DESIGN, OPTIMIZATION, AND SELECTIVITY OF INORGANIC ION-EXCHANGERS FOR RADIOACTIVE WASTE REMEDIATION

A Dissertation

by

DMITRY GENNADIEVICH MEDVEDEV

Submitted to the Office of Graduate Studies of
Texas A&M University
in partial fulfillment of the requirements for the degree of

DOCTOR OF PHILOSOPHY

August 2004

Major Subject: Nuclear Engineering

DESIGN, OPTIMIZATION, AND SELECTIVITY OF INORGANIC ION-EXCHANGERS FOR RADIOACTIVE WASTE REMEDIATION

A Dissertation

by

DMITRY GENNADIEVICH MEDVEDEV

Submitted to Texas A&M University
in partial fulfillment of the requirements
for the degree of

DOCTOR OF PHILOSOPHY

Approved in style and content by:

Abraham Clearfield (Co-Chair of Committee)	John Ford (Co-Chair of Committee)
Timothy R. Hughbanks (Member)	John W. Poston (Member)
	William E. Burchill (Head of Department)

August 2004

Major Subject: Nuclear Engineering

ABSTRACT

Design, Optimization, and Selectivity of Inorganic Ion-exchangers for Radioactive Waste Remediation. (August 2004)

Dmitry Gennadievich Medvedev, Diploma, D.I. Mendeleyev University of Chemical Technology of Russia

Co-chairs of Advisory Committee: Dr. Abraham Clearfield
Dr. John Ford

The processes of development of nuclear weapons resulted in accumulation of thousands of curies of high-level radioactive waste. Liquid waste produced in the US has been stored in carbon steel tanks in highly alkaline (1-3 M NaOH, 6 M sodium salts) media for fifty years and leakage has occurred.

One of the approaches to the solution of the problem of radioactive waste is to adsorb the nuclides on highly selective ion-exchange material, solidify in a glass matrix and dispose in a geological formation. The use of the ion-exchange technology is limited by the time of the sorbent-solution contact required to reduce the activity of the streams to acceptable levels. Inorganic ion-exchangers are promising materials due to their high radiation stability, extreme selectivity, and compatibility with the glass matrix. The contact time can be reduced by improving selectivities, kinetics, and capacities of the materials towards the target ions. This can be accomplished in part through understanding of the origin of ion-exchange selectivity.

Crystalline zeotypes with minerals sitinakite (ideal formula $Na_2Ti_2O_3SiO_4 \bullet 2H_2O$) and pharmacosiderite ($HM_3(TO)_4(GeO_4)_x(SiO_4)_{3-x}$ M = Cs^+, Na^+, K^+, T=Nb^{5+}, Ge^{4+}, Ti^{4+}) structures are excellent candidates for selectivity studies because of their ion-exchange properties tunable by alterations of synthetic procedures, and isomorphous framework substitution. The Nb-substitution in titanium sites reduces the framework

charge, whereas Ge substitution decreases the unit cell size if in titanium sites and increases if it in silicon sites. The compounds were hydrothermally synthesized in Ti/Si, Ti/Nb/Si, Ti/Ge/Si forms and characterized by structural and ion-exchange studies. The 25% Nb substitution in titanosilicate sitinakite resulted in enhanced selectivity for cesium and additional bond formation of cesium within the channel. The selectivity for cesium in germanium substituted pharmacosiderite also was correlated with the coordination environment within the channel.

In the advanced stages of this study semi-crystalline (sodium nonatitanate) and amorphous (monosodium titanate) materials also were considered because of their remarkable strontium selectivity. In situ X-ray diffraction techniques revealed that the sodium nonatitanate precedes the formation of the TS phase in hydrothermal synthesis. This knowledge allowed us to design and synthesize material for combined cesium and strontium removal.

To my family

ACKNOWLEDGEMENTS

I gratefully acknowledge Dr. Abraham Clearfield for strategic guidance throughout my research work which resulted in this dissertation and for giving me freedom in making independent decisions and choices over the course of this work. I was always treated like an individual and the feeling of that will stay in my memory forever. I very much value the knowledge and experience that I have received while working in his group.

My endless gratitude goes to Dr. Akhilesh Tripathi - structural "guru" of Clearfield's group. My dissertation would never have been completed without him. On top of that I developed a very close friendship with him which I hope will stay between us no matter where we go in our further careers.

I'd like to acknowledge other hard working members of the Clearfield group: Dr. Ekaterina Bakhmoutova, Dr. Naima Bestaoui, Dr. Joy Heising, Dr. Deyuan (Kitty) Kong, Dr. Sharath Kirumakki, Dr. Teresia Moller, Dr. Xiang Ouyang, Dr. Boris Speitzer, Dr. Ayyappan Subbiah and undergraduate student Jose Delgado. I am grateful for their comments, input, and help.

I am thankful to Dr. John Ford from Texas A&M's Department of Nuclear Engineering for his emotional support and useful advice.

I am indebted to Dr. Kenneth Lee Peddicord who encouraged me to come to study at Texas A&M.

This dissertation is a result of collaborative work. My special thanks go to Dr. May Nyman from Sandia National Laboratories, Dr. John Parise and Aaron Celestian from SUNY at Stony Brook, Dr. David Hobbs from Savannah River Company.

I am grateful to my parents, who supported me emotionally, my elder brother Pavel G. Medvedev, who helped me to start off a new life in the USA. My deepest gratitude goes to my wife, Natalia, and my daughter, Alexandra, for letting me spend quite a bit of time outside of home working on my dissertation.

This work was made possible by the U.S. DOE Environmental Management and Science Program, Grant DE-FG07-01ER63300 with funds supplied through the Westinghouse Savannah River Technology Center.

The research was carried out in part at the National Synchrotron Light Source, Brookhaven National Laboratory, which is supported by the U.S. Department of Energy, Division of Materials Sciences and Division of Chemical Sciences, through contract No. DE-AC02-98CH10886.

The FE-SEM acquisition was supported by the National Science Foundation under grant No. DBI-0116835.

Dr. Renald Guillemette of the Department of Geology and Geophysics, Texas A&M University is acknowledged for microprobe analysis of selected samples.

TABLE OF CONTENTS

LIST OF FIGURES

FIGURE Page

FIGURE Page

LIST OF TABLES

TABLE Page

CHAPTER I
INTRODUCTION

1.1. Defense high level waste: site locations and conditions of storage

Radioactive wastes accumulated in the USA as a result of the nation's nuclear weapons program pose a significant threat to the environment and population of the country. The situation became even more complicated after September 11 of 2001 and consequent events when the existence of terrorist organizations became obvious to the public. Temporary storage facilities for radioactive wastes may be used as a possible target for terrorist attacks. Untreated and undisposed, radioactive materials may be stolen and utilized as a component for so called "dirty bombs" - explosive devices designed to disperse radioactive material. The environmental damage due to leakages occurring over the time of storage seems rather small when compared to the scenarios mentioned above. The problem of radioactive waste remediation has to be solved in the near future. According to the General Accounting Office report that was quoted in one of the issues of Nuclear News magazine "after investing more than 20 years and about $18 billion the Department of Energy (DOE) acknowledges that the program to clean up its high level waste was far behind schedule, far over budget and in need of major change".[1]

The most significant part of the clean up effort is targeted towards High Level Waste (HLW), with 94 million gallons of untreated HLW in storage at DOE facilities at the Hanford Site in Washington, the Savannah River Site (SRS) in South Carolina, and the Idaho National Engineering and Environmental Laboratory (INEEL) near Idaho Falls. These industrial complexes were established across the United States during and after World War II to develop, manufacture, and store nuclear weapons.

This dissertation follows the style and format of *Chemistry of Materials.*

The accumulated liquid HLW has been stored in steel tanks for about fifty years and some leakage has occurred from the single-shell tanks. The migration of the radionuclides from tanks via ground water streams to the Columbia River (Hanford site) or Savannah River (SRS) is the most probable pathway of contamination of adjacent territories.

The operation of the Savannah River Site started in 1950 with production of isotopes, mainly, tritium and plutonium for defense programs. The site is located next to the Savannah River and the city of Augusta, Georgia. The tanks enclose large amounts of solids at the bottom, termed sludge. This sludge formed when the waste solution, which was 5-7 N in nitric acid, was neutralized with sodium hydroxide. All the insoluble oxides precipitated and amphoteric ones (like Al, Zn, etc) dissolved. The majority of the radioactive nuclides are concentrated in the sludge. Also, there is a thick salt cake on top of the fluid, formed after the alkaline waste solution was processed through evaporators to remove excess water.

Most of the activity in the tanks is due to actinides, strontium-90, and cesium-137. The general composition of SRS tank wastes is summarized in Table 1.1.[2]

Table 1.1. Chemical and Phase Composition of Tank High-Level Waste at SRS

	Sludge	Saltcake	Supernate	Total in solution	Total
Volume, m^3	9400	58400	65500	n/a	133000
Dry mass, tons	2500	22400	n/a	n/a	n/a
Cesium-137, MCi	5.9		88.8	95	95
Strontium-90, MCi	98		0.03	0.03	98
Total α, MCi	3.6		0.1	0.1	3.7

It is expected that half of the activity which is currently in insoluble form will dissolve during reprocessing activities.

1.2. The choice of remediation technology

One of the approaches to the radioactive waste problem is separation of the radioactive nuclides and solidification into a stable form with consequent isolation in a geological formation. Solidification allows significant volume reduction of the wastes, along with transformation of the activity into insoluble form.

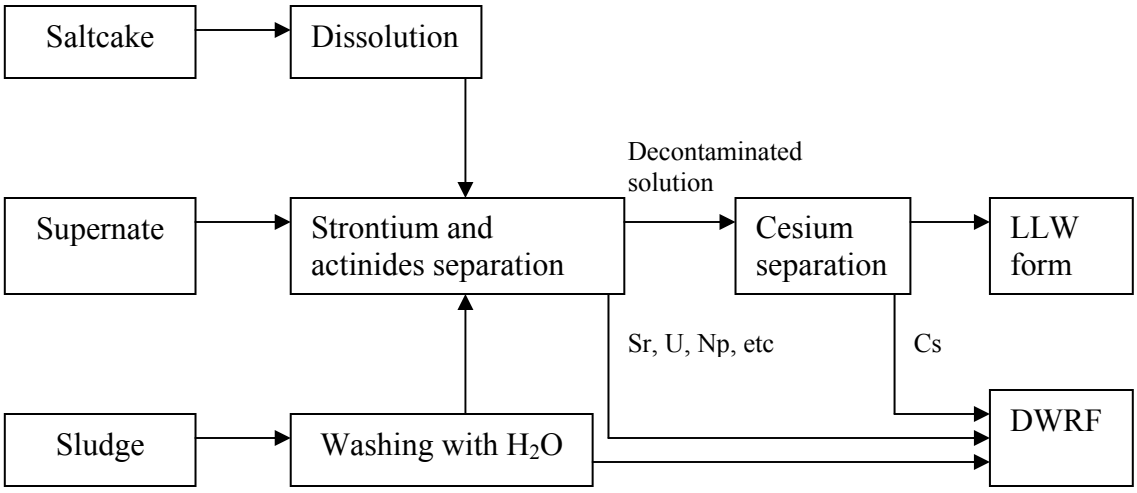

Figure 1.1. Schematic flow chart of HLW reprocessing at Savannah River Site

SRS plans to immobilize its waste in a borosilicate glass matrix (the process is usually referred as vitrification) and eventually dispose of the glass in a geological depository. The molten glass has to be poured into stainless steel canisters and will be kept on-site until the geological repository will be ready to accept them. The sequence of

operations, proposed for remediation of HLW at SRS[2] is shown in Figure 1.1. As can be seen from the flowchart SRS plans to utilize a two stage process. The first stage is the strontium and actinides removal which is followed by cesium removal in the second stage. The water from treated radioactive solution will be evaporated prior to introduction into the glass melting process in Defense Waste Processing Facility (DWPF). The sludge and the salt cake will be treated with water to transfer the activity to soluble form.

There are a number of technical challenges associated with separation of the content of the tanks due to high volume activity of the waste solutions, high ionic strength (> 5.6 M Na^+), and the lack of information about the real composition of the waste in each tank.

1.2.1. Solvent extraction

Separation of the nuclides by liquid extraction has a long history of success in spent nuclear fuel reprocessing and plutonium recovery. The removal of the nuclides in this process is based on differences in their solubilities in the aqueous stream solution and in the organic solvent. Generally, the process consists of several steps. First, the solvent is being contacted with the stream solution containing the nuclides in continuous mode. During this operation the targeted nuclides are being transferred (extracted) from the stream solution to the solvent. Since the aqueous solution and organic solvent are immiscible, the organic and aqueous phases can be separated by being left undisturbed. Second, the solvent, containing target nuclides is being contacted with another aqueous stream and the nuclides are removed selectively from the solvent. Third, the nuclide free solvent is recycled and directed to the head of the process.

Despite of several advantages, such as long successful experience of application in nuclear industry and the possibility of remote control, there are some specific shortcomings associated with this process. In particular, the following problems require further consideration:

- whether the solvent can be regenerated successfully
- whether "crud" will build up on the boundary between the phases
- whether the supply of the crown ether for this operation will be available with a high degree of reliability

1.2.2. Cs removal by in-tank precipitation procedure

As was noted above, the actinides, strontium, and cesium are planned to be removed in two separate steps. In the late 1970s and early 1980s the SRS developed a process for removing of Cs from solution by precipitation with sodium tetraphenylborate (NaTPB). The process can be described by reaction:

$$Na^+ + TPB^- + Cs^+ \rightarrow Na^+ + CsTPB\downarrow$$

The NaTPB was supposed to be added directly to the tank and the procedure is referred as "in-tank precipitation." The process was tested and removed most of the cesium but a complication arose due to flammable benzene generation presumably as a result of radiolytic reactions. This process was put on hold until the source of benzene generation was found.[2]

1.2.3. Ion-exchange technologies

DOE finally proposed to adsorb all radioactive elements into an ion-exchanger, or a series of exchangers. Several candidates have been proposed and the most promising are titanium silicates with open framework structures and amorphous and layered titanates.

Inorganic ion-exchangers are superior to the organic ion-exchange resins in their thermal stability and resistance to radiation. Organic ion-exchange resins consist of an elastic three-dimensional network of hydrocarbon chains which incorporate fixed ionic groups. The charge of the groups is balanced by mobile counter ions. The resins are insoluble but can swell to a limited degree. The ion-exchange properties of the resins

depend mostly on the nature of fixed ionic grouping. The framework of the resins in contrast to inorganic ion-exchangers is a flexible random network. Counter ions, associated with the fixed ionic grouping are preferred by the resins. The question, whether actual bonds are formed or the ions just being adsorbed in pores is still somewhat controversial.

Inorganic ion-exchange materials, such as zeolites and titanosilicates, are stable in highly basic media, and resistant to radiation and temperature. Another advantage is their ability to serve as a part of glass matrix, so the activity can be disposed while being trapped inside of ion-exchangers. Furthermore, crystalline ion-exchangers with regular framework structures often show higher selectivities than materials with irregular gel structures.

1.3. Baseline ion-exchangers

There has been an on-going search for inorganic ion-exchangers for the remediation activities. The current candidates are monosodium titanate (MST) proposed for strontium and actinides removal, and sodium titanium silicate (TS), which is usually, referred as crystalline silicotitanate (CST)[3-5] in its engineered form (IONSIV IE-911, UOP, Inc. Des Plains) that is suggested for cesium removal to replace earlier proposed in-tank precipitation of cesium with sodium tetraphenylborate.

The later procedure had to be revised due to generation of benzene as a result of the process. The cesium removal process has not received final approval yet. Solvent extraction by crown ethers is one of the alternative techniques for cesium removal. Modified in-tank precipitation procedure, designed for smaller volumes is also considered.

The choice of inorganic ion-exchangers for strontium removal is not final either. SRS considers layered sodium nonatitanates (SNT) and open framework titanium silicates with mineral pharmacosiderite topology (TSP) as alternatives to MST to speed

up the kinetics of strontium and actinides ion-exchange. The structural features of both baseline and alternative materials are introduced below.

1.3.1. Monosodium titanate (MST)

In 1976 R. Dosch from Sandia National Laboratories suggested the process of radioactive waste solidification by treatment of the solution with M'(MxOyHz) (M' is a cation, (MxOyHz) an anionic group, M = Ti, Zr, Nb, or Ta, and x = 2) to form a precipitate. The radioactive solution containing about 20 radioactive elements was treated with $NaTi_2O_5H$ taken in 10% stoichiometric excess. The removal of more than 50% of activity was reported.[6] The utilized compound is now referred as monosodium titanate.[7,8] MST in engineered form is an amorphous material with porous structure having pore sizes of the order of 500 to 2,000 Å.[9] The mechanism of the removal is presumably an ion-exchange reaction between sodium ions in the solid and radioactive ions in the solution coupled with absorption on the surface of particles.

1.3.2. Sodium titanium silicate (CST)

Synthetic sodium titanium silicate (referred to as TS in this dissertation) was developed as a result of collaboration of Sandia National Laboratories and Texas A&M University[3,10] in 1993. Its naturally occurring analog mineral sitinakite was discovered a few years earlier in Khibiny alkaline massif in the USSR.[11,12] The synthetic material has an ideal formula $Na_2Ti_2O_3SiO_4 \cdot 2H_2O$ and tetragonal unit cell, with a=7.8082 Å, c=11.9735 Å, and Z=4. The structure consists of clusters of four titanium-oxygen octahedra located around the unit cell corners, which are linked by silicate groups along two of the unit cell axes. This arrangement provides channels along the crystallographic axis suitable for selective adsorption of ions.[13] The remaining sodium ions reside in the framework, bonded to four silicate oxygens and two water molecules (Figure 1.2). It was

reported that this material is highly selective toward cesium and strontium and effective for removal of these elements from highly alkaline media.[3]

1.4. Alternative materials

1.4.1. Sodium nonatitanate (SNT)

Sodium nonatitanate with chemical formula $Na_4Ti_9O_{20}•xH_2O$ is a layered material with interlayered spacing varying from 6.9 to 10.0 Å depending on water content.[14] The exact structural information on this compound is not available because of its amorphous nature. It is presumed, however, that layers consist of titanium polyhedra sharing edges with each other.

Sodium ions are located between the layers and can be exchanged with cations from the solution.[14,15] SNT demonstrated excellent performance in alkaline media.

The distribution constants of the order of 21000 mL/g were reported for strontium in a solution of 55 ppm of Sr, 5M $NaNO_3$, and 0.1M NaOH.[16] Similarly to MST, the mechanism of removal is most likely a combination of ion-exchange and physical adsorption on the surface of the material.

1.4.2. Sodium titanium silicate pharmacosiderite (TSP)

In 1990 Chapman and Roe[17] reported synthesis and crystal structure of titanium silicate molecular sieves isostructural to naturally occurring mineral pharmacosiderite $KFe_4(AsO_4)_3(OH)_4.6\text{-}8H_2O$. The structure of TSP is somewhat similar to that of TS, described above.

Crystallized in a cubic unit cell, the structure consists of clusters of four Ti-O octahedra connected through silicon tetrahedra in all three crystallographic directions. Such an arrangement results in a three dimensional network of channels, where exchangeable cations, such as K^+, Cs^+ are located (Figure 1.2).

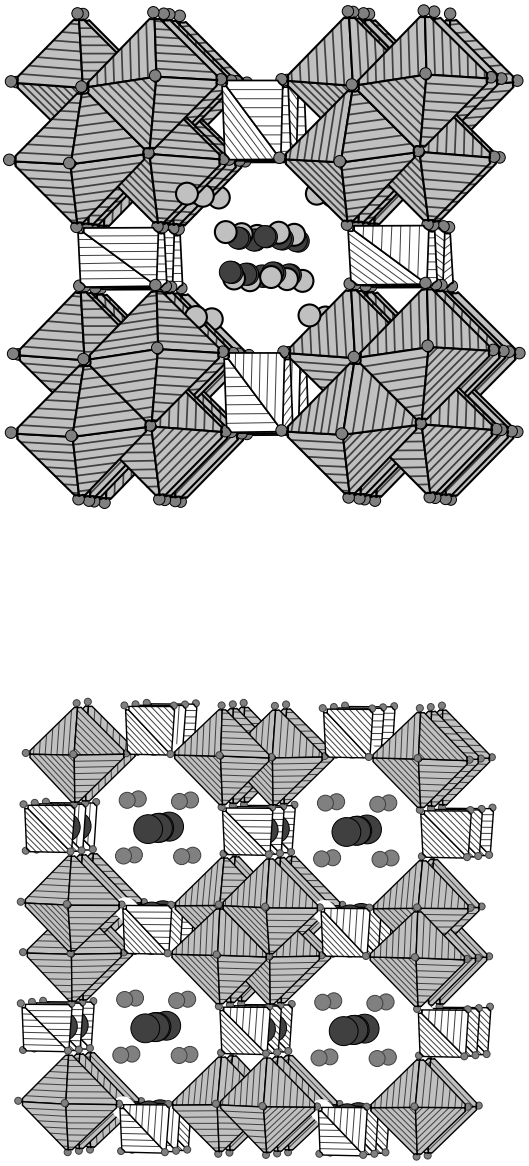

Figure 1.2. Polyhedral representation of crystal structure of the sodium form of TS along c-axis (top) and cesium form of TSP (bottom). Grey circles represent water molecules, black circles represent cations

Behrens and Clearfield[18] reported strontium distribution constants of potassium exchanged phase of 7100 mL/g in 2.5 M $NaNO_3$/1 M NaOH solution, and 3500 mL/g for a solution containing 5 M $NaNO_3$/1 M NaOH. This fact suggests that this material exhibits relatively high affinity towards strontium in highly alkaline media.

1.5. Purpose and overview

As was mentioned above the choice of the material for removal processes has not been finalized. The research activities related to evaluation and improvement of alternate materials has been initiated. The key to improvement of the materials lies in understanding of the reasons for ion exchange affinity of the particular ion-exchange towards the cation of interest. This dissertation focuses on investigation of the ion exchange process in tunnel type titanium silicates and amorphous titanates. Both structural and morphological reasons for selectivity will be considered.

Two approaches will be used to modify ion-exchange properties of titanosilicates: (1) modification of the synthetic procedure which affects morphology of the material and (2) is the alteration of the framework by isomorphous substitution for the titanium or silicon atoms.

In the second chapter the mechanism and conditions for crystallization of sodium titanium silicate with sitinakite topology (TS) is discussed. The results of ion-exchange studies of samples with different morphology are presented in Chapter III.

In Chapter IV we compare ion-exchange selectivities for cesium and strontium in Nb-substituted TS (Nb-TS) and pure (non-niobium) TS. Ion exchange studies will be correlated with structural features of exchanged phases.

Chapter V deals with ion-exchange properties of pharmacosiderites (TSP). Similarly, to TS the ion-exchange properties of samples with various germanium, or Nb substitutions will be correlated with structural studies.

Chapter VII is devoted to amorphous materials and their optimization in relation to the removal of strontium from HLW solutions.

CHAPTER II
CRYSTALLIZATION OF SODIUM TITANOSILICATE WITH SITINAKITE TOPOLOGY UNDER HYDROTHERMAL CONDITIONS

2.1. Introduction

2.1.1. Background

A search on the topic "hydrothermal synthesis" in the SciFinder literature database returned more than 20,000 references containing this concept. The earliest electronic reference dates back to the year 1918. Mooler and Koenigsberger[19] discovered that "when a mixture of all or some of the components K_2O, Na_2O, Al_2O_3, SiO_2, H_2O and CO_2 is heated in a pressure bomb at about 400^o C certain minerals, as, for example, orthoclase and leucite, may be formed".

Being initially a trial and error technique, hydrothermal synthesis was systematically studied after commercialization of zeolites. Zeolites are crystalline microporous alumosilicates utilized widely as catalysts in fluidized catalytic cracking of petroleum. Being porous on a molecular scale, their structure represents regular arrays of channels and cavities. The framework consists of repeating SiO_4 and AlO_4 units connected through oxygen atoms. The negative charge of the framework is balanced by group IA and group IIA ions. In a typical zeolite synthesis a mixture of sodium aluminate and sodium silicate is heated in an autoclave in alkaline media at temperatures from 80 to 200^{o}C. The gel is prepared from reactive sources of silica and aluminum. Being metastable, such a gel yields crystals which, depending on the temperature, reagents and time of reaction, may have different chemical structures and as a result different properties.[20-22]

Microporous titanosilicates where the titanium atoms are incorporated as octahedra TiO_6 connected with silicon tetrahedral units represent a new family of zeolite

type materials (zeotypes). Their possible applications are similar to that of zeolites: catalysis, separations, and ion-exchange. The number of such materials synthesized in the last few years has increased dramatically. Different types of materials have been synthesized such as small pore ETS-4 (Engelhard Titanosilicate-4), wide pore ETS-10, pharmacosiderites, CST, the family of AM titanosilicates, containing edge shared titanium chains. Some of the materials are counterparts of naturally occurring minerals, so the development of synthetic analogues was inspired by the nature.[23]

Sodium titanium silicate with mineral sitinakite topology and ideal formula $Na_2Ti_2O_3SiO_4 \bullet 2H_2O$ (TS), which is usually referred as crystalline silicotitanate (CST) in its engineered form (IONSIV IE-911, UOP, Inc. Des Plains) is considered as one of the baseline materials for cesium removal from alkaline HLW accumulated in the USA.[5,24-26] Besides being of great technological importance, TS is also of great academic interest because of diversity of its chemistry.[27] The substitution of heteroatom into the framework of this material allows the fine-tuning of its properties. The effects of such substitution will be described in the next chapters.

2.1.2. Aspects of zeolites crystallization relevant to titanosilicates synthesis

Several reviews have been published on zeolites crystallization.[21,22] Numerous systematic studies on synthesis have been carried out and have resulted in preparation of many materials with different structures. J. B. Nagy et al[22] have summarized general parameters influencing zeolite crystal growth. Among these are composition of the reaction mixture, time and temperature of crystallization. Though the effect of each synthesis parameter is different for different zeolite structures some common trends can be outlined.

Precursor composition. Due to a variety of complicated processes taking place during crystallization it is very unlikely for a zeolite to have the same Si/Al ratio as in the starting precursor. Attempts to change the Si/Al ratio in a zeolite by changing the Si/Al ratio in the starting mixture result are usually accomplished by trial and error

methods. They may result either in the desired product, or a completely different compound.

The hydroxide ion content strongly influences the nature of the species present in the solution, rate of hydrolysis and as a result rate of crystallization. The alkalinity of the gel can alter the type of the framework and its composition.

Silica speciation. Speciation of silica is highly dependent on hydroxide content in a starting precursor. The soluble species tend to polymerize. To simplify the notation of different silica species in the solution Q-units, first proposed by Engelhardt Corporation has been widely adopted. The Q symbol stands for a silicon atom tetrahedraly coordinated with 4 oxygens. Further more, the superscript indicates the number of other Q units, attached to the central atom. Depending on the conditions mono or polymeric species are present, serving as building units for the framework.

Time and temperature. Time and temperature are, perhaps, the most important parameters to control zeolite synthesis. The desired zeolite phases are often metastable and may be redissolved almost immediately after formation, so it is important to know the crystallization kinetics to prepare crystalline phases.

There are several ways in which the temperature can affect zeolite synthesis:

- the nature of the phase: higher temperature leads to more dense structures
- kinetics of crystallization: at higher temperature the processes completes faster

2.1.3. Approach to studies of titanosilicate crystallization

Despite similarities in structures and methods of synthesis between titanosilicates and zeolites there are some differences in chemistry of the precursors between the two. Titania species are much less soluble in the alkaline media than are aluminates and silicates, and this difference may affect the nucleation mechanism significantly. Considerable information on crystallization can be obtained in ex-situ experiments, by stopping the reaction at regular intervals, or by variation of synthetic parameters and

collecting X-ray diffraction patterns of the samples. However, this process is generally time consuming, provides limited information, and can be prone to misleading results if in the process of extracting samples the crystallizing reaction is affected.

In-situ X-ray diffraction provides a convenient tool to obtain more detailed data about crystal growth of a material, providing a continuous record of the crystallization process while leaving the reaction undisturbed. It provides easy and rapid information about any intermediate and short-lived phases formed during the hydrothermal reaction. Information about the kinetics of the reaction, which is uncertain in ex-situ experiments, can be obtained from in-situ experiments. In-situ measurements also eliminate the possibility of alteration of the product by quenching, since many species may exist only at high temperatures and may change during post synthesis treatment (filtration, drying).

In the present investigation we utilized a combination of ex- and in-situ experiments to study the crystal growth of TS. The parameters that influenced the crystallization and product composition were first detailed via ex-situ synthesis studies and were then followed by study of the in-situ crystallization process, using the synchrotron radiation facility at National Synchrotron Light Source, Brookhaven National Laboratory for collecting dynamic X-ray powder diffraction spectra. Based on the results of these studies a mechanism for TS crystallization has been suggested.

2.2. Experimental methods

2.2.1. Preparation of gels

Two groups of gels were used in these studies. In the first group, starting gels were prepared so that the titanium to silicon ratio (Ti/Si) was close to 1.0, while in the second group Ti/Si=0.5.

Preparation of gels with Ti/Si = 1. Several precursors with general composition, $1.0TiO_2$:$x SiO_2$:$y Na_2O$:$146.0H_2O$ were prepared by variation of one of the parameters and then treated hydrothermally for time τ at temperature T. The ranges of

variation of x, y, T and τ were as follows: $0.9 \leq x \leq 1.6$, $3.64 \leq y \leq 5.67$, $110^0C \leq T \leq 210^0C$, $2 days \leq \tau \leq 15$ days.

Generally synthetic parameters were varied one at a time. The gels were prepared by mixing $Ti(OC_3H_7)_4$ (Alfa Aesar) with $Si(OC_2H_5)_4$ (Aldrich) in a plastic beaker. Sodium hydroxide was added to the mixture in the form of a 6.32 M solution under constant stirring, followed by addition of 15 mL of doubly deionized (ddi) water. After vigorous agitation the mixture was sealed in a 100 mL Teflon lined pressure vessel and kept in the oven. In the experiments involving variation in the composition of the gel, hydrothermal reaction was carried out for 3.5 days at 170^o C.

After heating, the final products in all reactions were treated in the following fashion: pressure vessels were cooled down, the solid was separated by filtration, rinsed with ddi water and ethanol, and dried at 60^o C. X-ray powder patterns of the solids were routinely recorded on a Rigaku computer-automated diffractometer with rotating anode, operated at 50 kV and 100 mA with a copper target. Data were collected from $2\theta = 5$ to 60 degrees with a step size of 0.04^o and exposure of 1 sec/step.

Preparation of gels with Ti/Si = 0.5. A second group of precursors was prepared using a different source of silica. The general composition of these gels was $1.0TiO_2:1.98SiO_2:yNa_2O:218\ H_2O$. A total of 3.5 mL of titanium isopropoxide (Alfa Aesar) with 20 mL of ddi H_2O and 7 mL of 10 M NaOH were mixed in a plastic beaker. To this mixture, 1.469 g of $SiO_2.nH_2O$ (Fisher), dissolved in NaOH solution was added. The amount of added NaOH varied according to desired gel compositions specified later. After agitation, the mixture was sealed in a Teflon lined pressure vessel and heated in the oven at the conditions outlined later. The X-ray powder patterns of the solids were recorded on a Bruker-AXS D8 powder high resolution parallel beam X-ray diffractometer, operated at 40 kV and 40 mA. Data were collected from $2\theta = 5$ to 60 degrees with a step size of 0.04 and exposure of 1 sec/step.

2.2.2. Studies of kinetics of crystallization

In the present investigation the process of crystallization was studied using ex-situ batch experiments as well as in-situ scattering techniques.

Batch type ex-situ experiments. The gel of desired composition was divided into several 20 mL pressure vessels (12 mL of gel in each liner), which were then sealed, and heated in an oven at pre-determined temperature. The pressure vessels were taken out after different periods of time, and treated as described above.

In-situ experiments. In-situ synthesis experiments were carried out at the X7B beamLine of the National Synchrotron Light Source (NSLS) at Brookhaven National Laboratory.

A gel of composition, $1.0TiO_2$:$1.98SiO_2$:$6.77Na_2O$:$218H_2O$ was prepared by mixing of 3.5 mL of titanium isopropoxide in 20 mL of ddi H_2O, 8.5 mL of 10 M NaOH with 27 mL of 0.86 M silica solution in 2.6 M NaOH. The gel was filled into a 0.5 mm sapphire capillary mounted on a goniometer head with Swagelock T-piece. An external nitrogen pressure of 250 atm was applied through the connected tubing and a hot air stream was used to slowly heat the capillary to 220^{o}C at a constant rate for (2 hours), and followed by 14 hour synthesis at this temperature. Thus hydrothermal conditions were achieved in the heated part of the capillary.[28,29]

Diffracted X-ray (λ=0.9223Å) data were collected on a MAR 345 imaging plate (IP) detector with a built in scanner for online reading. Erasing, exposing and reading the IP limits the time resolution to about 2.5 minutes. Data were acquired for 60 s exposures. A large dynamic range can be obtained with IPs that in turn allows intensity data to be extracted from the image for Rietveld refinement of in-situ powder diffraction data. The wavelength, sample detector distance, zero point, and imaging plate tilt were determined from a LaB_6 standard.[28,29]

The crystallization progress was determined from IP images using integrated intensities of diffraction lines. After data collection, IP data were integrated using the program Fit2D.[30,31] These files were saved as a CHI file (2θ vs. intensity file), and then

converted to DiffracPlus and CPI format by the program ConvX.[32] These formats were used in the programs EVA (data plotting),[33] CRYSFIRE (automated indexing),[34] XFIT (peak profiling),[35] and EXPGUI[36] (Retvield refinement) for the processing of data for structure refinement.

2.2.3. Recording of the NMR spectra

Si-29 NMR spectra of several gel filtrates and filtrates from final products were recorded on a Varian Inova 400 NMR spectrometer equipped with a 5 mm multinuclear probe head. Gels for NMR experiments were prepared using D_2O as a solvent. Chemical shifts were recorded with respect to $Si(CH_3)_4$ in $CDCl_3$ locked at $CDCl_3$. A 2 s acquisition time, 20 s relaxation delay, and 45^o pulse was used to obtain the spectra. During the acquisition the field was locked at D_2O. A 2.620 ppm standard shift from zero was added to the chemical shifts of peaks and peak assignment was done based on corrected values.

2.3. Results and discussion

As a first step the effect of various parameters on the yield and crystallinity of the final products was examined. The group of gels, having Ti/Si=1 were prepared for this purpose. Gels with other compositions were studied subsequently.

2.3.1. Experiments with gels having Ti/Si=1

Effect of amount of Na_2O. First attempts to synthesize TS from the gel with composition $1.0TiO_2$:$1.01SiO_2$:$5.26Na_2O$:$146.0H_2O$ resulted in crystallization of two phases: the TS phase and sodium titanium oxide silicate Na_2TiSiO_5 (STOS), a synthetic

analog of naturally occurring mineral natisite, whose crystal structure and chemical formula were reported previously.[37,38] In this structure titanium-oxygen square pyramids share corners with silicon tetrahedra forming layers that are separated by sodium ions.[39] The sodium ions are trapped in four member rings formed by two TiO_5 square pyramids and silicon tetrahedra and are not exchangeable. Figure 2.1 shows the XRD patterns of various phases obtained from the above gel under different conditions. In particular, the initial amount of Na_2O in the gel was varied from 3.6 to 5.6 moles per mole of TiO_2. These syntheses resulted in a mixture of STOS and TS phases when the *y* variable (see preparation of gels with Ti/Si=1) was set above 3.65.

To quantify the relative amount of each phase in a mixture of products we compared the ratio of the most intense reflection in the TS phase (d=7.808 Å, I=100%, hkl=100) to that in the STOS phase (d=2.709 Å, I=100%, hkl=201) for each value of *y* (amount of Na_2O). The results are plotted against y and NaOH concentration in Figure 2.2. As can be seen from the plot, the STOS phase yield increases with alkalinity of the starting gel, resulting in a pure STOS phase when the *y* value was above 5.7 ($[OH^-]$=4.3 M). Unlike the STOS phase, the conditions for TS phase formation are favorable at lower Na_2O content. The pure TS phase can be synthesized at *y* values below 3.5 ($[OH^-]$=2.76 M), but the crystallinity of the product deteriorates. Figure 2.2 shows the effect of the initial NaOH concentration on crystallinity of the TS phase expressed as the value of full width at half maximium (FWHM) of the most intense TS peak (d=7.808 Å, I=100%, hkl=100).

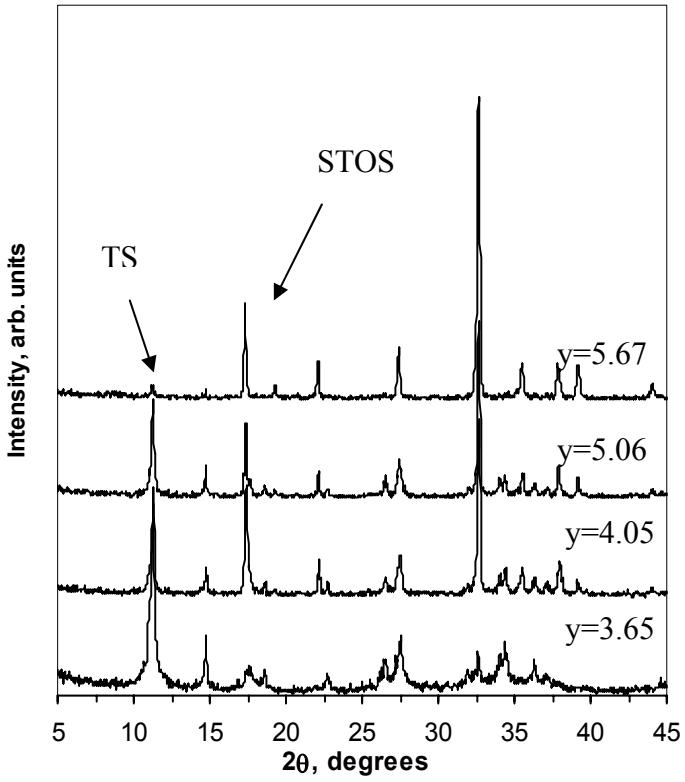

Figure 2.1. XRD powder patterns of phases obtained from $1.0TiO_2$:$1.01SiO_2$:$y Na_2O$:$146.0H_2O$. Reaction time-84 hours, temperature-170^o C. Samples ID: DM1-38-2 (y=5.67), DM1-41-2 (y=5.06), DM1-37-1 (y=4.05), DM1-44-1 (y=3.65)

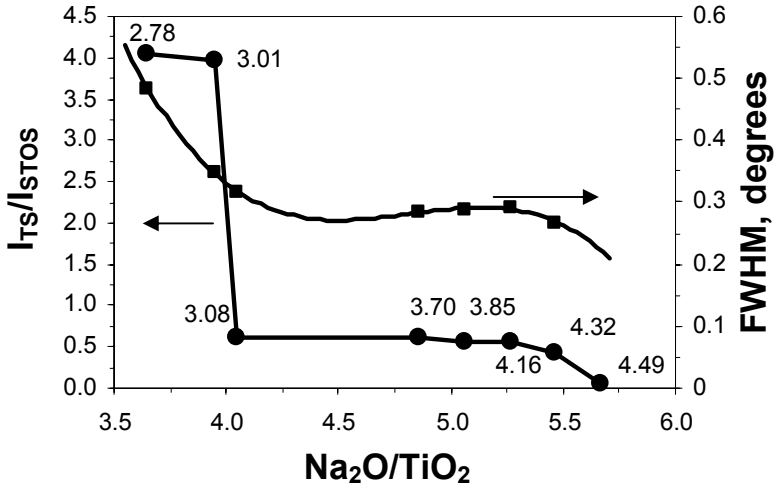

Figure 2.2. Crystallinity (FWHM) and the ratio of the most intense reflections (I TS/ I STOS) for the gels of composition 1.0 TiO_2 : 1.01 SiO_2 : y Na_2O : 146.0 H_2O, temperature 170^0C, time 3.5 days for 3.0 <y<6.0. The labels next to data points indicate initial NaOH concentration in gels

As the concentration drops below 3.7 M NaOH the FWHM value starts increasing and reaches half a degree in 2θ. Transition from the pure TS phase to pure STOS phase is not gradual and in this region two phases coexist with each other with the yield of STOS slightly increasing with increasing alkalinity.

Variation of Ti/Si ratio. According to the chemical formula of TS the ratio of Ti/Si=2:1.[13] Synthetic procedures attempted from gels with this ratio resulted in formation of mixtures of several phases, including layered sodium nonatitanate $Na_4Ti_9O_{20}•nH_2O$ (SNT) and STOS (Figure 2.3).[14,40] Further increase of the amount of silicon over titanium reduces the alkalinity of the gel as NaOH is consumed in the reaction for silicate formation.

As a result the yield of TS increases as the amount of Si in the starting gel increases. Similar to the effect of decreasing Na_2O, the crystallinity of the product reduces as Si loading becomes higher.

Temperature variation. The temperature of the hydrothermal reaction is one of the key parameters controlling hydrothermal synthesis.[21,22] Open-framework compounds typically crystallize under hydrothermal conditions with temperatures up to 250° C.[22,41] In the present study it was found that SNT is formed both at low (110° C and 145° C) and high (210° C) temperatures. At the temperatures above 160° C mixtures of STOS and TS phases formed. The yield of the TS phase reduced as the temperature increased, resulting in an almost negligible value at 210° C. The phases and FWHM values of their 100% reflection (TS d=7.808 Å, hkl=100; STOS d=2.709 Å, hkl=201; SNT d=9.5-10.0 Å, hkl=001) are summarized in Table 2.1.

As can be seen from the values of FWHM shown in Table 2.1 the crystallinity of the products increases with the temperature of hydrothermal reaction. There is ~ 40% decrease in the FWHM value of (100) reflection in TS as the temperature increases by 10° from 160° C. The FWHM of (001) reflection in SNT at 110° C is three times broader than that at 210°C.

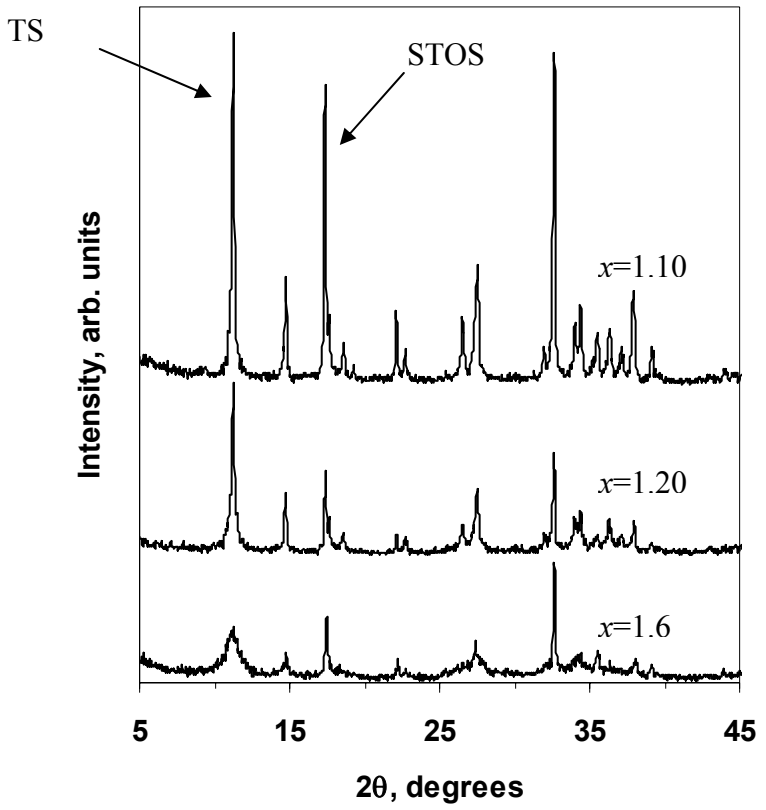

Figure 2.3. XRD powder patterns of phases obtained from gel $1.0TiO_2$:$xSiO_2$:$5.62Na_2O$:$146.0H_2O$. Reaction time-84 hours, temperature-170^o C. Samples ID: DM1-45-2 (x=1.10), DM1-44-3 (x=1.20), DM1-44-2 (x=1.6)

Table 2.1. Phases Obtained from Gel with Composition of $1.0TiO_2:1.01SiO_2:5.26Na_2O:146.0H_2O$. All reactions were carried out for 84 hours

Sample ID	Temperature, ^oC	Phases	FWHM, degrees		
			SNT (001)	STOS (201)	TS (100)
JD1-17-1*	110	SNT	0.4160	-	-
JD1-17-2	145	SNT	0.4680	-	-
DM1-45-4	160	TS; STOS	-	0.1960	0.2080
DM1-38-1	170	TS; STOS	-	0.1920	0.1240
DM1-45-3	210	SNT, STOS	0.1520	0.1400	-

Several conclusions can be drawn from the experiments regarding optimization of the conditions for TS synthesis. Firstly, out of two impurity phases that are formed along with TS phase, the SNT phase ($Na_4Ti_9O_{20}\cdot xH_2O$) does not contain any silicon, while the STOS phase (Na_2TiSiO_5) has 50 mol% more silicon and sodium per titanium compared to the TS phase. Modifying synthesis condition changes the relative amount of each phase. Secondly, we believe it is the concentration of sodium hydroxide that makes a major contribution in the purity of the TS product. An increase in starting concentration of NaOH improves the crystallinity of the product, but reduces the yield of the TS phase. In fact, when the concentration of hydroxide ion is about 2.7 M, conditions for the TS phase formation are more favorable, but the crystallinity of the product is reduced (Figure 2.2). To further support and generalize the above conclusions we prepared gels with completely different composition by increasing the amount of silica in the starting precursors and changing the source of silica as well.

2.3.2. Experiments with gels having Ti/Si=0.5

Ex-situ batch crystallization. Starting concentrations of titanium and silicon in gels were decreased to 0.2 M compared to 0.8 M in Ti/Si=1 group of gels. We prepared

* Samples were synthesized by an undergraduate student, Jose Delgado, as a part of his training.

gels with two compositions: in the first one (TS gel) the TS phase was targeted. The gel composition was $1.0TiO_2$:$1.98SiO_2$:$6.77Na_2O$:$218H_2O$. The second gel (STOS gel) had composition of $1.0TiO_2$:$1.98SiO_2$:$10.53Na_2O$:$218H_2O$. The hydrothermal reaction temperature was 210^o C to ensure good crystallinity (see Table 2.1). The TS gel resulted in moderately crystalline TS phase in 24 hours (DM5-381-1), and in highly crystalline TS phase in 5 days with about 2-5% impurity of the STOS phase (DM5-38-1). The STOS gel resulted in highly crystalline STOS phase both in 5 (DM5-38-2) and in 24 hours.

It should be noted that in both cases Na_2O/TiO_2 ratios were above 5.7, which in terms of this parameter corresponds to the conditions of pure STOS phase formation (Figure 2.2). The concentration of NaOH however, was set so that conditions were favorable to formation of the TS phase in the first case (2.7 M), and STOS phase (4.2 M) in second case. When compared to the results of experiments with Ti/Si=1 gels, the values of Na_2O/TiO_2 are higher for the gels with Ti/Si=0.5. However, the values of OH^- concentration are the same. This means that the parameter of initial concentration of NaOH, which accounts for the amount of solvent (H_2O) present in the system should be used to predict the yield and crystallinity of the TS phase in different systems rather then the Na_2O/TiO_2 values. Being empirically obtained from the previous experiments, the values of initial NaOH concentration, favorable for either TS or STOS formation are the same for gels with different Ti/Si ratios. The X-ray diffraction powder patterns of dried STOS (DM5-38-2 gel) and TS gels (DM5-38-1 gel) are shown in Figure 2.4. As can be seen from the plot both powder patterns have a very broad low angle peak, centered at 9.5-10 Å, which corresponds to the interlayer spacing of the SNT phase. This implies that the SNT phase forms at an early stage even at room temperature. As the synthesis proceeds, the crystallinity of this phase increases and then SNT grows into titanium silicate. In-situ crystallization studies were carried out to support this hypothesis.

Time-resolved in-situ diffraction studies Figure 2.5 shows a three-dimensional plot of the XRD spectra as a function of time during the TS gel (DM5-38-1) heating. As

can be seen from the figure the process starts with formation of a phase having a broad peak at 10 Å.

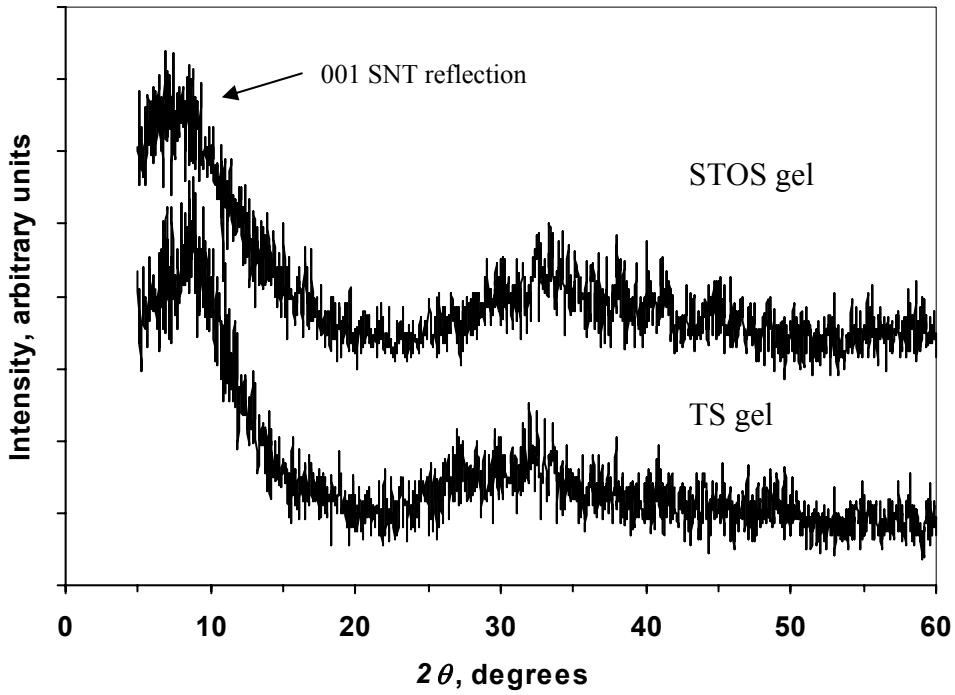

Figure 2.4. X-ray diffraction powder pattern of dry STOS (DM5-38-2 gel) and TS (DM5-38-1 gel) precursors

This phase was identified as layered sodium nonatitanate. The phase starts forming at room temperature, which is confirmed by collecting of X-ray diffraction powder pattern of the dried starting gel.

The intensities of the peaks are much higher than at room temperature but they do not change as the reaction progresses. The process of transformation of the SNT phase to the TS phase started after 1 hour of heating, with rapid decrease of SNT peaks and growth of TS peaks.

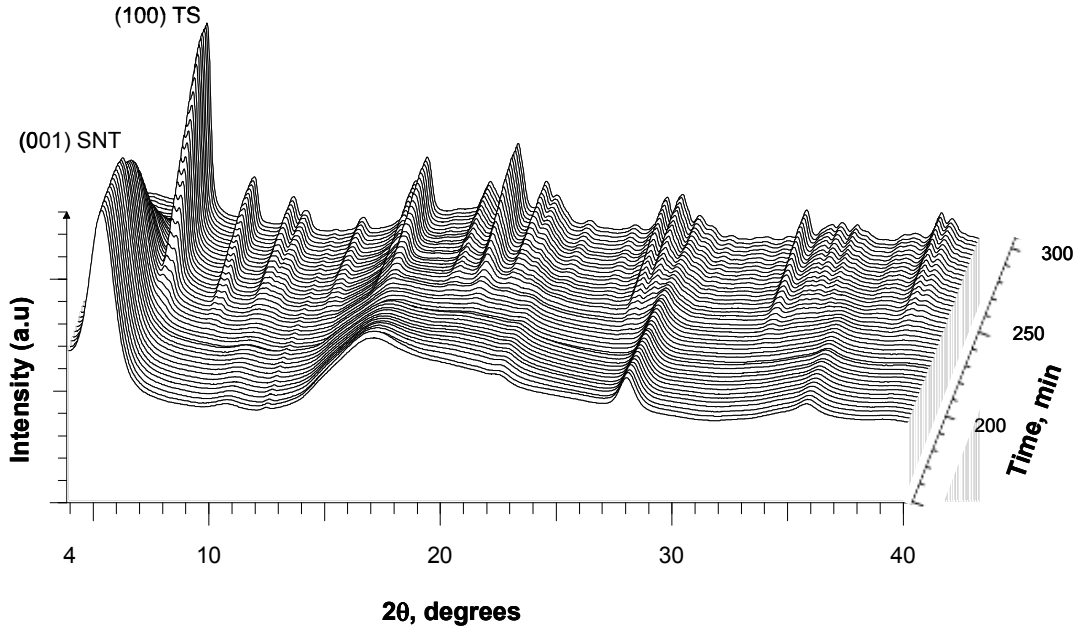

Figure 2.5. Time-resolved X-ray powder diffraction spectra of TS crystal growth from the gel with composition of $1.0TiO_2$:$1.98SiO_2$:$6.77Na_2O$:218 H_2O

The whole process of transformation lasted about 50 minutes. During the period followed by transformation no significant changes occurred, except a slight increase in peak intensities. No impurity phases were formed after 12 hours of experiment.

Ex-situ studies of kinetics of crystallization. Figure 2.6 shows the changes that occur in the powder pattern of the STOS precursor as a function of the time of hydrothermal reaction. The SNT phase remains as the only product of the reaction after 9 hours of heating. Peaks, attributed to the STOS phase first appear after 12 hours of heating. The intensity of the STOS peaks keeps increasing as the gels are heated further. The peaks, attributed to the SNT phase completely disappear after 17 hours of heating. The reaction route is a complete SNT - STOS conversion, with no intermediate phases formation. Formation of the SNT phase as a parent phase is also supported by the temperature variation studies, undertaken with Ti/Si=1 precursors (Table 2.1), where the SNT phase was obtained at 110^{o} and 145^{o} C. At these temperatures dissolved Si does not react with the SNT phase.

The ex-situ crystallization of the TS phase was monitored in the same fashion. Similar to our observation in in-situ crystallization, the SNT phase starts forming at the beginning of the reaction and becomes more crystalline after 1 hour of heating (Figure 2.6). In 10 hours, the intensity of (100) reflection in TS reaches almost the same value as the (001) reflection of SNT. In 24 hours, the SNT phase is completely converted to the TS phase. The route of the reaction in this case is a complete transformation of the SNT phase to the TS phase.

Silica speciation in solutions. As was mentioned above, the difference between the STOS and TS gels lies in the initial concentration of NaOH. In spite of that, both systems have the same Si species in the solution. Figure 2.7 shows typical Si-29 NMR spectra of the filtrates obtained from the starting gels and filtrates from the final products. The spectra of the starting filtrates show that only two types of species are present in the solution in both syntheses.

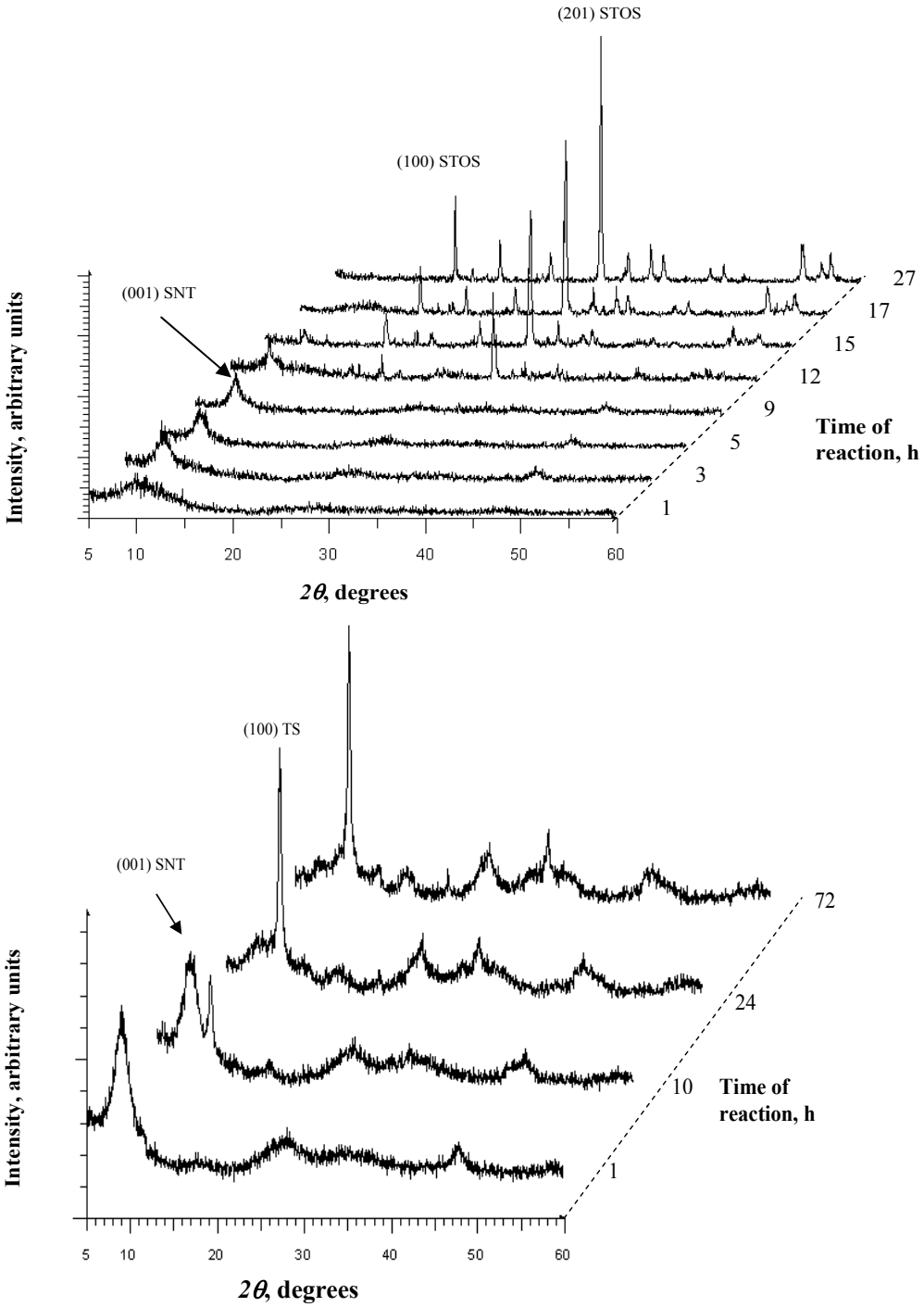

Figure 2.6. Dynamic XRD spectra of evolution of STOS phase (top) from gel of composition $1.0TiO_2$:$1.98SiO_2$:$10.53Na_2O$:$218H_2O$, T=200^o C and TS phase (bottom) from gel of composition $1.0TiO_2$:$1.98SiO_2$:$6.51Na_2O$:$250H_2O$, T=200^{0}C obtained in ex-situ experiments

The narrow, low field peak $(Q_0)^{\Upsilon}$ corresponds to monomeric silicate species, while the peak, denoted as Q_1 corresponds to end group Si atoms (i.e those, connected through oxygen to another silicon).[42] From the ratio of the peaks it is obvious that the relative amount of dimeric species is small, compared to the

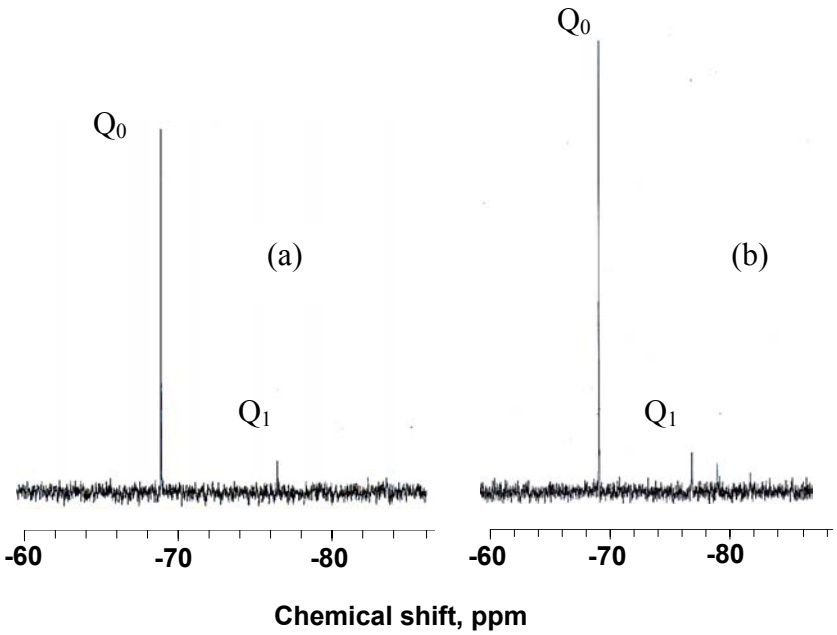

Figure 2.7. Si-29 NMR spectra of STOS (a) and TS (b) gel filtrates

monomeric species. The spectra of the final filtrates show that only monomeric silicate species are present in the solution. The NMR studies showed that there is no difference

$^{\Upsilon}$ The symbol Q was used to denote a tetrahedrally connected silicon atom to oxygen atoms. The superscript below represents the number of other Q-units attached to the silicon tetrahedron.

in Si speciation for these gels. No changes were observed in the spectra of the filtrates after 24 hours of crystallization.

3.2.3. Mechanism of crystallization

In situ X-ray powder diffraction studies provide a unique opportunity to follow the process of crystal growth and observe the formation of phases during the synthesis without gel alteration due to quenching and without the ambiguity from utilizing several vessels to monitor crystallization. The sequence of powder patterns collected as often as every 2 minutes. Based on such studies, combined with ex-situ experiments it is possible to suggest with a certain degree of confidence the mechanism of the reaction in this system. There are several steps that can be distinguished in the process of products crystallization. The first step is the formation of layered SNT ($Na_4Ti_9O_{20}$•xH_2O) phase which can be described by the reaction shown below. This reaction starts with hydrolysis of titanium (IV) isopropoxide at the stage of admixing of reagents:[43]

$$Ti(OR)_4+4H_2O \rightarrow Ti(OH)_4 + 4ROH \text{ (hydrolysis)}$$

$$9Ti(OH)_4 + 4NaOH + xH_2O \rightarrow Na_4Ti_9O_{20}.xH_2O \text{ (SNT formation)}$$

The second step is the diffusion of soluble silicate species towards the centers of nucleation sites, which in this case are the species of the SNT phase. We believe that the possible number of routes of the consequent reaction is limited to three, depending on the alkalinity of the gels. Route A is the transformation of the SNT phase to the STOS (Na_2TiSiO_5) phase while route B is the transformation of SNT to pure TS ($Na_2Ti_2O_3SiO_4.2H_2O$) phase. The other possibility, route C is the transformation of the SNT phase to a mixture of TS and STOS phases. The difference between these transformations is the amount of Si and Na consumed in the reaction. In the STOS phase the stoichiometric ratio of Ti/Si is 1:1, and in TS it is 2:1 which implies that in route A, twice as much Si is consumed compared to route B, when the same amount of titanium

was used. In the case of STOS the diffusion is more successful, since more silicate species were delivered to the centers of nucleation.

The structure of the SNT phase is unknown, although an idea has been posited. It was reported[14,40] that SNT is a layered compound whose interlayer spacing depends on its water content. The layers are most likely composed of titania octahedra, connected by Ti-O-Ti linkages. In the TS structure, titanium forms four atom clusters that are connected by silicon tetrahedra along the *a* and *b* axes, and by Ti-O-Ti linkages along the *c* direction. During transition from the SNT phase to the TS phase the titanium layers are required to regroup and form cubane-like clusters connected by silicate groups around the Na ions. The pieces of layers consisting of 2 Ti atoms may serve as building blocks for the titanium clusters. In the Ti_4O_4 cubane clusters the titanium atoms are present as octahedra sharing edges. Two of the six oxygens in each TiO_6 octahedron are silicate oxygens with each silicate group bonding to four Ti. Thus, the SNT layers, which have an O/Ti ration of 2.22, could break up into fragments under the influence of the SiO_4 groups into Ti_4O_8. Cubane units plus the four oxo-oxygens cross linked in the *xy* plane to form sheets. These sheets could come together to form the final framework structure by elimination of half of the oxo-groups. It is likely that under the influence of NaOH the oxo-groups would exist as hydroxo-groups. The sheets would have the composition $[(TiO)_4(OH)_4(SiO_4)_2]^{4-}$. These sheets could come together layer by layer condensing out two moles of water per unit to form the three-dimensional framework structure with sodium ions filling the framework cavity sites and the tunnels to balance the charge.

Obviously, STOS has a simpler structure than TS and is almost certainly the more thermodynamically stable compound. That is the reason it forms preferentially at higher temperatures and in more concentrated base solutions. Because the more complex TS is less stable thermodynamically it is more difficult to synthesize and can be done so in limited base concentrations and temperatures.

In the STOS crystallization process it is likely that higher NaOH concentration causes complete disintegration of the layers and the atoms arrange in a condensed

structure, in the simplest way, where each titanium polyhedra is linked to the silicon tetrahedra through oxygen. When the mixture of phases forms, a combination of processes occurs. The transformation starts with formation of the STOS phase, and once enough NaOH is consumed in the reaction of the STOS formation and the concentration decreases, the TS phase starts forming.

The main result of this study is the discovery of the route of TS crystallization. The fact that the SNT precedes the formation of the TS phase is of particular interest because SNT itself has the ability to remove strontium and actinides from highly alkaline media. In fact, the National Research Council referred to the utilization of SNT for strontium and actinides removal as "an appealing alternative from the standpoint of reliable sources". Furthermore, "… a range of possibilities can be considered – for example SNT could be used in an ion-exchange mode, either alone or in some combination with crystalline silicotitanate".[2] Being used for cesium removal, the TS phase when utilized in combination with SNT would remove both cesium, and strontium and the actinide fraction of liquid HLW. Besides, the mixtures of SNT and TS phases in different ratios can be synthesized from one precursor by modification of the hydrothermal treatment time which implies that both of the materials can be manufactured in one process, which would cut the expenses dramatically.

2.4. Conclusions

Studies of the crystallization of titanium silicate with sitinakite topology suggest the composition of the final product and its crystallinity depend on the sodium hydroxide concentration in the starting gels. The synthesis resulted in either pure TS phase, or a pure STOS phase, or mixtures depending on the hydroxide ion concentration in the starting gels. Higher concentrations conditions are more conducive for the formation of the Si-rich STOS phase with dense structure. The open framework TS phase formed at lower concentration, and the mixtures were formed in the intermediate region. We

believe that higher hydroxide concentrations provide better diffusion of silicate species to the SNT phase which precedes the silicates formation.

In-situ studies revealed the route of the TS crystallization and allowed us to optimize the conditions for synthesizing mixtures of SNT and TS phases with different ratios. The SNT phase is being considered as an alternative material for strontium and actinide removal phase in the process of liquid HLW remediation at Savannah River site. It was suggested that it might be possible to coat the TS particles used in the cesium ion-exchange process with strontium/actinide absorbing agent.[2] We believe that the SNT/TS combination product synthesized from one precursor is a promising material for combined actinides and cesium removal. Ion-exchange properties of this material will be discussed in Chapter VI.

CHAPTER III
OPTIMIZATION OF SODIUM TITANIUM SILICATE FOR STRONTIUM REMOVAL BY ALTERATION OF SYNTHETIC PROCEDURE

3.1. Introduction

In the late sixties and early seventies, Clearfield and coworkers published a series of papers concerning ion-exchange processes in zirconium phosphate.[44-46] The ion-exchange behavior of zirconium phosphates was correlated with the degree of crystallinity of the samples. It was found that the crystallinity of the ion-exchanger affected ion-exchange properties. In fact, the least crystalline exchanger exhibits the higher preference for cations (Na^+, Cs^+) in acidic media than in alkaline media. The highly crystalline exchangers exhibit the reverse behavior.[44]

Crystalline sodium titanium silicate (TS) is highly selective towards cesium in both basic and acidic solutions.[3,47] Inspired by the results of the earlier zirconium phosphate studies, we synthesized both amorphous and crystalline TS and compared ion-exchange properties in them. Since the Cs affinity has been studied previously,[48] we concentrated our effort on optimization of the TS for strontium removal by modification of the synthetic procedure. The reasons for the differences in the selectivities of amorphous and crystalline samples have been suggested.

3.2. Experimental methods

3.2.1. Synthetic procedures

Synthesis of highly Crystalline TS (C-TS). A total of 24 mL of dounly deionized (ddi) H_2O was added to 6.66 mL of $TiCl_4$ (Alfa Aesar) under constant stirring followed by addition of 40 mL of 30% H_2O_2, 150 mL of ddi H_2O and 40 mL of 10 M NaOH. Sodium silicate solution (4.3 g of $SiO_2 \bullet nH_2O$ in 200 mL of 1 M NaOH) was added as a last ingredient. The pH of the mixture was brought up from initial value (12.4) to 12.8 by dropwise addition of 10 M NaOH solution (4 mL). The mixture was sealed in a Teflon lined pressure vessels and heated for 10 days at 200 ^oC. The pressure vessel was taken out, cooled; the solid was separated by filtration, rinsed with ddi H_2O and ethanol, and dried in the oven at 55 ^oC (DM3-15-1).

Synthesis of Poorly crystalline TS (P-TS). A total of 4.39 mL of 40% colloidal silica (Ludox 40) was mixed with 8.7 mL of 10 M NaOH and 25 mL of ddi H_2O in a plastic beaker. To this mixture, 5.7 mL of Titanium isopropoxide (Alfa Aesar) was added. The mixture was stirred, sealed in a Teflon lined pressure vessel, and heated in the oven at 170^oC for 3.5 days. After reaction, the solid was treated similarly to case C-TS. The sample name is DM1-37-4.

3.2.2. Ion-exchange

pH titrations of H-forms of TS. Sodium forms of TS were converted to the hydrogen form by treatment with 0.1 M HCl solution and exhaustive washing with ddi H_2O to remove excess HCl.[48] Titrations were carried out by the batch method. About 50 mg of dry ion-exchanger were weighed out in polyethylene bottles and equilibrated with exact combination (10 mL) of 0.05 M ($SrCl_2$-$Sr(OH)_2$) solution for 5 days at ambient temperature. To avoid $SrCO_3$ precipitation strontium solutions were prepared using boiled ddi H_2O under nitrogen flow. Base to salt ratio in the strontium solution varied

from bottle to bottle to ensure a progressive increase of the equilibrium pH. After equilibrium was attained (5 days) solutions were filtered off and the Sr concentration (C_{eq}) was analyzed by atomic absorption spectroscopy (AAS) and the pH of the solutions were measured using an Ion Analyzer 250 with glass electrode. Uptake (U) of strontium was calculated by equation 3.1:

$$U = \frac{(C_{in} - C_{eq}) \times V}{m}, \tag{3.1}$$

where C_{in} – initial concentration of Sr in the solution, C_{eq} – equilibrium concentration of Sr in the solution, V, m – volume of the solution and mass of the ion-exchanger, respectively.

Distribution coefficients measurements. As a part of this study we assessed ion-exchange properties through measurement of ^{89}Sr distribution coefficients in a ground water simulated solution utilizing the batch technique. The simulant having composition 0.0025 M KNO_3, 0.04 M $NaNO_3$, 0.0075 M $Ca(NO_3)_2.4H_2O$, was traced with the ^{89}Sr isotope. About 40 mg of dry ion exchanger in sodium form was equilibrated with 10 mL of the solution at ambient temperature in 25 mL polyethylene vials for various periods of time, ranging from 6 minutes to 24 hours. Solutions were filtered through an Acrodisk LC 13 mm Syringe Filter with 0.2 μm PVDF (polyvinylidene fluoride) membrane. Filtrates were counted on a Wallac 1450 liquid scintillation counter (LSC) for ^{89}Sr content. The values of distribution constants (K_d, mL/g) and recovery (R, %) of the nuclide were calculated for each point of time using the following equations:

$$K_d = \frac{A_0 - A_t}{A_t} \times \frac{10}{m} \tag{3.2}$$

and

$$R = \frac{A_0 - A_t}{A_0} \times 100\%, \tag{3.3}$$

where

A_0 – initial count rate of the solution, cpm/mL; and

A_t - final count rate of the solution , cpm/mL

Assessment of ion-exchange properties in nuclear waste simulant solutions. The composition of the simulant prepared for this experiment is shown in Table 3.1.

Table 3.1. Simulant Composition

Species	NaOH	$NaNO_3$	$NaAl(OH)_4$	$NaNO_2$	Na_2SO_4	Na_2CO_3	Sr
C, mol/L	1.33	2.6	0.0429	0.134	0.521	0.026	603 μg/L

The simulant solution was traced with radioactive strontium, so that the count rate would be about 4000-5000 cpm/mL. One hundred milliliters of such solution was introduced to 40 mg of dry ion-exchanger in a 250 mL plastic bottle. The suspension was sampled after appropriate periods of time to assess the kinetics of Sr removal. The sampled suspension was filtered and the filtrate was counted on a LSC. The concentration of strontium at time *t* concentration (C_t) was calculated using equation:

$$C_t = \frac{A_t}{A_{in}} \times C_{in}, \tag{3.4}$$

where

A_t –count rate at time *t*, A_{in} – initial count rate and C_{in} – initial concentration of nonradioactive strontium.

3.2.3. Surface area measurements

The surface area of the samples was determined by adsorption of nitrogen. Sorption-desorption isotherms were obtained with a Quantachrome Autosorb-6 automated N_2 gas adsorption unit. The samples (0.2-0.6 g) were preheated at temperatures specified later on the Quantachrome degasser at the pressure of 2×10^{-3} Torr. The isotherms were collected at 77 K and analyzed by the BET method. The micropore volume was determined by the DeBoer t-plot method, and the micropore distribution was calculated by the MP method.

3.3. Results

3.3.1. Synthesis

X-ray powder patterns of both amorphous and crystalline samples are shown in Figure 3.1. As can be seen for the figure the powder pattern of P-TS resembles that of C-TS in terms of peaks positions. The reflections of the P-TS pattern have higher values of Full Width at Half Maximum (FWHM) which is a measure of the crystallinity of the product. The conditions for synthesis were set up according to the results of our studies on optimization described in Chapter II. In particular, in the case of C-TS, the initial NaOH concentration was set up below 2.0 M (1.4 M) to ensure complete absence of the STOS phase. The high crystallinity was achieved through amplified time of the hydrothermal (10 days) reaction. In the case of P-TS the concentration of hydroxide ion was set up to 1.98 M; and the time and temperature of the reaction were less aggressive compared to the C-TS (see experimental part).

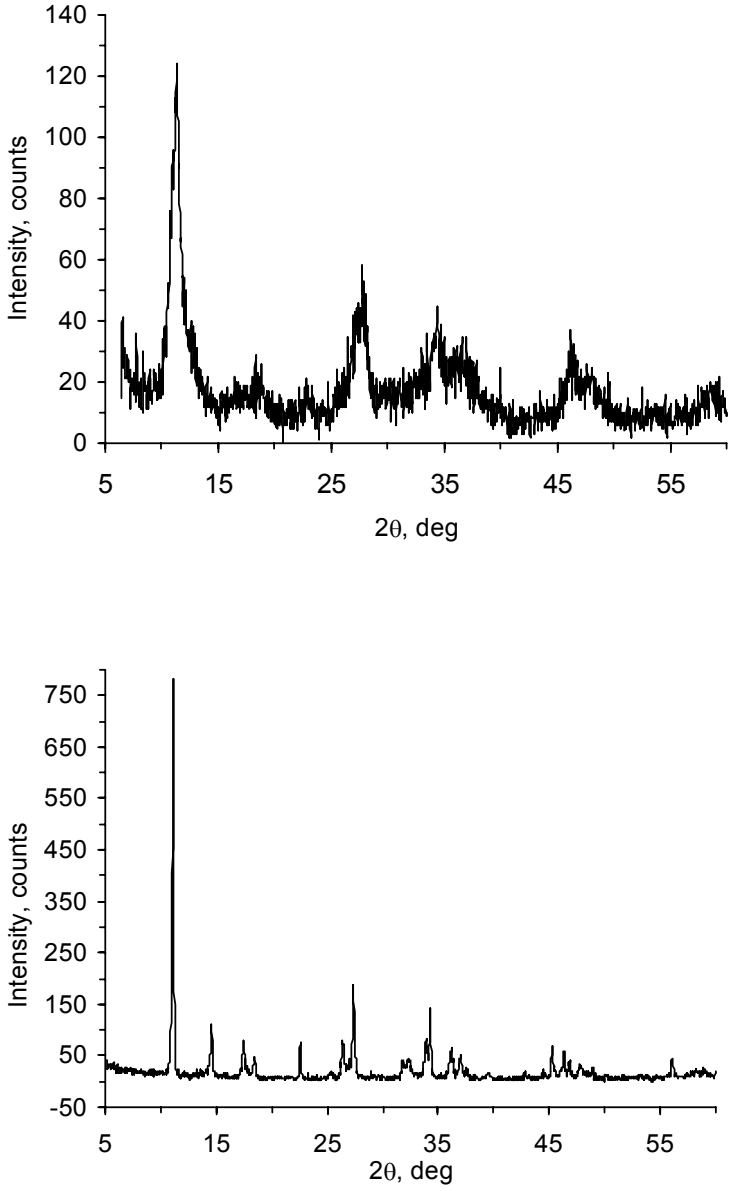

Figure 3.1. X-ray powder pattern of sodium forms of poorly crystalline P-TS (top) and highly crystalline C-TS (bottom)

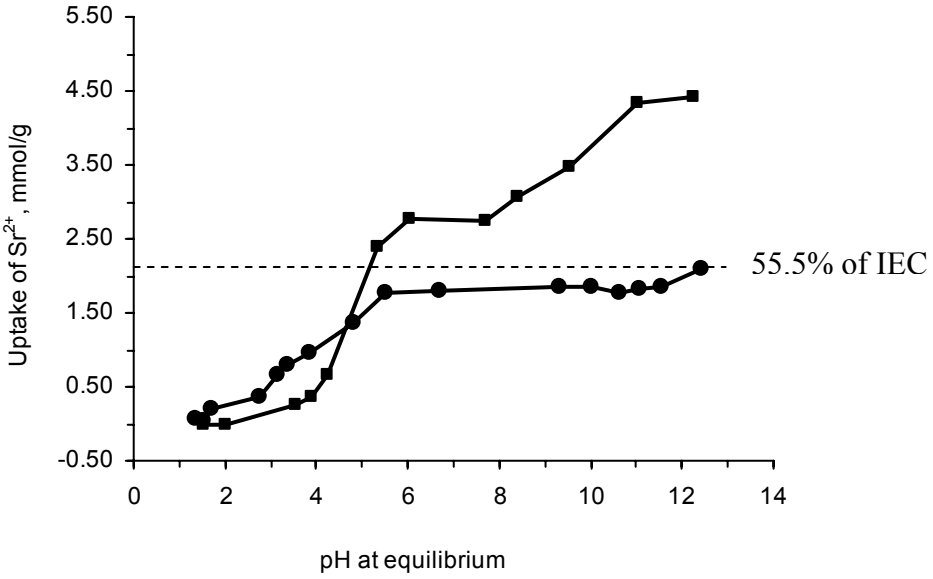

Figure 3.2. Potentiometric titration curves of highly crystalline (● C-TS) and poorly crystalline (■ P-TS) phases of $H_2Ti_2O_3SiO_4 \bullet 1.5H_2O$. Titrant: 0.05 M ($SrCl_2$-$Sr(OH)_2$). To achieve values of pH below 3 a 0.1 M HCl solution was used

3.3.2. Ion-exchange studies

Potentiometric titrations. The strontium potentiometric titration curves for H-forms of both phases are shown in Figure 3.2. The P-TS exchanger exhibited better selectivity for strontium at pH higher than 5 than the C-TS phase. However, the selectivities are just the opposite over the region of lower pH. The chemical formula $H_2Ti_2O_3SiO_4 \bullet 1.5H_2O$ was assumed for both samples based on previous studies.[47]

According to this formula the theoretical ion-exchange capacity (IEC) of the TS is 7.55 mequiv/g which is equivalent to 3.78 mmol/g for doubly charged cations. The ion-exchange behavior is different in the phases of different crystallinity. In the case of the P-TS sample the uptake values steeply increase over the region of pH from 4 to 6 followed by moderate increase over the region of higher pH values.

The maximum capacity achieved in the P-TS phase is about 4.4 mmol/g, which corresponds to 116% of theoretical capacity and almost triple of the capacity of the highly crystalline phase. In the acidic region the ion-exchange behavior of the phases is the opposite of that at the higher pH. A negligible amount of Sr was exchanged in the poorly crystalline sample whereas the highly crystalline phase performed somewhat better taking up 0.2 mmol/g of Sr at pH=1.7. The two curves intersect at pH=5 indicating that the selectivities are reversed for acidic and neutral to alkaline regions for the two phases.

Sr removal from groundwater simulant. The ^{89}Sr distribution constants obtained in the ground water simulant, containing 0.0025 M K^+, 0.04 M Na^+, 0.0075 M Ca^{2+}, are plotted in Figure 3.3 for both phases against time of agitation. As can be seen from the curve the P-TS phase exhibited better removal rate than the C-TS phase. In fact, after 120 min the strontium K_d value reached 25000 mL/g for the P-TS phase removing 98% of the radioactivity and only 2500 mL/g for C-TS which corresponds to 90% of recovered activity. After 2 hours of agitation the C-TS phase continued removing strontium and, eventually, the distribution constant reached a value of 25918 mL/g in 24 hours. No significant difference was observed in the recovery values for both samples

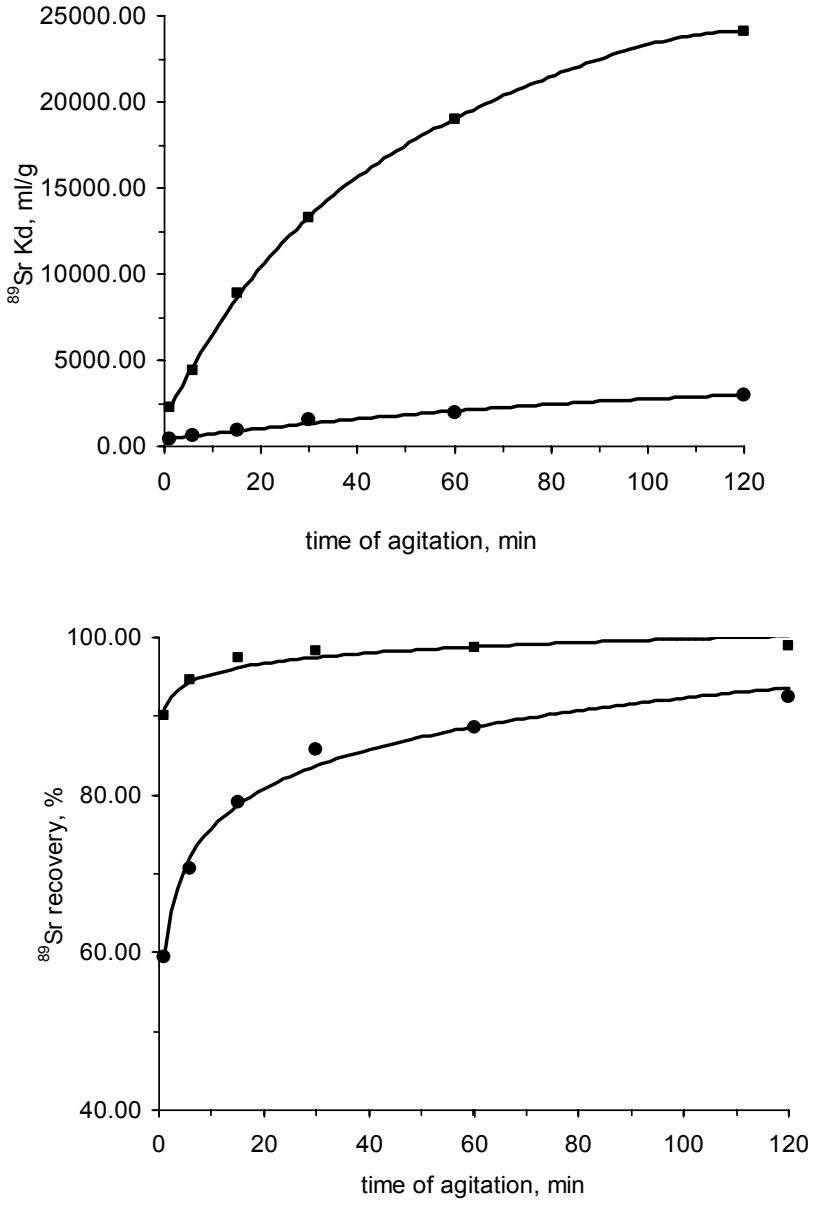

Figure 3.3. K_d values (top) and recovery of Sr-89 (bottom) from groundwater simulant as a function of time of agitation with C-TS (●) and P-TS (■) phase

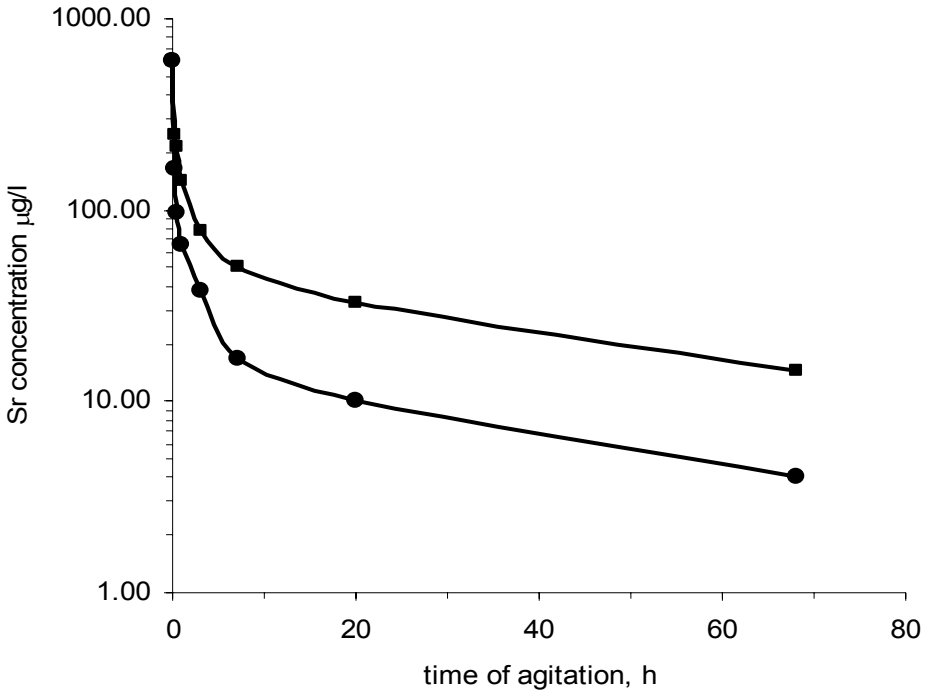

Figure 3.4. Kinetics of Sr removal from radioactive waste simulant by H-forms of poorly (● - P-TS) and highly (-■- -C-TS) crystalline phases of TS

after 24 hours of agitation. Since the strontium was present in trace amounts both phases were exchanged below the capacity limit. The kinetics of the removal was quite different, with the P-TS phase being more efficient. The reasons for such a behavior are provided in the discussion.

Sr removal from radioactive waste simulant. Unlike the ground water simulant, the radwaste simulated solution contains a significant amount of strontium. The decrease in concentration was quantified using trace amounts of ^{90}Sr. Figure 3.4 shows the plot of strontium concentration, remaining in the solution after agitation with the ion-exchanger in proton form, plotted against the time of agitation. Similarly to the experiment with the ground water simulant the P-TS phase behaved better. Besides faster kinetics it exhibited higher strontium capacity. After 30 minutes of agitation the concentration of Sr in the solution, treated with P-TS dropped from 600 μg/L to 96 μg/L, whereas the concentration of the solution treated with C-TS decreased only to 215 μg/L.

The rate of strontium removal became the same for both phases after 20 hours of shaking, which can be concluded from the parallel nature of the last section of the curves represented in Figure 3.4.

3.3.3. Morphology Characterization

Surface area measurements. TGA analysis of the H-form of the phases indicated that both C-TS and P-TS samples stopped losing weight at the temperature of 210^{o} C (Figure 3.5). X-ray diffraction powder patterns of the residues showed that the structure of the H-form collapses at these temperatures. Therefore, for indicative surface area measurements both phases were outgassed at lower temperature (150^{o} C) to remove water molecules attached to the surface. We believe that under such conditions the coordinated water molecules are being removed from the tunnels and the structure is not being destroyed. The XRD powder pattern revealed that only slight amorphization of the highly crystalline material occurred. The results of surface area measurements are summarized in Table 3.2. The Brunauer, Emmett, and Teller (BET) surface area of P-TS

phase calcined at 150°C is almost twice that of the C-TS phase. The contribution of microporous part in the C-TS phase is 13% which is due to the surface within the tunnels. The P-TS phase does not make any microporous contribution in the total surface area. When the samples were calcined at 210°C the surface area of the C-TS phase was only due to macropores and resulted in a value of 8 m^2/g. This indicates that the structure has collapsed and the tunnels no longer existed. The SA of the P-TS phase preheated at 210°C remains the same within experimental error, which means that its nature cannot be attributed to the phase structure.

Table 3.2. Surface Area (SA) in m^2/g of the P-TS and C-TS Phases Calcined at Different Temperatures

	Calcination temperature			
	150° C		210° C	
	BET SA	Microporous SA	BET SA	Microporous SA
P-TS	196.00	0.00	205.00	0.00
C-TS	85.70	11.10	8.43	0.00

Adsorption-desorption isotherms for both phases are shown in Figure 3.5 b,c. For the C-TS phase the isotherm of the sample calcined at 210°C shifted down compared to the position of the isotherm for the sample calcined at 150°C showing almost negligible nitrogen adsorption. No change in isotherm shape was observed both in the case of P-TS and C-TS phases as the temperature of calcination increased. According to IUPAC classification the isotherm of the P-TS phase is a type III isotherm, which is typical for nonporous or macroporous materials (pore diameter > 50 nm) whereas the isotherm of C-TS is of type I, which is usual for microporous materials (pores diameter < 2 nm).[49,50]

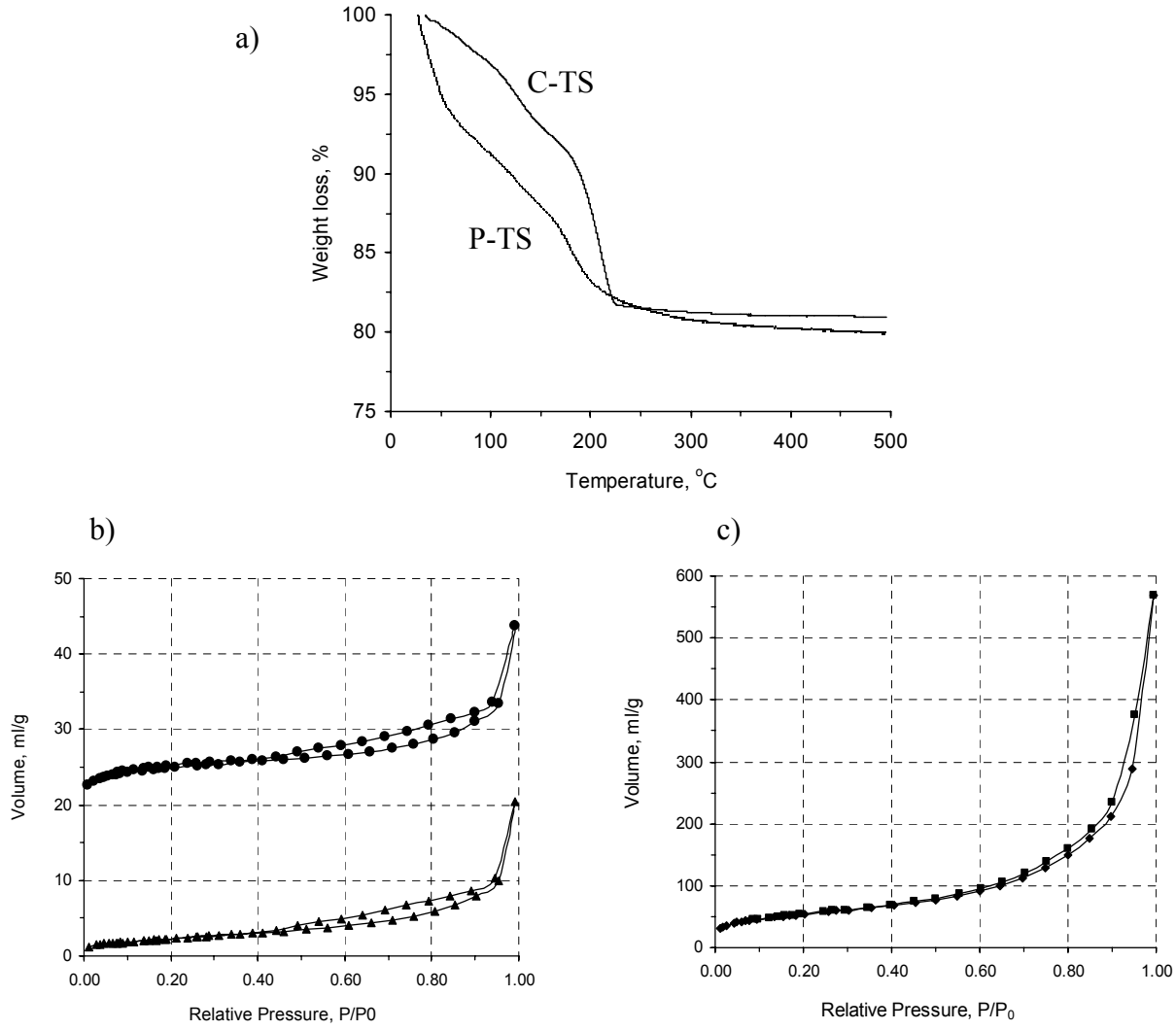

Figure 3.5. TGA curves (a), nitrogen adsorption-desorption isotherms of the C-TS phase (b) calcined at 150°C and 210°C and the P-TS phase (c) calcined at 150°C

a)

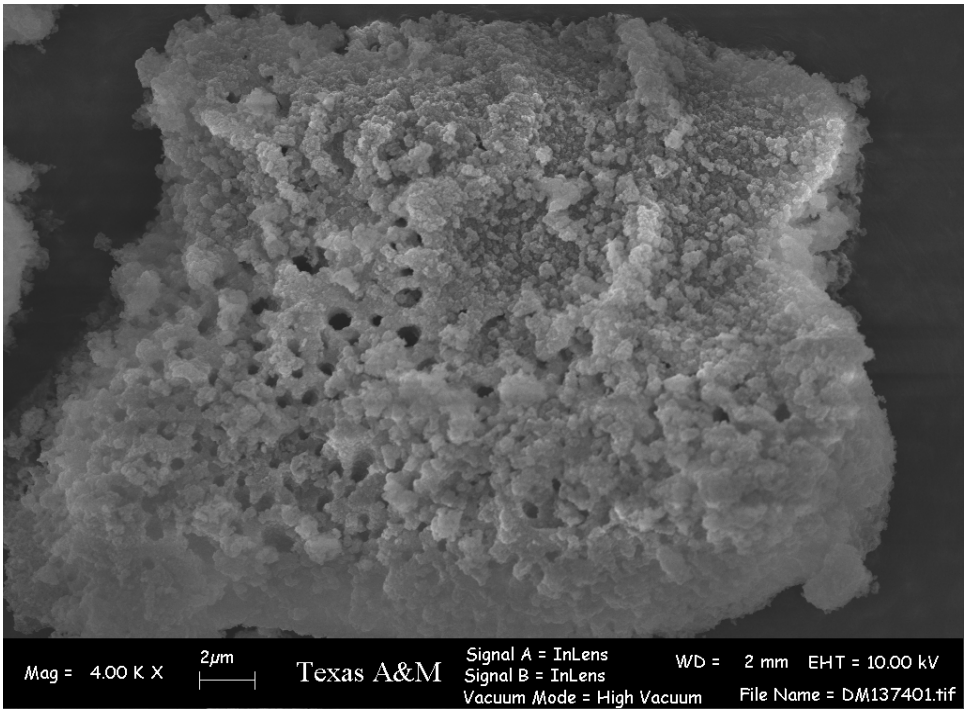

b)

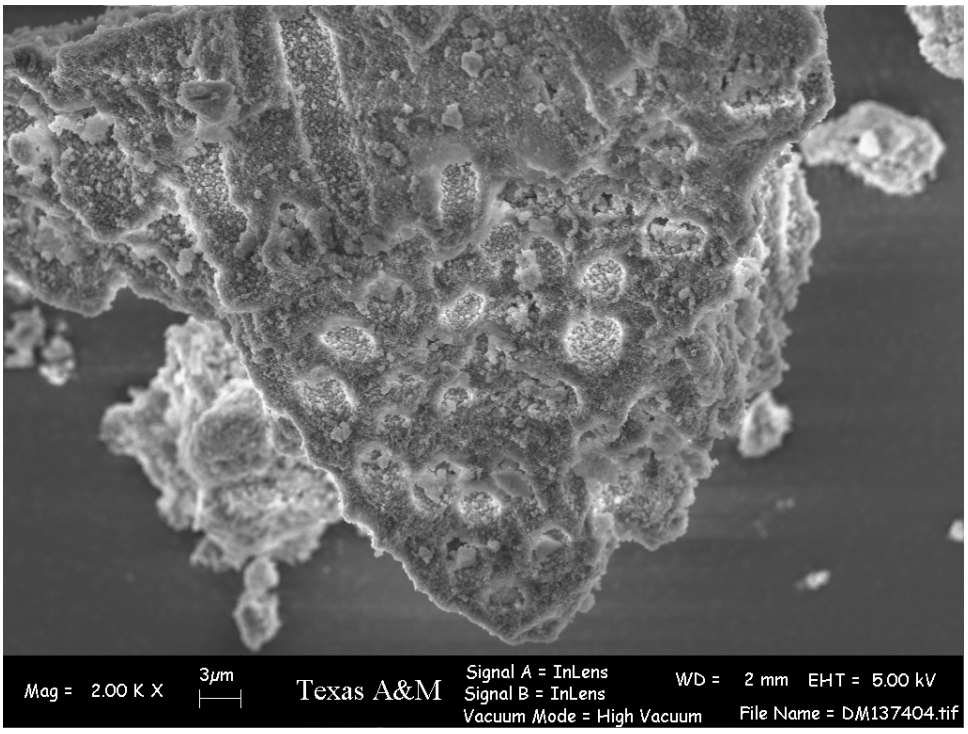

Figure 3.6. SEM images of P-TS (a, b) and C-TS (c) phases of the TS.

c)

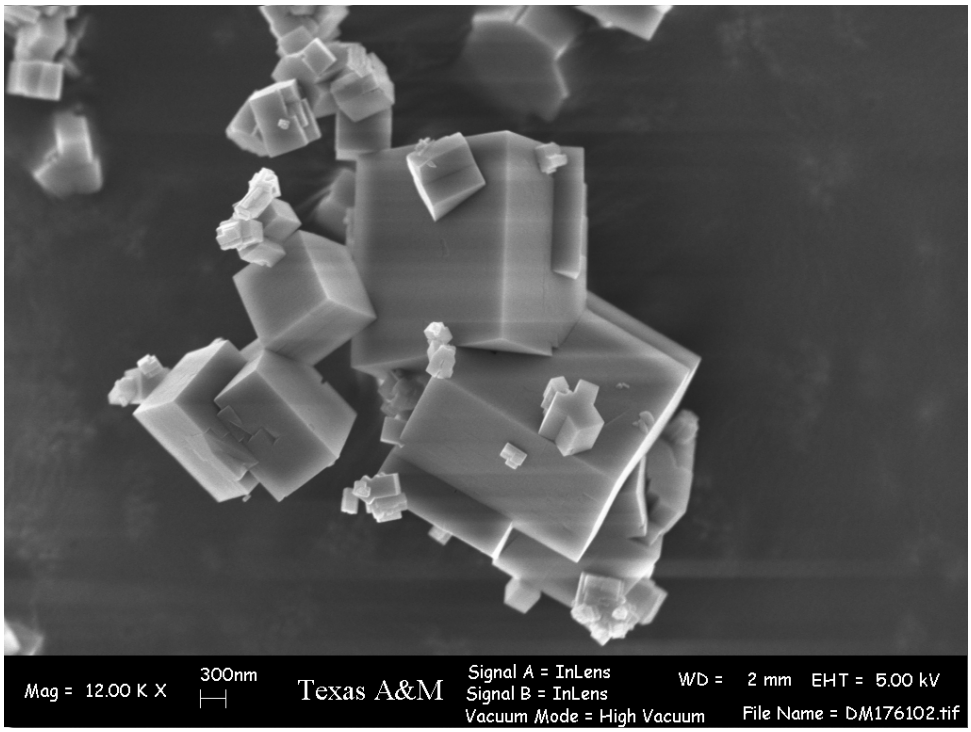

Figure 3.6. (Continued).

The upward curvature of the isotherm at higher pressure corresponds to adsorption of the nitrogen in the cavities, formed by neighboring particles.

Scanning electron microscopy. Scanning electron microscopy (SEM) of the C-TS phase revealed crystalline tetragonal-shaped particles with sizes ranging from 0.25 to 3 μm (Figure 3.6a). The SEM image of the P-TS phase suggests that the material consists of large agglomerates with a size reaching several microns (Figure 3.6 b,c) The large particles however, appeared as though they consist of small undeveloped crystallites glued to each other. The particles are arranged so that they form pores streaming through the agglomerates. There is no regularity in these pores. The diameter

of the pores is ranging from 1 to 3 microns, which allows us to classify them as macropores. The existence of pores of this size in P-TS was also suggestive through the adsorption isotherm.

3.4. Discussion

In order to tune the ion-exchange properties of TS we prepared a less crystalline sample based on the prior studies on the effects of crystallinity on ion-exchange properties of zirconium phosphate. Generally speaking the poorly crystalline TS phase exhibited faster removal kinetics for and higher ion-exchange capacity. The reasons for such a difference between the two phases can be explained from structural and morphological perspectives.

The structure of C-TS was described elsewhere.[13,47] The tunnel framework consists of repeating cubane-type clusters of edge sharing titanium octahedra connected through Ti-O-Ti linkages along the c-axis and sharing corners with silicon tetrahedra in the a and b directions. In the fully exchanged sodium form half of the sodium ions occupy framework sites with another half filling the tunnels.[13,47]

The framework of the acid form is completely free of the cations and is protonated; the tunnels are filled with water molecules disordered over several positions.

Crystallographic studies of the fully exchanged strontium samples revealed that it consists of a mixture of tetragonal (82%) and orthorhombic (18%) phases.[51] The tetragonal phase has strontium at 61% of theoretical capacity and $Sr_{0.61}H_{0.78}Ti_2O_3SiO_4 \bullet 2.2H_2O$ formula, whereas the orthorhombic phase with composition $Sr_{0.25}H_{1.5}Ti_2O_3SiO_4 \bullet 2.2H_2O$ has 25% of Sr. Thus, the total amount of strontium loaded in the sample is 54.5% of theoretical capacity which almost exactly corresponds to the maximum uptake value (55.5%) obtained by potentiometric titration (Figure 3.2). In the orthorhombic (26%) phase strontium occupies positions at (½ 0.1 ½) with occupancy factor of 0.5 and is coordinated to 5 water molecules and 5 framework oxygens. The strontium in this position is disordered with water molecules which mean that on average

half of the unit cells have strontium, half have water molecules. This site is being filled until the pH is about 4 and the uptake value at this point corresponds to 25% of IEC on the titration curve. However, the share of this phase in the fully exchanged sample is only 18%. This means that additional strontium ions are being exchanged not only in the unit cells with water molecules at (½ 0.1 ½) but also in unit cells where strontium occupies this position. The ions are being moved from (½ 0.1 ½) to the positions at (0.36 0 0) or (0.92 ½ 0) where their coordination number varies from 7 to 10. With that the transformation from orthorhombic to tetragonal phase occurs.

The sodium forms of TS were used in the experiments with groundwater simulant. Since a relatively small amount of electrolytes is present in the solution, the sodium ions are being hydrolyzed out from the tunnel. Apparently, strontium has no complication in arranging itself inside the tunnel. We believe that the coordination of strontium in this case corresponds to the one in the orthorhombic phase, described above.

The H-form of the TS phases was used with the radioactive waste simulant for two reasons. First, the protons liberated from the ion-exchanger would combine with hydroxide ions to form water which would drive the ion-exchange reaction. Second, the sodium ions from the solution would first attack framework sites letting strontium enter the channels.

The same reasoning is not compelling for the poorly crystalline phase. Though a limited amount of information can be obtained about the ion-exchange processes in amorphous materials since the structural tools are not applicable, some data can be acquired using other techniques. It is obvious from surface area and an SEM results that in the P-TS phase the tunnels are not developed. The macropores that can be seen on the SEM photograph exceed the cations in size and the cations cannot be trapped there. We believe that the cations bond to the surface Ti or/and Si polyhedra through oxygens. The water molecules arrange themselves around cations, sticking from the surface resulting in the whole assembly being loosely bonded ("hanging") compared to the 10 coordinate complex in highly crystalline material. A somewhat disordered and chaotic arrangement

of Ti and Si polyhedra on the surface provides more opportunities for cations to attach resulting in higher ion-exchange capacity in alkaline media. In acidic media the surface of P-TS became easily protonated and strontium is not being picked up (Figure 3.2) .In the case of C-TS the bonds are stronger and the affinity towards strontium is higher.

Faster kinetics of ion-exchange in the P-TS phase is also justified in terms of above considerations. In the C-TS phase strontium ions have to diffuse towards the site at (½ 0.1 ½) whereas in P-TS the ions are located on the surface. The diffusion within the macropores is not a concern since their size is much bigger, compared to the size of cations.

3.5. Conclusion

In this section we discussed synthesis and ion-exchange properties towards strontium of poorly and highly crystalline phases of sodium titanium silicate with sitinakite topology. The poorly crystalline phase exhibited higher ion-exchange capacity in alkaline media and faster kinetics of strontium removal both in groundwater and radioactive waste simulant. The differences in properties are due to major dissimilarities in mechanisms of ion-exchange in the phases. In the case of the highly crystalline phase the ions arrange themselves within the channels bonding both to framework oxygens and water molecules. In the poorly crystalline phase the tunnels are not developed and the ions are being picked up on the surface resulting in uptake values exceeding theoretical ion-exchange capacity. This investigation suggests that the poorly crystalline phase of TS in H-form is a promising candidate for strontium removal from alkaline solutions.

CHAPTER IV
IMPROVED CESIUM SELECTIVITY WITH ISOMORPHOUS FRAMEWORK SUBSTITUTION IN TITANOSILICATE WITH SITINAKITE TOPOLOGY**

4.1. Introduction

The incorporation of a heteroatom in the framework of the compound is an extremely important process because it can modify the properties without changing the structure of the parent phase. A considerable amount of work has been done on substitution in zeolite frameworks by direct synthesis.[52-56] In fact, the use of the elements other than Si/Al in zeolite synthesis led to the discovery of numerous metallosilicates containing titanium, vanadium, boron, niobium, zirconium and etc. A successful substitution of silicon with phosphorus, germanium, and boron was also achieved. The insertion of heteroatoms in the framework results in either known structures identical to the alumosilicate analogues or in novel compounds.

Significant efforts were expanded in the area of substitutions in microporous titanosilicates – a relatively new family of zeotype materials. Rocha and coworkers synthesized and characterized a series of microporous analogs of the mineral nenadkevichite, with Ti/Nb molar ratios ranging from 0.8 to 17.1 - substituted derivatives of ETS-4 titanosilicate.[57] Another titanium silicate, ETS-10 (Engelhard Titanium Silicate), was modified by introduction of aluminum and gallium into tetrahedral silicon sites to improve the acidity of the material.[23] In 1990 Chapman and Roe[17] prepared a novel microporous Ti silicate - a structural analog of the naturally occurring mineral pharmacosiderite with composition of $K_3[Fe_4(OH)_4\ (AsO_4)_3]\bullet 5H_2O$.

**Part of the data reported in this Chapter is reprinted from Journal of Solid State Chemistry, Vol 175, A. Tripathi, D.G. Medvedev, M. Nyman, A. Clearfield, *Selectivity for Cs and Sr in Nb-substituted titanosilicate with sitinakite topology*, pp 72-83, 2003, with permission from Elsevier.

Behrens et al[58] further synthesized mixed Ti/Ge-Ge/Si molecular sieves with pharmacosiderite topology with Ge both in octahedral (titanium) and tetrahedral (silicon) sites.

The choice of the "guest" atoms for substitution is often inspired by nature. That is the case with the titanium silicate sitinakite (TS) which is one of the materials of interest in this dissertation. Its natural analog with composition of $(Na_{2.251}K_{0.693}Ca_{0.004}Sr_{0.062}Ba_{0.026}Ce_{0.004})(Ti_{3.816}Nb_{0.195}Fe_{0.014}Zr_{0.006})Si_{1.928}O_{13}(O_{0.045}H_{0.455})\bullet 3.7H_2O$ was found in the Khibiny alkaline massif, Kola Peninsula, USSR.[11] Clearfield and coworkers reported the ideal formula $Na_2Ti_2O_3SiO_4\bullet 2H_2O$ and structure of this material solved from powder by ab-initio methods.[59] The structure of this material was described previously in the text (see Chapter I, pp. 8-9). As can be seen from the composition of the naturally occurring mineral about 5% of titanium is substituted with Nb atoms. Anthony et al[60] showed that a silicotitanate (TAM 5) has remarkable Cs removal capabilities with Nb/Ti = 0.4. However, the structural and chemical reason for enhanced selectivity has never been found. Recently, Luca and coworkers[27] postulated multiple cesium environments in the Nb-doped and Nb-free phases based on the results of ^{133}Cs NMR studies. It was stated that "different cesium environments are clearly dependent on the amount of water in the channels. …further experiments are needed to more clearly define the water structure in Cs^+ exchanged sitinakite channels...".[27]

The work presented in this chapter was carried out to pinpoint the different hydration water environments of Cs^+ and Sr^{2+} ions that influence the selectivity upon Nb^v substitution in TS. To accomplish this, a 25% Nb substituted sample with the composition of $Na_{1.3}H_{0.2}Nb_{0.5}Ti_{1.5}O_3SiO_4\cdot 2H_2O$ (Nb-TS) was synthesized and the Cs and Sr exchanged forms were studied using Retvield refinement. The coordination of cesium and strontium in the framework was determined and correlated with ion-exchange behavior of the phases in various simulated solutions.

4.2. Experimental methods

4.2.1. Synthetic procedures

A crystalline titanium silicate (TS) was synthesized by a hydrothermal reaction similar to that for C-TS described in Chapter III.

A 25% Nb-substituted titanium silicate (Nb-TS) was synthesized by a modified procedure reported previously by Poojary et al.[47] Two modifications have been made. First, $TiCl_4$ was replaced by titanium isopropoxide ($Ti(OC_3H_7)_4$), and second, the amount of silica was increased three-fold. Furthermore, 25 mol% of titanium was replaced by niobium utilized in the form of $NbCl_5$. In general, 1.3 g of titanium isopropoxide was mixed with 0.405 g of $NbCl_5$ in 10 mL of ddi H_2O followed by addition of 4 mL of 30% H_2O_2 and 8 mL of 10 M NaOH. A solution of 1.26 g of $SiO_2 \bullet nH_2O$ (Fisher) in 20 mL of 3M NaOH was added as a last step. The mixture was stirred, sealed in a Teflon lined pressure vessel and heated at 200^oC for 10 days. A highly crystalline white powder was separated by filtration, rinsed with water and ethanol, and dried in an oven at 60^oC for 24 hours.

4.2.2. Ion exchange

Preparation of Sr^{2+} and Cs^+ exchanged samples. Strontium and cesium exchange in Nb-TS was performed in a similar fashion. A total of 400 mg of dried sample was equilibrated with 100 mL of 0.025 M solution of $SrCl_2$ for 12 hours. The solid was separated by filtration, rinsed with ethanol and dried in an oven for 12 hours at 60 ^oC. An exact amount of dry sample was dissolved in HF and the solution was analyzed for Sr and using Atomic-Absorption (AA) spectroscopy. The calculated composition, $Sr_{0.19}Na_{0.61}HNb_{0.5}Ti_{1.5}O_3SiO_4 \cdot H_2O$, determined using AA spectroscopy, TGA and charge neutrality, closely matched the composition obtained by X-ray diffraction analysis.

Due to the collaborative nature of this work, Nb-TS in Na-form and cesium exchanged samples of Nb-TS were supplied by Sandia National Laboratory and used "as is". A series of Cs-exchanged Nb-TS materials were prepared by ion exchange. For each ion exchange, 3 g of Nb-TS was combined with 50 mL of an aqueous CsCl solution, containing the appropriate amount of CsCl to obtain a Cs-exchange with the Nb-TS sample with 3.8, 6.4, 9.0 and 9.6 wt % cesium. The Nb-TS samples were shaken with the CsCl solutions at room temperature for 12 hours, and the Cs-exchanged samples were collected by filtration. Inductively Coupled Plasma Mass Spectroscopy (ICP MS) was used for compositional analysis of these Cs-exchanged Nb-TS materials. Powder X-ray diffraction was used to examine phase identification, purity and crystallinity, and thermogravimetric analysis (TGA) was used to determine water content.

Absorption measurements of Sr^{2+} and Cs^{+} in the presence of $NaNO_3$. In the present study we determined uptake of Sr^{2+} and Cs^{+} from the solutions having different Na^{+} concentrations. To simulate the concentrations of the actual nuclear wastes, we prepared solutions using non-radioactive metals with concentrations high enough to make the ion-exchangers saturated to their maximum capacity by the target ion. In particular, we prepared 5 solutions with 340-350 ppm of Sr^{2+} and 5 solutions with 630-770 ppm of Cs^{+}. The sodium ion concentrations were 0, 0.5, 1.0, 2.5 and 5.0 M. The exchange was carried out for 24 hours as described above. Amounts of Sr^{2+} and Cs^{+} in solutions were analyzed by AA spectroscopy and the pHs of the solutions were measured using an Ion Analyzer 250 with glass electrode. Uptake (meq/g) of the cations was calculated using equation 3.1, Chapter III

Kinetic studies. Kinetics of the removal of ^{89}Sr and ^{137}Cs from radioactive waste solutions was examined using the radioactive tracer method. Solutions were prepared by dissolving appropriate amounts of $NaNO_3$ and NaOH in ddi H_2O to give 4.27 M NaCl and 1.33M NaOH and then spiked by either the ^{137}Cs or the ^{89}Sr. Solids were batch-equilibrated with the solutions as described above during various periods of time. Cs-137 and Sr-89 in the filtrates were measured using a Wallac 1450 liquid scintillation counter

(LSC). Recovery, R, of the nuclide at each point of time was calculated using equation 3.3, Chapter III.

Assessment of ion exchange properties of the materials in nuclear waste type solutions. To assess the behavior of the ion-exchangers in nuclear wastes solutions, distribution constants (K_d) for ^{137}Cs and ^{89}Sr were determined in alkaline simulants with various Na^+ contents. Two sets (6 solutions each) were prepared for Sr and Cs series. Each of the solutions in the Cs and Sr set was spiked with ^{137}Cs and ^{89}Sr, respectively. The specific activity of the solutions was about 500-600 cps/mL. All solutions were 1M in NaOH and 0 to 4.5 M in $NaNO_3$. The equilibrating time was 24 hours. Filtrates were counted on a LSC. K_d values in mL/g were calculated using equation 3.2, Chapter III

4.2.3. X-ray powder diffraction data collection, structure solution, and Rietveld refinement

X-ray powder data were collected for six phases. The samples were packed into a flat plastic holder and the data were collected using a Bruker-D8 advanced computer-automated X-ray diffractometer. The X-ray source was a sealed tube operating at 40 kV and 40 mA with a copper target. Data were collected at room temperature between 8.5 and 85^o in 2θ with a step size of 0.02^o and a count time of 60 s/step. The powder patterns were indexed using the program NTREOR incorporated in the program EXPO. The solution, which indexed all peaks, corresponded to a tetragonal cell with cell parameters close to $a \sim 7.83$ Å and $c \sim 11.94$ Å in all the cases. The systematic absences were consistent with the space group $P4_2/mcm$, previously reported for TS.

Each data set was treated individually, using the same general procedure described below. The data were analyzed using the Rietveld technique. Atomic positions reported for the framework atoms of TS were used to model and refine the framework cations of all Nb-TSs. The individual site occupancies for the disordered framework Nb^V and Ti^{IV} atoms were set equal to the ratio determined from the ICP-MS analysis (1/3) and their sum was constrained to a value equal to 1. The positions of the Cs^+, Na^+, Sr^{2+}

ions and water molecules in each of the structures were obtained by difference Fourier maps, followed by Rietveld refinement of the full patterns.

4.3. Results

4.3.1. Structure of Nb substituted phases

Crystallographic parameters for the Nb-TS, three cesium loaded phases and strontium phase are summarized in Table 4.1. The chemical formulas for each phase are shown in Table 4.2. Fractional atomic coordinates and occupancy factors are presented in Tables 4.3-4.7. Table 4.8 contains information on interatomic distances for the Cs and Sr loaded phases.

The powder patterns of Nb-TS and its cesium and strontium forms were similar to those reported for non-substituted TS.[13] The space group does not change upon Nb-substitution, or upon cesium cation exchange. All 5 phases were successfully refined in the $P4_2/mcm$ space group reported previously for TS. The solution corresponded to a tetragonal cell with parameters close to a=7.83 Å and c=11.94 Å. Although the overall framework structure of Nb-TS and its exchanged forms are not much different from the parent TS phase, some differences in ion positioning inside the channels take place. The parent compound is briefly described below. The structure consists of Ti octahedra occurring in clusters of four and sharing edges to form a cubane like unit. The clusters are connected to each other along the *a* and *b* axes by silicate tetrahedra whose oxygen atoms form part of the cluster. The unit cell is tetragonal with $a \approx 7.8$ Å and $c \approx 12.0$ Å. Along the *c* axis the titania- clusters are connected through oxo-bridging. This arrangement forms a framework enclosing a one-dimensional tunnel parallel to the c-axis direction. There are two crystallographic positions for the eight Na^+ ions in the unit cell. Half of the sodium ions reside within the framework at (0, 1/2, 1/2) bonded to four silicate oxygen atoms and two water molecules.

Table 4.1. Crystallographic Parameters for Different Titanosilicate Phases

	Nb-TS	Cs1-Nb-TS	Cs2-Nb-TS	Cs3-Nb-TS	Sr-Nb-TS
Pattern range (2θ), ^{o}	8.5-85	8.5-85	8.5-85	8.5-85	8.5-85
Space group	$P4_2/mcm$	$P4_2/mcm$	$P4_2/mcm$	$P4_2/mcm$	$P4_2/mcm$
a (Å)	7.8331(4)	7.8339(4)	7.8397(4)	7.8690(2)	7.8463(2)
c (Å)	12.0074(7)	12.0339(5)	12.0321(6)	12.0890(3)	11.9985(6)
V(Å^3)	736.7	738.5	739.5	748.6	738.7
Z	4	4	4	4	4
No. of reflections	366	421	143	122	323
χ^2	6.368	4.80	2.12	1.626	2.82
wRp	9.09%	9.81%	14.61%	8.54%	13.07%
Rp	7.95%	7.37%	11.60%	6.65%	9.84%

$$R_p = \frac{\sum |I_o - I_c|}{\sum I_c},\ wR_p = \left(\frac{\sum w(I_o - I_c)^2}{\sum w{I_o}^2} \right)^{1/2},\ \chi^2 = \sum \frac{w(I_o - I_c)^2}{N_{obs} - N_{\text{var}}}$$

Table 4.2. Chemical Formulas of the Phases and Their Designation

Identification	Chemical formula
Nb-TS	$H_{0.2}Na_{1.3}Nb_{0.5}Ti_{1.5}O_3SiO_4{\cdot}2H_2O$
Cs1-Nb-TS	$Cs_{0.1}H_{0.4}NaNb_{0.5}Ti_{1.5}O_3SiO_4{\cdot}2H_2O$
Cs2-Nb-TS	$Cs_{0.2}H_{0.3}NaNb_{0.5}Ti_{1.5}O_3SiO_4{\cdot}H_2O$
Cs3-Nb-TS	$Cs_{0.3}H_{0.2}NaNb_{0.5}Ti_{1.5}O_3SiO_4{\cdot}2H_2O$
Sr-Nb-TS	$Sr_{0.2}Na_{0.6}H_{0.5}Nb_{0.5}Ti_{1.5}O_3SiO_4{\cdot}H_2O$

Table 4.3. Refined Fractional Atomic Coordinates and Occupancy Factors for Nb-TS

Atom	Site	*x*	*y*	*z*	Occ.
Ti/Nb	*8o*	0.1392(2)	0.1392(2)	0.1541(2)	0.75/0.25
Si	*4e*	0	0.5	0.25	1
O1	*16p*	0.1195(9)	0.3876(8)	0.1710(5)	1
O2	*8o*	0.1126(8)	0.1126(8)	0.3295(8)	1
O4	*4i*	0.1445(12)	0.1445(12)	0	1
Na1	*4f*	0	0.5	0.5	1
OW1	*4j*	0.2744(13)	0.2744(13)	0.5	1
OW2	*8o*	0.4479(15)	0.4479(15)	0.1117(13)	0.5

Table 4.4. Refined Fractional Atomic Coordinates and Occupancy Factors for Cs1-Nb-TS

Atom	Site	*x*	*y*	*z*	Occ.
Ti/Nb	*8o*	0.1407(2)	0.1407(2)	0.1547(2)	0.75/0.25
Si	*4e*	0	0.5	0.25	1
O1	*16p*	0.1316(7)	0.3873(6)	0.1721(4)	1
O2	*8o*	0.1121(8)	0.1121(9)	0.3324(9)	1
O4	*4i*	0.1486(9)	0.1486(9)	0	1
Na1	*4f*	0	0.5	0.5	1
Cs1	*2d*	0.5	0.5	0.25	0.08
Ow1	*4j*	0.2894(12)	0.2894(12)	0.5	1
Ow2	*8o*	0.4443(9)	0.4443(9)	0.1105(9)	0.5

Table 4.5. Refined Fractional Atomic Coordinates and Occupancy Factors for Cs2-Nb-TS

Atom	Site	*x*	*y*	*z*	Occ.
Ti/Nb	*8o*	0.1418(2)	0.1418(2)	0.1528(2)	0.75/0.25
Si	*4e*	0	0.5	0.25	1
O1	*16p*	0.1382(8)	0.3935(7)	0.1675(5)	1
O2	*8o*	0.1154(6)	0.1154(6)	0.3344(7)	1
O4	*4i*	0.1564(11)	0.1564(11)	0	1
Na1	*4f*	0	0.5	0.5	1
Cs1	*2d*	0.5	0.5	0.25	0.3
Cs2	*4h*	0.5	0.5	0.1263(15)	0.1
Ow1	*4j*	0.2824(12)	0.2824(12)	0.5	0.5
Ow2	*4j*	0.5916(25)	0.5916(25)	0.5	0.5

Table 4.6. Refined Fractional Atomic Coordinates and Occupancy Factors for Cs3-Nb-TS

Atom	Site	x	y	z	Occ.
Ti/Nb	*8o*	0.1400(1)	0.1400(1)	0.1531(1)	0.75/0.25
Si	*4e*	0	0.5	0.25	1
O1	*16p*	0.1222(4)	0.3870(4)	0.1662(3)	1
O2	*8o*	0.1153(4)	0.1153(4)	0.3266(4)	1
O4	*4i*	0.1494(6)	0.1494(6)	0	1
Na1	*4f*	0	0.5	0.5	1
Cs1	*2d*	0.5	0.5	0.25	0.42
Cs2	*4h*	0.5	0.5	0.1582(9)	0.12
OW1	*4j*	0.2451(2)	0.2451(2)	0.5	0.5
OW2	*4i*	0.4264(1)	0.4264(1)	0	0.5
OW3	*8n*	0.2496(17)	0.3473(12)	0.5	0.5

Table 4.7. Refined Fractional Atomic Coordinates and Occupancy Factors for Sr-Nb-TS

Atom	Site	x	y	z	Occ.
Ti/Nb	*8o*	0.1435(3)	0.1435(3)	0.1548(3)	0.75/0.25
Si	*4e*	0	0.5	0.25	1
O1	*16p*	0.1256(13)	0.3978(14)	0.1663(7)	1
O2	*8o*	0.1190(8)	0.1190(8)	0.3234(9)	1
O4	*4i*	0.1559(11)	0.1559(11)	0	1
Na1	*4f*	0	0.5	0.5	0.737
Sr1	*4j*	0.3969(19)	0.3969(19)	0	0.197
OW1	*4j*	0.2683(20)	0.2683(20)	0.5	1

Table 4.8. Selected Interatomic Distances (Å)

Cs1-Nb-TS		Cs2-Nb-TS		Cs3-Nb-TS		Sr-Nb-TS	
Non Framework Cations							
Na1-O1	2.483(5)x4	Na1-O1	2.436(6)x4	Na1-O1	2.399(4)x4	Na1-O1	2.366(10)x4
Na1-O4	3.000(4)x2	Na1-O4	2.960(4)x2	Na1-O4	2.999(2)x2	Na1-O4	2.964(7)x2
Na1-Ow1	2.814(2)x2	Na1-OW1	2.794(2)x2	Na1-OW1	2.7827(4)x2	Na1-OW1	2.781(2)x2
				Na1-OW2	2.303(12)x2		
Cs1-O1	3.171(6)x8	Cs1-O1	3.119(6)x8			Sr1-O1	2.91(2)x4
		Cs1-OW2	3.175(9)x4	Cs1-O1	3.264(3)x8	Sr1-O4	2.67(3)
		Cs2-O1	2.998(7)x4	Cs1-OW2	3.132(4)x4	Sr1-OW1	2.81(2)x2
		Cs2-OW1	2.95(1)x2	Cs2-O1	3.104(3)x4		
				Cs2-OW1	3.421(19)x4		
				Cs2-OW3	2.998(12)x2		

The remaining sodium ions reside in the tunnels at (x x z) with x ~ 0.435, z ~ 0.059 with partial occupancies as these positions are close to each other. Instead, protons substitute for Na^+ ions and the actual formula is $Na_{1.64}H_{0.36}Ti_2O_3SiO_4 \cdot 1.84H_2O$.[13]

The unit cell dimensions of Nb-TS are larger than TS due to the 25% Nb^V in the framework since Nb is slightly larger than Ti (γ_{Ti} = 0.605 Å, γ_{Nb} = 0.69 Å). The volume expansion is 1% above that of the TS phase due to the combined effects of niobium substitution and additional water present in the tunnel. Similar to the TS phase, in Nb-TS, sodium occupies two types of sites: framework (Na1) at (0 ½ ½) and channel sites. The framework sites are 100% occupied. There are two water positions within the tunnel (Table 4.3). One (Ow1) is at (x x ½) with x = 0.2744, which is almost the same as the position of Ow1 in the TS phase and fully occupied. Another site (Ow2) is at (0.4479 0.4479 0.1117) which is actually closer to the face of the tunnel than in TS. This site is about 70% occupied and disordered with Na2. The amount of Na was calculated from microprobe analysis and taking into account results of TGA. The final formula was refined close to $Na_{1.3}H_{0.2}Ti_{1.5}Nb_{0.5}O_3SiO_4 \bullet 2.0H_2O$.

Similar to the cesium form of TS, the sodium atoms at (0 ½ ½) remain intact in all cesium loaded phases of Nb-TS. There are two cesium positions in Nb-TS: one is at (½ ½ ¼) and another one at (½ ½ z) with z varying from 0.1263 in Cs2-Nb-TS to 0.1582 in Cs3-Nb-TS (Table 4.3-4.7).

In Cs1-Nb-TS the cesium *2d* site is only 8% occupied whereas the second site is empty. The other channel sites are occupied by two water molecules (Table 4.3). Only one water site was observed in pure TS.[13] The water site, OW1, is fully occupied and this water is coordinated to Na1. The occupancy of the site with disordered OW2 is 50%. OW2 is hydrogen bonded to residual protons and framework oxygen atoms. The Cs1 forms an eight-coordinated complex with the framework oxygens similar to the one observed in the case of TS (Table 4.8).

Cs2-Nb-TS has the same hydration as the Cs-TS, $Cs_{0.2}Na_{1.49}H_{0.31}Ti_2O_3SiO_4 \cdot H_2O$. Therefore, a 5.86 $Å^3$ (0.79%) increase of volume over TS is due to 25% Nb substitution as the hydration level remains the same. The water molecules, however, are distributed

in a different manner. Two partially occupied water sites were found. The water OW1 at (x, x, ½) with x ~ 0.273 is bonded to Cs2 and Na1 with environment similar that observed in the case of OW1 in TS (Table 4.5). However, OW2 at (x, x, ½) with x ~ 0.591 was not found in the TS phase resulting in an alteration of the Cs1 coordination. Coordination number varies from eight (8 framework oxygens) to twelve. Four additional bonds originate from four disordered waters at a distance of 3.175(9) Å from cesium (Table 4.8).

The maximum Cs^+ exchanged sample Cs3-Nb-TS, with the composition, $Cs_{0.3}H_{0.2}NaNb_{0.5}Ti_{1.5}O_3SiO_4 \cdot 2H_2O$, shows further difference in the water sites position and the cesium environment. The volume increase over the Cs2-Nb-TS phase is 9.12 $Å^3$ (1.22 %) and can be attributed to both the increase in water content in the tunnel and the Cs occupancy. The six coordinate oxygen environment around Na1 remains the same as in the TS phase, though in this case it is bonded to two statistically occupied water molecules instead of one fully occupied water molecule in TS. Three statistically occupied water sites were observed (Table 4.6). The OW1 at (x, x, ½) with x ~ 0.24 is similar to OW1 observed in the case of the Cs-TS phase. The second water, OW2 at (x, x, 0) with x ~ 0.426 is in a four-fold site and is involved in bonding with Cs1 whereas OW3 at an eight-fold site (x, y, ½) is bonded to Na1, Cs1 and Cs2. The two statistically occupied Cs^+ ions have more hydration water compared with Cs^+ ions in TS and in the low Cs substituted Nb-TS discussed above. Cs1 is bonded to eight O1 atoms at 3.264(3) Å and four OW2 at 3.132(4) Å (Table 4.8). These two sites containing water with 50% water population can be simultaneously occupied. Although, it is difficult to assign an exact CN to Cs1 due to the statistical nature of the waters, OW2 and OW3, a CN of 12 can be assigned to Cs1. The 12 coordinate connectivity of cesium ions is shown in Figure 4.1. The other disordered Cs2 ion also is located along the tunnel but is displaced 1.109(10) Å away along the *c*-axis from Cs1 compared with 1.425 Å in the case of TS. It has a bonding environment with four oxygens of the framework, two OW1 and four OW3. The waters, OW1 and OW3 are too close to be simultaneously occupied. In this case a CN of eight can be assigned.

In the Sr^{2+} exchanged sample of Nb-TS, a seven coordinate Sr was observed at (x, x, 0) with x ~ 0.3977 (Table 4.7, Figure 4.1). Unlike other Cs-Nb-TS samples the framework Na site is only partially (73%) occupied in this case. There is only one water site containing OW1. The Sr^{2+} exchange resulted in a mixture of phases in the case of TS. Preliminary results from structure solution of the two phases indicate a mixture of tetragonal and orthorhombic phases. The tetragonal phase has a ten coordinate Sr.[51]

4.3.2. Ion exchange properties

Cs^+ uptake measurements. The experimental values of the uptake of Cs^+ ions by pure TS and Nb-TS as a function of sodium ion concentration are plotted in Figure 4.2. For Na^+ concentrations ranging from 0-5 M, Nb-TS shows higher uptake values in agreement with those observed by Dosch and Anthony.[3] Particularly, in the region of sodium ion concentrations higher than 0.5 M, pure TS picks up almost no Cs^+, whereas Nb-TS shows much higher uptake especially in strong salt solutions. Equilibrium pH values of Cs^+ solutions are plotted in Figure 4.2. Though both the curves have similar shapes, the pH for the Nb-TS solution is lower. This may be attributed to partial hydrolysis. Metal ion forms of TS type materials could be considered as insoluble salts formed by a strong base such as those of alkali metals and a very weak insoluble acid $H_2Ti_2O_3SiO_4 \cdot 2H_2O$. The hydrolysis of the sodium form of the TS type material in water solutions could be described by the following reaction:

$$\overline{Na}^+ + H_2O \Leftrightarrow \overline{H}^+ + Na^+ + OH^-$$

According to Le Chatlier's principle the equilibrium can be altered by changing the concentration of sodium and protons in the solution, as well as the amount of sodium ions residing within the framework of the ion exchanger. The increase of Na^+ concentration causes the downward slopes of the both curves because equilibrium shifts to the left.

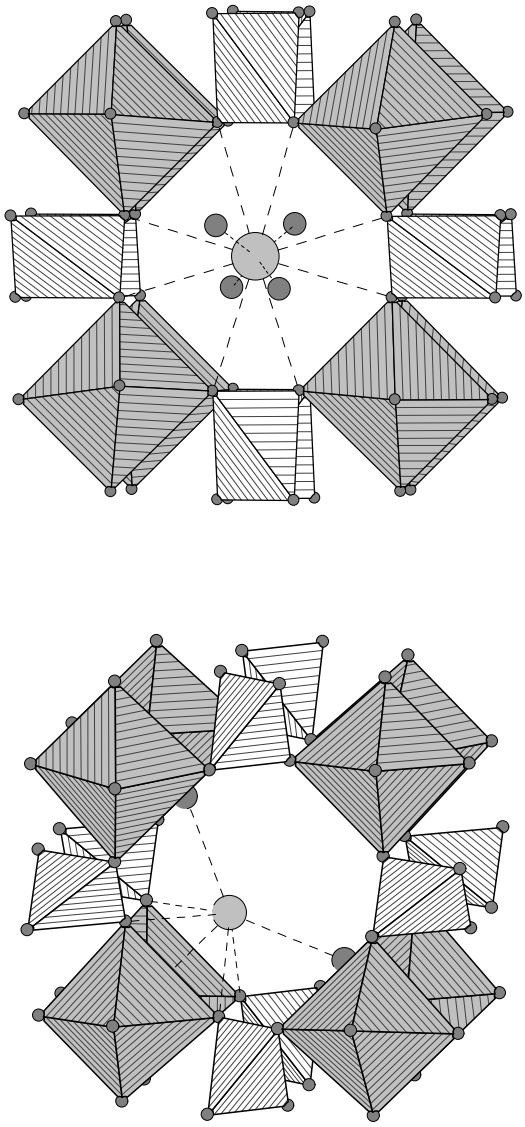

Figure 4.1. Connectivity of 12 coordinated Cs2 (top) and 7 coordinated Sr in 25% substituted Nb-TS (bottom) in the tunnel arranged from TiO_6 (grey, hatched) and SiO_4 (white hatched) polyhedra. Medium-grey circles represent water molecules, light-grey circles represent cations

The amount of hydrolysable sodium ions is also crucial for equilibrium. Since the amount of sodium ions in Nb-TS is 15% less than in pure TS, under similar conditions, the pH of the Nb-TS equilibrium solution is lower.

Sr^{2+} uptake measurements. The experimental values of Sr^{2+} uptake by pure TS and Nb-TS plotted against sodium ion concentration are shown in Figure 4.3. Unlike Cs^{+} uptake, the Sr^{2+} absorption shows two distinct regions. Below 1.0 M Na the uptake of Sr^{2+} in Nb-TS is higher but in more concentrated solutions pure TS behaves better than Nb-TS. In particular, the Sr^{2+} uptake value from 5 M sodium ion solutions is twice for pure TS than for Nb-TS. The pH curves for Sr^{2+} solutions look similar for both the materials (Figure 4.3). As in the case of Cs^{+} the equilibrium pH values are generally lower for Nb-TS. The pH remains nearly neutral for solutions with high sodium ion content in the case of Nb-TS. Hydrolysis is suppressed and only ion exchange occurs.

Kinetic studies. Recovery of ^{89}Sr and ^{137}Cs from alkaline media as a function of time was studied to compare the kinetics of Sr^{2+} and Cs^{+} uptake for Nb-TS and the TS phase. A total of 5.6 M Na^{+} was present as a competitive ion for the framework sites. As observed in Figure 4.4, the kinetics of recovery of ^{89}Sr from such a solution is the same for both Nb- and pure TS. In both the systems equilibrium was reached in twenty minutes, and no more nuclide was recovered from solution after that. Also, both the materials used up to ~90% of their equilibrium uptake for ^{89}Sr under these conditions in one minute. However, it can be emphasized that, pure TS removed almost 99.6% of ^{89}Sr from solution compared to 85.3% removal by Nb-TS. The K_d values at equilibrium were 60,000 mL/g for pure TS and about 1,500 mL/g for Nb-TS. The recovery curve for pure TS is shifted up 15 units compared to the Nb-TS curve. The similarity in the shapes of the curves suggests that although $Nb^{5+} \leftrightarrow Ti^{4+}$ substitution increased the tunnel capacity, it did not affect Sr diffusion rates inside the tunnel.

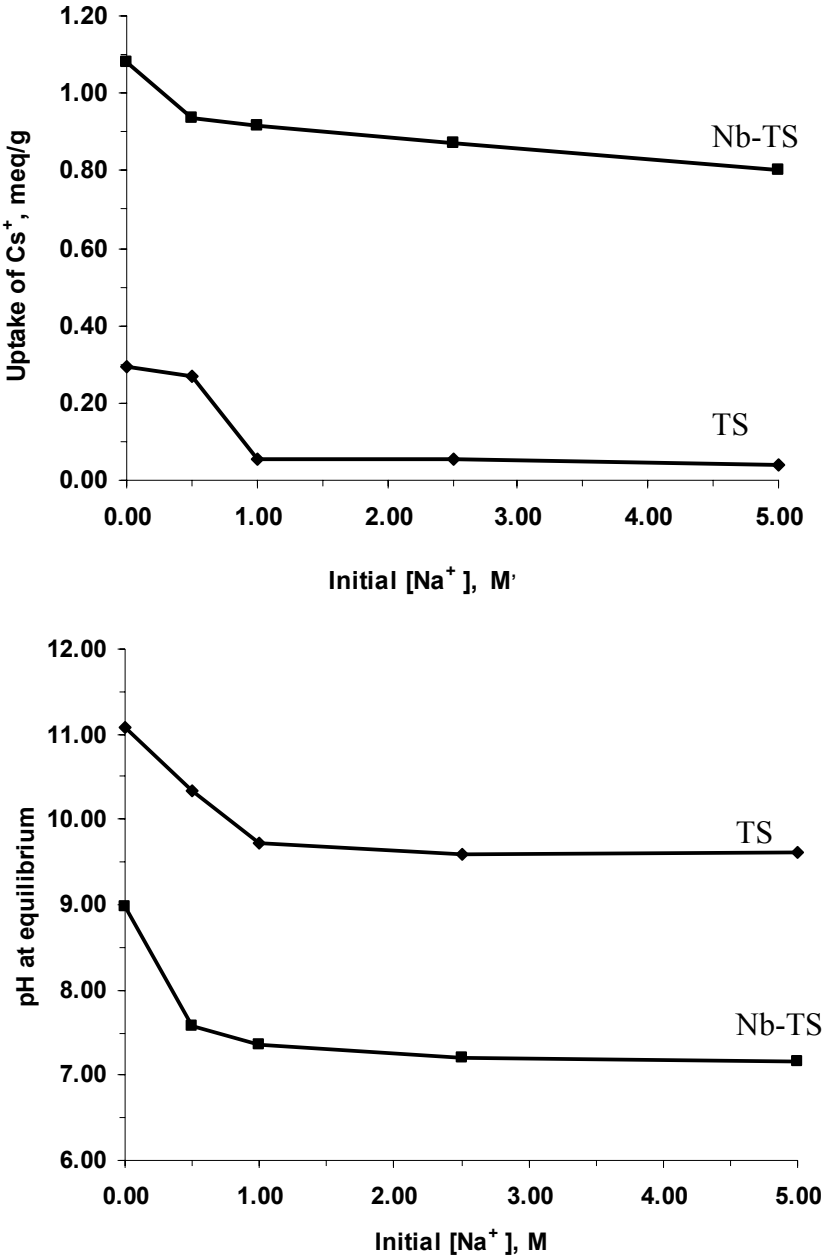

Figure 4.2. Uptake of Cs^+ (top) and equilibrium pH values (bottom) as a function of initial Na^+ concentration in solution for Nb-substituted and non-Nb phases

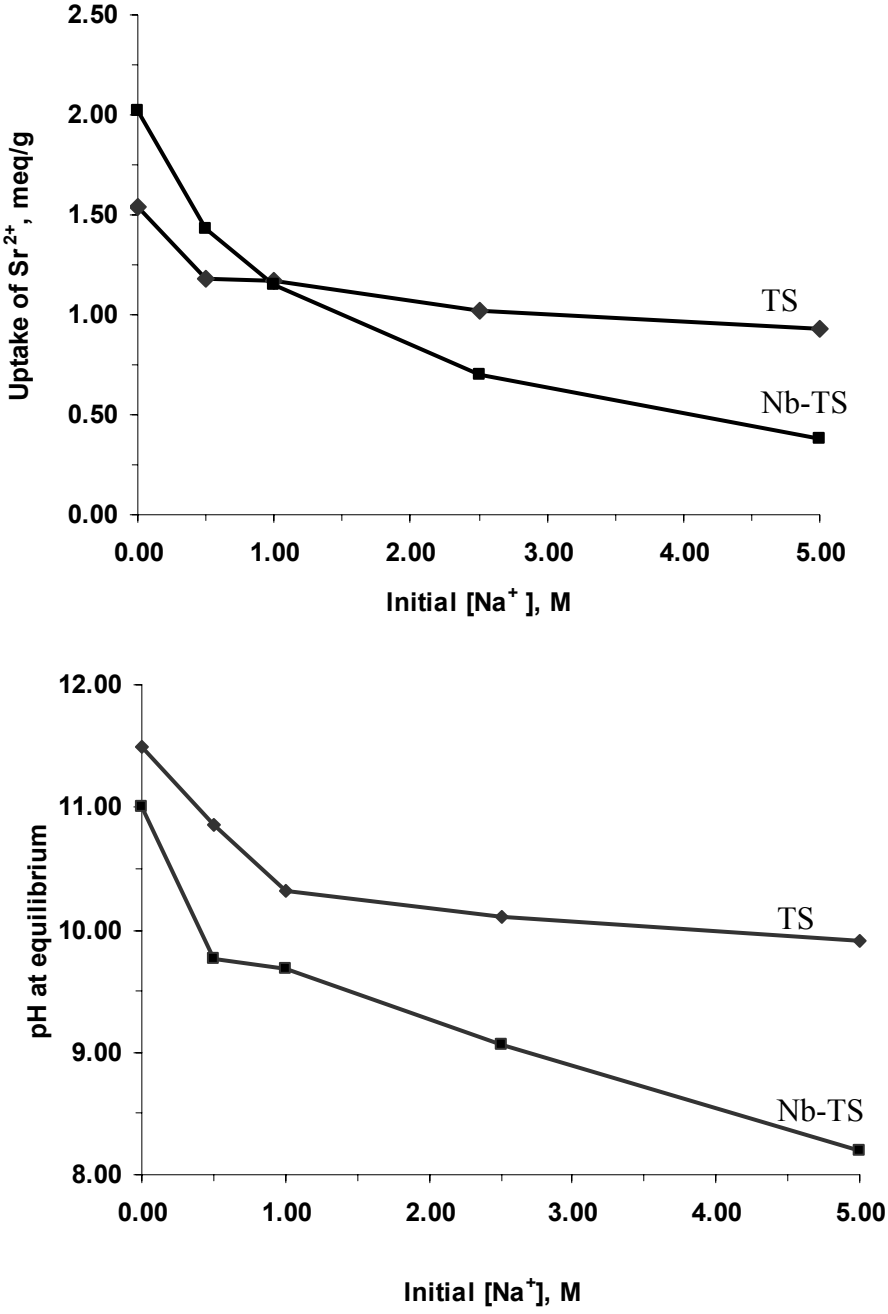

Figure 4.3. Uptake of Sr^{2+} (top) and equilibrium pH values (bottom) as a function of initial Na^{+} concentration in solution for Nb-substituted and non-Nb phases

The ^{137}Cs uptake experiments indicated that Cs^+ was not absorbed by TS only. For pure TS, differences in the remaining activity of the Cs^+ solution at each point of time did not exceed the counting error. Almost no Cs^+ was picked up after 2 hours of equilibration. Unlike ^{89}Sr uptake, the Nb-TS phase exchanged to only 40% of its final (120 min point in Figure 4.4) amount of ^{137}Cs after one minute, and in 2 hours, 80% of all ^{137}Cs was recovered from the solution. The recovery value continued to increase after 60 min (Figure 4.4) implying that the kinetics of ion exchange of Cs^+ in Nb-TS is much slower than that for Sr^{2+}. As Cs^+ is larger than Sr^{2+}, its diffusion rate is expected to be lower than that of Sr^{2+} as shown by the data. To assess the behavior of the ion-exchangers in nuclear waste solutions, distribution constants (K_d) for ^{137}Cs and ^{89}Sr were determined in alkaline simulants with varying Na^+ concentration. In all the solutions the concentration of NaOH was 1M. In addition, $NaNO_3$ was added to each solution, so that the concentration in the simulants varied from 0 to 4.5 M. The Cs and Sr simulants for K_d value determination were spiked by ^{137}Cs and ^{89}Sr, respectively so that the initial activity of the solutions is about 2000 times higher than the background. Figure 4.4 shows the plots of experimental K_d values for Nb-TS and pure TS for Cs and Sr against $NaNO_3$ concentration in the simulant. All simulants were 1M in NaOH to begin with, so the total Na^+ concentration is (n+1) M, where n equals the molarity of $NaNO_3$. As evident from the curves, the Nb-TS is more selective for Cs^+, compared with the pure TS. The K_d value of Cs^+ for Nb-TS in 1M NaOH is about 23,000 mL/g, which is 24 times higher than for pure TS. This ratio holds up to a concentration of 2 M $NaNO_3$, however, at higher concentrations both materials lose their ability for Cs^+ uptake. The distribution constants show a reverse situation in the case of Sr^{2+}. Pure TS outperforms Nb-TS with a K_d value of 25×10^6 mL/g at 1 M NaOH, and 5×10^5 mL/g at 4.5M $NaNO_3$/1 M NaOH compared with 11,000 mL/g and 2400 mL/g in similar conditions for Nb-TS.

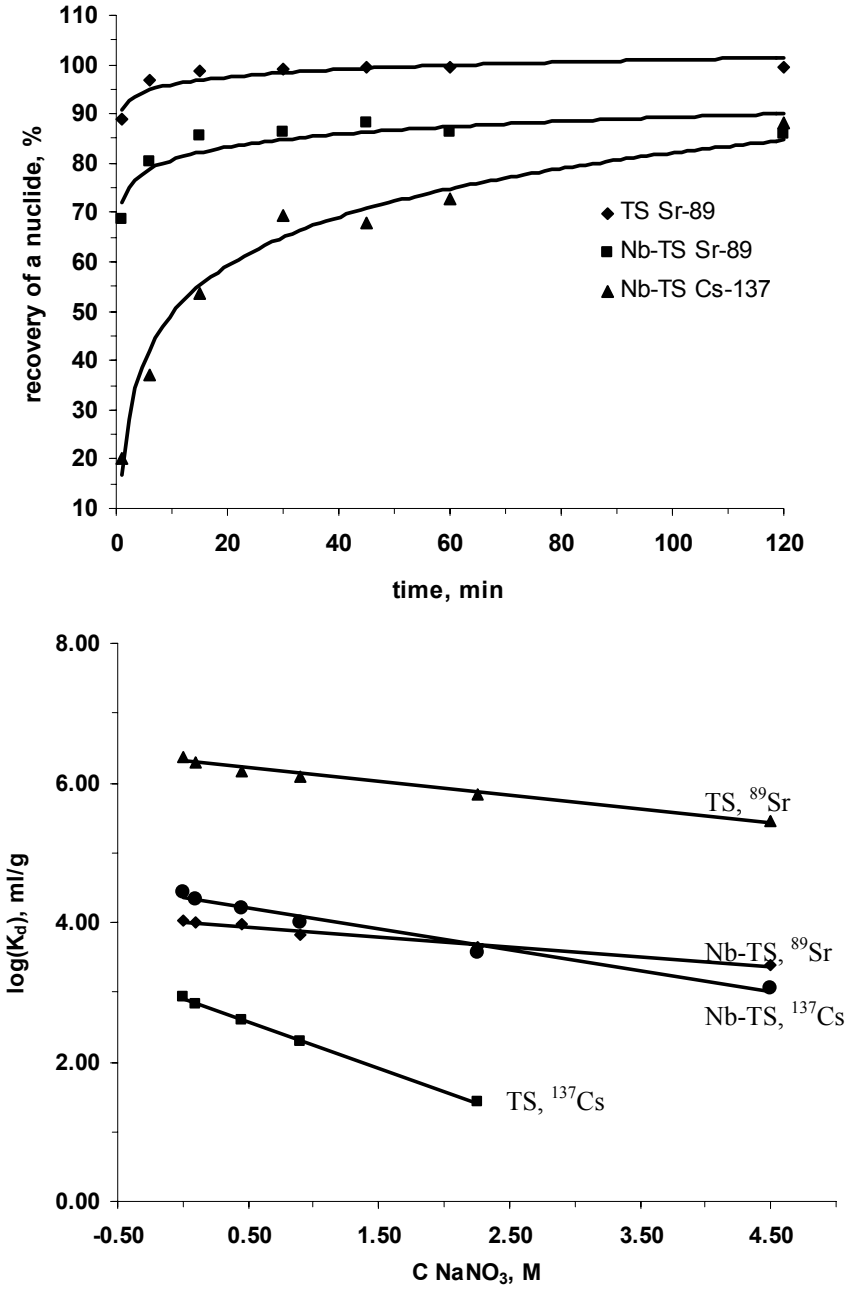

Figure 4.4. Kinetics of recovery of ^{137}Cs and ^{89}Sr from radioactive waste simulant (top) and log Kd values from solutions with increasing sodium concentrations (bottom) for Nb-TS and TS phases

4.4. Discussion

Heteroatom framework substitution is essential, because the properties of the material can be tuned. The structural studies and comparison of properties of parent and substituted derivatives often can shine light on the nature of the phenomena. We compared Nb-substituted TS phase with a parent compound from structural and ion-exchange perspectives to understand the reasons for differences in ion-exchange selectivities reported previously.[3]

The results can be interpreted in the scope of Eisenman theory.[61] Suppose a monovalent ion is to be taken from the bulk of a dilute solution and brought into contact with the ionic grouping of the opposite charge inside an ion-exchanger. Consider an ion-exchange reaction, where the ion-exchanger is in the A form, and B is a counter ion, and A is partially replaced by B. The bar indicates the ion in the solid phase:

$$\overline{A} + B \Leftrightarrow \overline{B} + A\,.$$

Two types of interactions are involved in such a process: (1) the electrostatic interaction between the fixed ionic grouping and the exchanging ions and (2) hydration of the exchanging ions and ionic grouping of an ion-exchanger. Eisenman treated the fixed grouping and the counter-ion as point charges. The energy of electrostatic interaction between ions A^+(radius r_{A^+}) and fixed ionic grouping (radius r_{f^-}) is:

$$W_{f^-,A^+} = \frac{e^2}{r_{f^-} + r_{A^+}} \text{ or} \qquad (4.1)$$

$$W_{f^-,B^+} = \frac{e^2}{r_{f^-} + r_{B^+}} \text{ for ion } B^+ \text{ of radius } r_{B^+}\,. \qquad (4.2)$$

For the above ion-exchange reaction the change of free energy due to electrostatic interaction is:

$$\Delta G^0{}_E = W_{f^-,A^+} - W_{f^-,B^+} \qquad (4.3)$$

To account for the free energy changes due to hydration, we consider the sequence of the following processes: (1) hydration of the ion A^+ which is leaving an ion-

exchanger followed by hydration of the fixed ionic group [-($\Delta G_{f^-} + \Delta G_{A^+}$)] and (2) dehydration of the fixed ionic group followed by dehydration of the ion B^+, approaching this dehydrated group inside an ion-exchanger ($\Delta G_{f^-} + \Delta G_{B^+}$). Since ΔG_{f^-} cancel out each other, then the net free energy change for hydration is

$$\Delta G_h^0 = -(\Delta G_{A^+} - \Delta G_{B^+}) \tag{4.4}$$

and the overall free energy change for the reaction is

$$\Delta G_{B/A}^0 = \left(\frac{e^2}{r_{f^-} + r_{A^+}} - \frac{e^2}{r_{f^-} + r_{B^+}} \right) - (\Delta G_{A^+} - \Delta G_{B^+}) \tag{4.5}$$

The equilibrium constant for the exchange reaction is related to this free energy by equation (4.6).

$$\Delta G_T^0 = -RT \ln \mathrm{K}_{T\,B}^{\,A} \tag{4.6}$$

Thus, from the knowledge of ionic radii and free energy of hydration, it is possible to explain the selectivities for alkaline metal cations as a function of r_f.

In ion-exchange resins the order of preference of the alkali cations is usually $Li^+ < Na^+ < K^+ < Rb^+ < Cs^+$. The usual order may be explained if we assume that the binding force is electrostatic and that the ions within the resin are hydrated approximately as they are outside it. The ion with the smallest hydrated radius (Cs^+) will be able to approach closely to the negative site and hence be held more strongly.[62]

The situation is different for zeotype materials, since the role of coordination bonds becomes more important. As was mentioned previously, framework Na1 ions remain intact in Cs-loaded phases. Since only tunnel sodium ions are removed, the sites can be considered homogeneous.

The sodium ion forms 6 bonds within the tunnel: 2 bonds with framework oxygens and 4 bonds with water molecules. The bonds with the framework are weak as they are ~ 9% longer than the sum of effective ionic radii of Na^+ and oxygen.[63] The Na^+ in the solution is 6 coordinate forming $Na(H_2O)_6^+$ species with a hydration energy of 406 kJ/mol.[62]

Cesium positions itself at the center of the tunnel and forms 8 strong bonds with framework oxygens in pure TS and an additional 4 bonds with water molecules in the Nb-TS phase. The hydration energy of aqueous Cs^+ is 264 kJ/mol, which is smaller than that for Na^+. The equation 4.5 can be rewritten for the ion-exchange process of Cs in Na form of TS:

$$\Delta G^0_{Cs^+/Na^+-TS} = \left(\frac{e^2}{r_{TS^-} + r_{Na^+}} - \frac{e^2}{r_{TS^-} + r_{Cs^+}} \right) - (\Delta G_{Na^+-aq} - \Delta G_{Cs^+-TS}) \qquad (4.7)$$

Assuming that $r_{TS}^- = r_{Nb\text{-}TS}^-$, the difference between free energies of ion-exchange, i.e selectivities, of Cs in pure TS and Nb-TS can be expressed as:

$$\Delta(\Delta G^0) = \left|\Delta G^0{}_{Cs^+/Na^+-TS}\right| - \left|\Delta G^0{}_{Cs^+/Na^+-Nb-TS}\right| = \left|\Delta G_{Cs^+-TS}\right| - \left|\Delta G_{Cs^+-Nb-TS}\right| \qquad (4.8)$$

As can be seen for equation 4.8 the difference in free energies of ion-exchange, i.e selectivities for TS and Nb-TS, arises only from free energies of hydration of Cs inside the ion-exchangers. The Cs^+ hydration is higher in Nb-TS, therefore the free energy of hydration is higher (in absolute value) therefore the Nb-TS is more selective for Cs compared to pure TS. Consequently various cesium coordinations were observed in the three Cs^+ exchanged samples for both the 2*d* (½, ½, ¼) and the 4*h* (½, ½, z) positions. We compared Nb-TSs with the Cs-TSs reported by Poojary, et al[13] and no attempts were made to prepare higher Cs substituted TS. Indeed, this average structural analysis using X-ray powder diffraction method is insufficient to pinpoint all the water sites due to static disorder of the tunnel constituents (particularly Na^+ cations and water molecules) and their statistical occupancy of multiply closed sites. However, the study shows that a key factor in the selectivity for a metal ion is the coordination environment around it. The 25% Nb^V substitution for Ti^{IV} results in 50% less Na^+ in the tunnel (see equation below), thus facilitating the uptake of extra water, possibly as a hydrated Cs complex, into the less crowded tunnels.

$$Na^+ + Ti^{4+} \leftrightarrow Nb^{5+}$$

As the Cs^+ uptake increases, the protons/hydronium ions are displaced from the tunnel which in turn modifies the amount and coordination by water molecules. Several additional bonds formed with water in the case of Cs1 and Cs2 result in thermodynamically more favorable complexes in the case of Nb-TS compared with the TS. The results are consistent with the higher uptake of Cs^+ in Nb-TS compared with TS.

Through our structural studies it was found that strontium forms a 7 coordinate complex in Nb-TS and a 10 coordinate complex in the non-substituted phase. As it is obvious from Figure 4.3 the TS phase is more selective at the sodium concentration above 1M which in general, correlates with the Eisenman theory. However, at concentrations below 1M the Nb-TS phase is more efficient. The reasons for such a behavior can be found if we consider the processes which accompany ion exchange.

Let's consider the sodium TS phase which was brought into contact with 0.05 M Sr solution. The sodium ions in the tunnel are loosely bonded[13] and will be hydrolyzed out as evident from the pH values corresponding to 0 M Na concentration. Unlike Cs^+ ion which occupied the central position in the eight ring tunnel, the Sr^{2+} cation in Nb-TS is located inside the tunnel close to the smaller six-membered rings. This site is less spacious for a large amount of water molecules to reside in. Sr^{2+} will exchange in the tunnel, causing depopulation of the framework sodium site (Na1). This process is more successful if less sodium was hydrolyzed from the tunnel and now being in solution suppressing the depopulation. Since there are less sodium ions residing in the tunnel in Nb-TS phase (see Table 4.2-4.3) the pH of the solution at equilibrium is lower and the depopulation of Na1 site is more successful and Sr uptake is higher, although the coordination of strontium is lower then in the case of pure TS. Generally speaking, in order for strontium to be exchanged it has to squeeze out Na1 and form bonds within the framework. Removing Na1 is more problematic in the case of TS since more sodium is being hydrolyzed from the tunnel, than in the Nb-TS case and now trying to occupy the Na1 site. When the concentration of sodium progressively increases, the role of hydrolysable tunnel sodium ions diminishes and the coordination of strontium within the

framework becomes crucial. As a result TS removes more strontium at higher sodium concentrations, forming the thermodynamically more stable 10 coordinate complex. The Eisenman theory was developed assuming that ion-exchange sites are homogenous. In the case of TS type of materials Na occupies inhomogeneous sites. The sites which are being depopulated in ion-exchange/hydrolysis should be carefully examined.

4.5. Conclusion

In this chapter we discussed the results of our studies of framework substituted titanium silicate with sitinakite topology. For a 25% Nb-substituted phase its cesium and strontium loaded phases were structurally investigated. It was found that $Ti^{iv} \leftrightarrow Nb^{v}$ substitution resulted in depopulation of the tunnel due to the decreased negative charge of the framework compared to non-substituted phase. Additional water molecules were found disordered over the sodium sites within the tunnel. A Nb-TS phase demonstrated enhanced selectivity towards cesium in highly alkaline media. The reasons for selectivity are in the coordination environment of cesium within the framework. Cs forms a 12-coordinate complex in Nb-TS and only an 8-coordinate complex in the TS phase. The situation appears to be reversed in the case of Sr exchange. The TS phase is more effective for Sr in highly alkaline media, having Sr 10 coordinated in contrast to 7-coordinated in the case of Nb-TS.

CHAPTER V
SUBSTITUTION OF GERMANIUM AND NIOBIUM IN TITANOSILICATE WITH THE MINERAL PHARMACOSIDERITE STRUCTURE

5.1. Introduction

In Chapter IV we discussed the results of comparative studies on titanium silicate sitinakite and its 25% Nb-substituted derivative. It was found that Nb incorporates in octahedral (titanium) sites and being a +5 charged cation decreases the negative charge of the anionic grouping. This results in depopulation of sodium sites within the tunnel and increase in hydration of the Nb-substituted derivative. Structural studies of the cesium loaded phase revealed that the additional water molecules arrange themselves around Cs cations leading to an increase in the coordination number of the latter. We believe that such a phenomenon is the reason for an improved ion-exchange selectivity towards cesium in the Nb-substituted phase.

In this chapter we consider another class of materials with mineral pharmacosiderite structure. Pharmocosiderite is a naturally occurring mineral with a composition of $KFe_4(OH)_4(AsO_4)_3$. The framework consists of clusters of 4 edge shared FeO_6 octahedra connected through AsO_4 tetrahedra in all three directions to form a three-dimensional network of channels. The negative charge of the framework is compensated by cations, residing in the channels. Several types of substitution are possible in this structure. In 1990 Chapman and Roe[17] reported synthesis and structure of microporous compounds with titanium in octahedral and silicon in tetrahedral sites. The fully substituted phases with Ge in octahedral and tetrahedral sites, $M_3HGe_7O_{16} \bullet nH_2O$ ($M=K^+$, Rb^+, Cs^+) were prepared previously by ion-exchange from the parent $(NH_4)_3HGe_7O_{16} \bullet nH_2O$ phase.[64] Further, the titanium silicate (TSP) and germanate modifications of this material was exploited very heavily mainly because of their possible application for radioactive waste remediation. In 1993 Nenoff et al[65] reported a

rhombohedrally distorted germanium pharmacosiderite phase, $Na_3H_x(H_2PO_4)_x[(GeO)_4(GeO_4)_3].4H_2O$ with anion/cation exchange capabilities. Furthermore, a sodium form of the titanium silicate rhombohedrally distorted pharmacosiderite analogue was studied. Behrens at al[66] reported the selectivity series for a proton form of the TSP phase showing that that the selectivity increases with the size of an exchanged ion and correlating it with hydration energies of ions in the bulk solution. The partially germanium substituted phases demonstrated enhanced affinity towards cesium and strontium compared to the parent titanium silicate phases.[58]

In our quest for selectivity reasons we decided to look deep into the titanium silicate pharmacosiderite phases. In the first approach we prepared a series of germanium substituted titanium silicate phases. Unlike the Nb^{+5}, germanium, being +4 charged does not alter the framework charge. However, having ionic radius smaller than Ti^{4+} (r = 0.605Å) and larger than Si^{4+} (r = 0.26 Å), Ge^{4+} (r = 0.40 Å) can be used to decrease the unit cell size when it occupies octahedral (titanium) sites and increase the unit cell size, when it substitutes for silicon. We carried out an ion-exchange and structural characterization of the Cs-loaded phases to see the differences if any in the structure and to correlate it with ion-exchange properties.

In the second approach, similar to the one for TS, we prepared a novel 20% Nb substituted potassium titanosilicate pharmacosiderite phase and a fully germanium substituted phase and compared its selectivity with potassium titanosilicate. The substitution of Nb^{5+} for Ti^{4+} in the framework decreases the amount of cations required in the channels to balance the framework charge and, hence, can modify ion exchange behavior. In this chapter, the modified ion exchange properties will be discussed from a structural perspective in light of these changes.

5.2. Experimental methods

5.2.1. Synthesis and composition of pharmacosiderite phases

Seven phases with pharmacosiderite structure were studied. Four Ti/Ge/Si samples with increasing germanium substitution at the tetrahedral site were prepared using Cs cations as a charge compensating counter cation in the channels while Ti/Si (K-TSP), Ti/Nb/Si (K-NbTSP), and Ge/Ge (K-GeGeP) phases were prepared in K-forms for the structural studies. The synthesis procedures are outlined below.

Synthesis of Cs-forms of germanium substituted phases. The partially Ge substituted Cs-forms of pharmacosiderite were prepared by modification of the technique described previously.[58] In particular, the overnight aging and washing steps utilized in the reported technique were omitted as it was discovered that they do not influence the crystallinity of the products. The synthetic procedure began with agitating fumed silica and titanium isopropoxide with doubly deionized (ddi) water in a plastic beaker. The mixture was stirred for 30 minutes and combined with GeO_2 dissolved in 50% CsOH solution. The composition of the starting gels was designed with increasing amounts of Ge and correspondingly decreasing amounts of silicon. Four precursors were prepared with compositions, shown in Table 5.1. The mixtures were placed in four 100 mL Teflon lined stainless steel pressure vessels and heated in an oven at 200^{o}C for 2 days. Highly crystalline solids were filtered off and dried in an oven at 55^{o}C. Stoichiometric formulas of the final products and the composition of the precursors are shown in Table 5.1. The samples were converted to hydrogen forms as described in the ion-exchange section. X-ray powder patterns of the obtained Cs-forms are shown in Figure 5.1. Figure 5.2 shows a comparative plot of Cs and H-form.

Synthesis of K-forms of pharmacosiderites. Synthesis of K-TSP: A total of 0.66 mL (6 mmol) of $TiCl_4$ (Alfa Aesar) was mixed with 40 mmol of HCl in ddi water in a plastic beaker. To this solution, 5 mL of 30% H_2O_2 was added under constant stirring

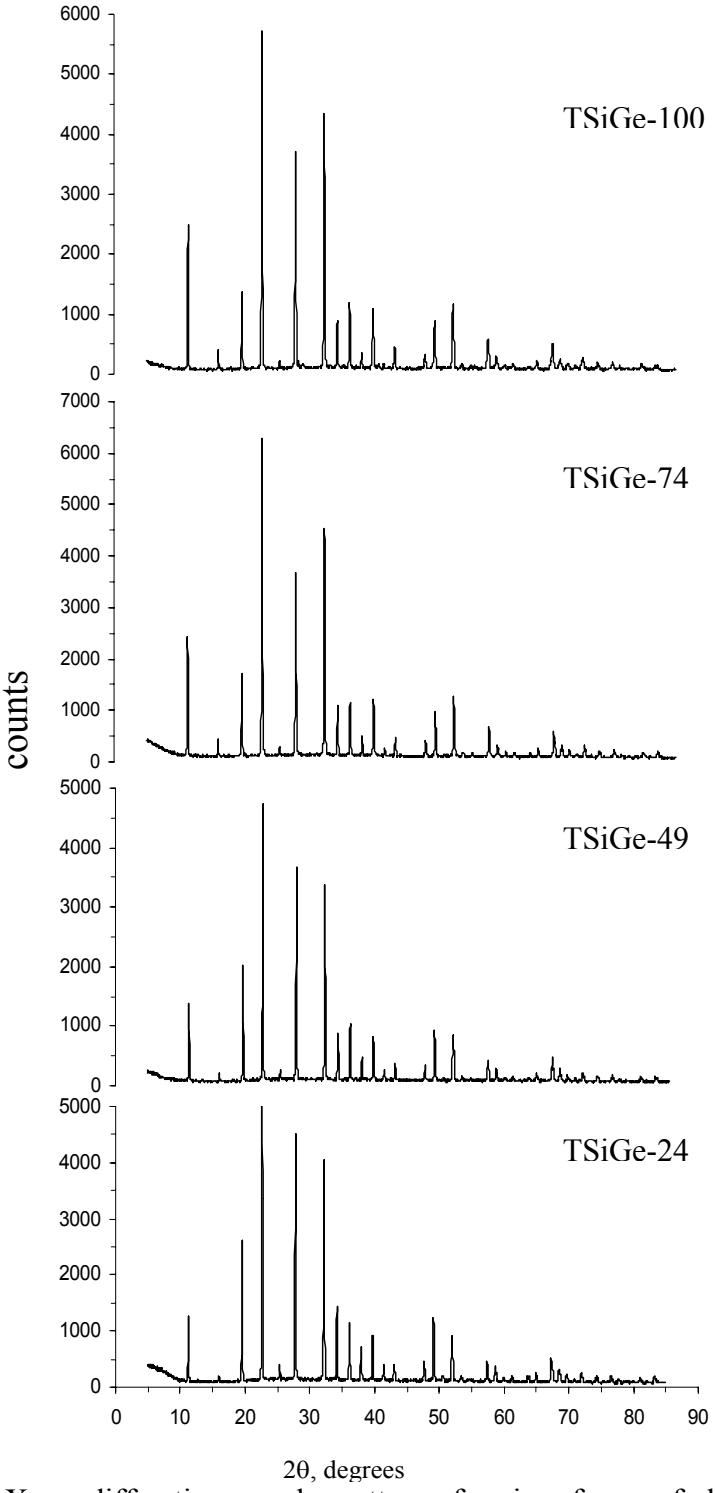

Figure 5.1. X-ray diffraction powder pattern of cesium forms of pharmacosiderites with different germanium substitution. See Table 5.1 for phase identification

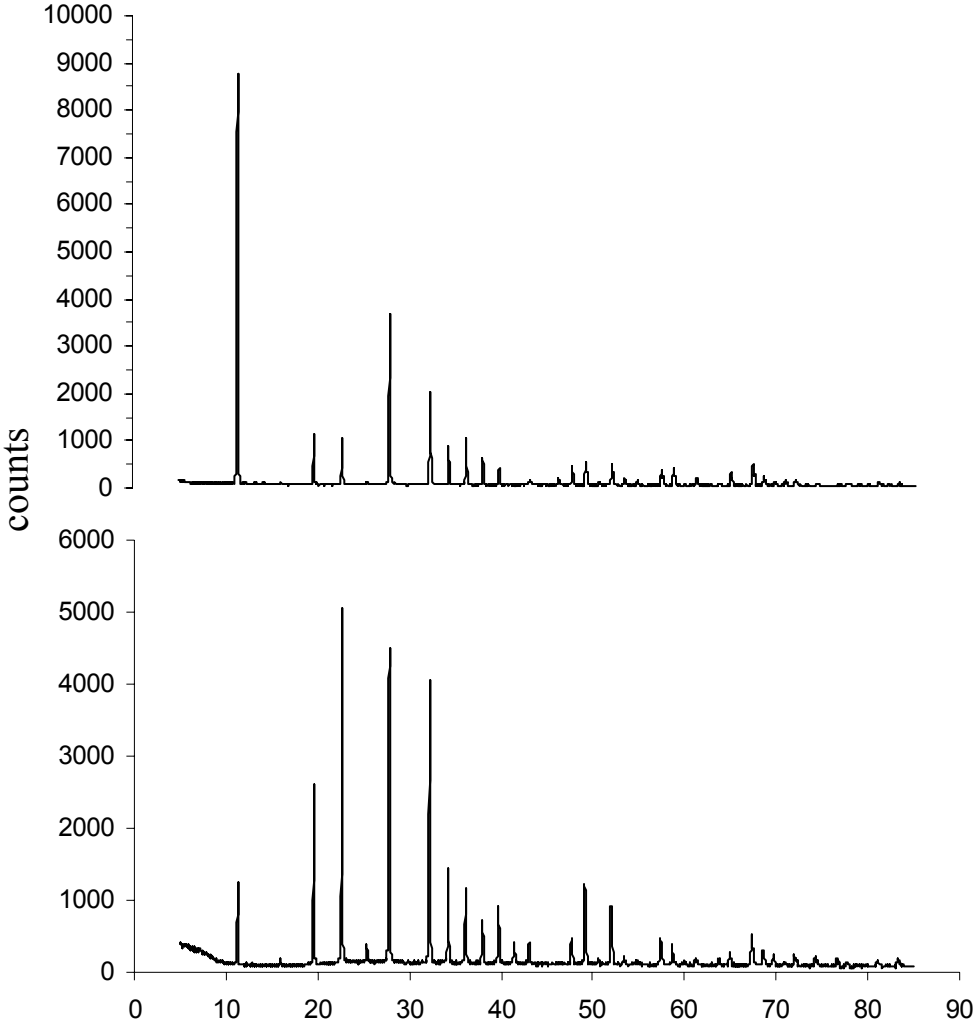

Figure 5.2. A typical X-ray diffraction powder patterns of the H-form (top) and the Cs-form (bottom) of germanium substituted pharmacosiderite phase (TSiGeP-24)

Table 5.1. Composition of Gel Precursors and Resultant Phases for Ti/Si/Ge Group

Preparation ID	Gel composition	Phase ID	Phase composition
DM3-35-1	TiO_2:0.75GeO_2:2.33SiO2: 10.73Cs_2O : 240.4 H_2O	TSiGeP-24*	$HCs_3(TiO)_{3.86}(GeO)_{0.14}(SiO_4)_{2.21}(GeO_4)_{0.82}$•4$H_2O$
DM3-34-2	TiO_2:1.40GeO_2:1.59SiO2: 10.53Cs_2O : 236.0 H_2O	TSiGeP-49	$HCs_3(TiO)_{3.72}(GeO)_{0.28}(SiO_4)_{1.53}(GeO_4)_{1.47}$•4.5$H_2O$
DM3-34-1	TiO_2:2.05GeO_2:0.66SiO2: 9.74Cs_2O : 218.0 H_2O	TSiGeP-74	$HCs_3(TiO)_{3.55}(GeO)_{0.45}(SiO_4)_{0.77}(GeO_4)_{2.21}$•5$H_2O$
DM3-37-1	TiO_2:3.08GeO_2: 11.28Cs_2O : 252.7 H_2O	TGeP-100	$HCs_3(TiO)_{3.55}(GeO)_{0.45}(GeO_4)_3$•4.5$H_2O$

*-indicates % of Ge substitution in tetrahedral site

Table 5.2. Composition of Gel Precursors and Resultant Phases for the Phases Synthesized in K-form

Preparation ID	Gel composition	Phase ID	Phase composition
DM4-13-2	1.0TiO_2:4.0 SiO_2:17.5 K_2O:416.0 H_2O	K-TSP	$HK_3Ti_4O_4(SiO_4)_3$ 4H_2O
DM4-41-1	0.8TiO_2:0.1 Nb_2O_5:4.0 SiO_2:17.5K_2O:416.0 H_2O	K-Nb-TSP	$HK_{2.2}Ti_{3.2}Nb_{0.8}O_4(SiO_4)_3$•4$H_2O$
DM4-48-1	1.0GeO_2:13.5KF:138.8H_2O	K-GeGeP	$HK_3Ge_4O_4(GeO_4)_3$•4H_2O

Table 5.3. Composition of H-forms Ti/Si/Ge Group of Phases

Preparation ID	Phase composition	Phase ID
DM3-35-1H	$H_{3.64}Cs_{0.36}(TiO)_{3.86}(GeO)_{0.14}(SiO_4)_{2.21}(GeO_4)_{0.82}$•7.2$H_2O$	H-TSiGeP-24
DM3-34-2H	$H_{3.62}Cs_{0.38}(TiO)_{3.72}(GeO)_{0.28}(SiO_4)_{1.53}(GeO_4)_{1.47}$•7.2$H_2O$	H-TSiGeP-49
DM3-34-1H	$H_{3.59}Cs_{0.41}(TiO)_{3.55}(GeO)_{0.45}(SiO_4)_{0.77}(GeO_4)_{2.21}$•7.0$H_2O$	H-TSiGeP-74
DM3-37-1H	$H_{3.65}Cs_{0.35}(TiO)_{3.55}(GeO)_{0.45}(GeO_4)_3$•7.1$H_2O$	H-TGeP-100

Table 5.4. Composition of Cs-exchanged for the Samples Synthesized in K-form

Preparation ID	Phase composition	Phase ID
DM4-13-2Cs	$HCs_{2.8}K_{0.2}Ti_4O_4(SiO_4)_3$ 4H_2O	KCs-TSP
DM4-41-1Cs	$HCs_{2.1}K_{0.1}Ti_{3.2}Nb_{0.8}O_4(SiO_4)_3$•4$H_2O$	KCs-Nb-TSP
DM4-48-1Cs	$HCs_{1.77}K_{1.23}Ge_4O_4(GeO_4)_3$•4$H_2O$	KCs-GeGeP

followed by 10 mL of 10 M KOH solution and 20 mL of 1.06 M $SiO_2.nH_2O$ (Fisher) solution in 3 M KOH. The mixture was vigorously stirred for 15 minutes followed by the addition of 5 mL of 10 M KOH solution. It was placed in Teflon lined stainless steel pressure vessel and heated in an oven at 200^oC for 7 days.

Synthesis of K-NbTSP: A total of 0.34 g (1.25 mmol) of $NbCl_5$ (Aldrich) was mixed with 10 mL of ddi water and 1.4 g of titanium isopropoxide (TIP, Alfa Aesar) in a plastic beaker. Similar to the synthesis for K-TSP, 5 mL of 30% H_2O_2 was added under constant stirring followed by 10 mL of 10 M KOH solution and 20 mL of 1.06 M $SiO_2.nH_2O$ (Fisher) solution in 3 M KOH. Mixture was sealed and heated in the oven at 210 ^oC for 10 days.

Synthesis of K-GeGeP: Pure germanium pharmacosiderite was synthesized by adding 0.41 g of GeO_2 (Alfa Aesar) to 10 mL of 5.4 M KF solution under constant stirring. To this mixture 6 mL of 0.5 M urea solution was added. The resulting mixture was stirred for 15 minutes, sealed, and then placed in an oven at 200^oC for 4 days.

Products obtained after hydrothermal reaction in each of the above three syntheses were treated likewise: the pressure vessel was cooled to RT; solid was separated by filtration, rinsed with ddi water and pure ethanol and dried in air at 55 ^oC. Cesium forms of samples were prepared by ion exchange as described below. Gel composition of the precursors and stoichiometric formulas of obtained products are given in Table 5.2. Chemical compositions of phases prepared by ion-exchange are shown in Tables 5.3-5.4.

Analytical and instrumental. The composition of the Ti/Ge/Si phase was determined by pressed-pellet microprobe analysis using a Cameca 5-50 electron microprobe at an accelerating voltage of 15 kV and operating with a beam current of 20 mA using a wavelength-dispersive spectrometer (WDS). Calculation of the chemical compositions of the non-hydrated phase, $HCs_xH_{3-x}(TiO)_y(GeO)_{4-y}(SiO_4)_z(GeO_4)_{3-z}$ was based on the idea that Ti occupies only octahedral sites, and Si occupies tetrahedral. Germanium was distributed between tetrahedral and octahedral sites so that the atomic ratios were equal to those obtained from microprobe analysis. The water content was

determined by thermogravimetric analyses (TGA) conducted on a TA 950 unit at a heating rate of 10 ^{o}C/min. Alternatively, the compositions and water content was verified through Retvield refinement of the phases.

The compositions of the K-TSP, K-NbTSP, and K-GeGeP phases and its cesium loaded forms were determined in a similar fashion. The ratios of Cs to K were determined from Atomic Adsorption (AA) analysis by dissolving a 0.04 g of the phase in diluted HF. In addition, the microprobe analysis of the phases was conducted similarly to the above procedure. The amount of water was derived based on combined TGA and Rietveld refinement studies.

5.2.2. Ion exchange

Preparation of phases for structural investigation. All the four Ti/Ge/Si phases (Table 5.1) were converted to the H-form by shaking about 2 g of dry solid with 100 mL of 1 M HNO_3 for 6.5 hours, after filtration the solid was again shaken with 100 mL of 0.25 M HNO_3 for 11.5 hours. The final product was separated by filtration, washed with ddi H_2O and ethanol and dried in an oven at 55 ^{o}C. Chemical compositions of acid treated phases are shown in Table 5.3.

Cs-forms of K-TSP, K-NbTSP, and K-GeGeP were obtained by ion-exchange from the K-forms (Table 5.2). Generally, about 0.5 g of dry solid was shaken with 100-130 mL of 0.1 M solution of soluble salt of Cs for 18 hours. The solids obtained were separated by filtration, rinsed with ddi H_2O and ethanol and dried in an oven at 55^{o}C (see Table 5.4 for composition).

Ion-exchange studies. The K-TSP, K-NbTSP, and K-GeGeP phases were tested for cesium removal in alkaline simulated solution. The prepared solution was traced with ^{137}Cs so that the count rate was about 4000-5000 cpm/mL. A total of 100 mL of this solution was introduced to 40 mg of dry ion-exchanger in a 250 mL plastic bottle and agitated on a Barnstead Labline shaker. The suspension was sampled after appropriate periods of time to assess the kinetics of Cs ion removal. The sampled suspension (0.8

mL) was filtered through Millex® 13 mm Syringe Filter with 0.2 μm PVDF (polyvinylidene fluoride) membrane and filtrate (0.5 mL) was counted on Wallac 1450 Liquid Scintillation Counter (LSC). The distribution constant at time t (K_{dt}, mL/g) was calculated using equation:

$$K_{dt} = \frac{A_0 - A_t}{A_t} \times \frac{V}{m}, \qquad (5.1)$$

where,

A_t –count rate (cpm/mL) of a filtrate at time t, A_0 – initial count rate (cpm/mL), V-total volume of solution (mL), m-mass of the inorganic ion-exchanger (g).

A batch technique was used to determine the distribution coefficients for proton forms of Ti/Ge/Si phases. In general, about 40 mg of dry ion exchanger was equilibrated on an orbital shaker with 10 mL of solution for 48 hours. The remaining count rate of the filtrate was measured on the LSC and K_d values (mL/g) were calculated using the equation given above.

5.2.3. X-ray Powder Diffraction Data Collection, Structure Solution, and Rietveld Refinement

The samples were packed into a flat plastic or aluminum sample holder and data were acquired in the Bragg-Brentano geometry at room temperature. Two X-ray sources were utilized: for some samples a Bruker-D8 advanced computer-automated X-ray diffractometer operating at 40 kV and 40 mA was used and for some others a Rigaku RU-200 automated powder diffractometer operating at 50kV and 180 mA was used. Both diffractometers have a copper target. The same step size of 0.02^o but count times of 60 s/step and 15 s/step were used in Bruker-D8 and Rigaku, respectively. Atomic positions reported for the framework atoms of cubic and tetragonal TS-Ps were used to model and refine the framework cations of the mixed metal TS-Ps reported in this study.[58,66] In each case the individual site occupancies for the disordered framework Ti/Ge, Ti/Nb and Ge/Si atoms.

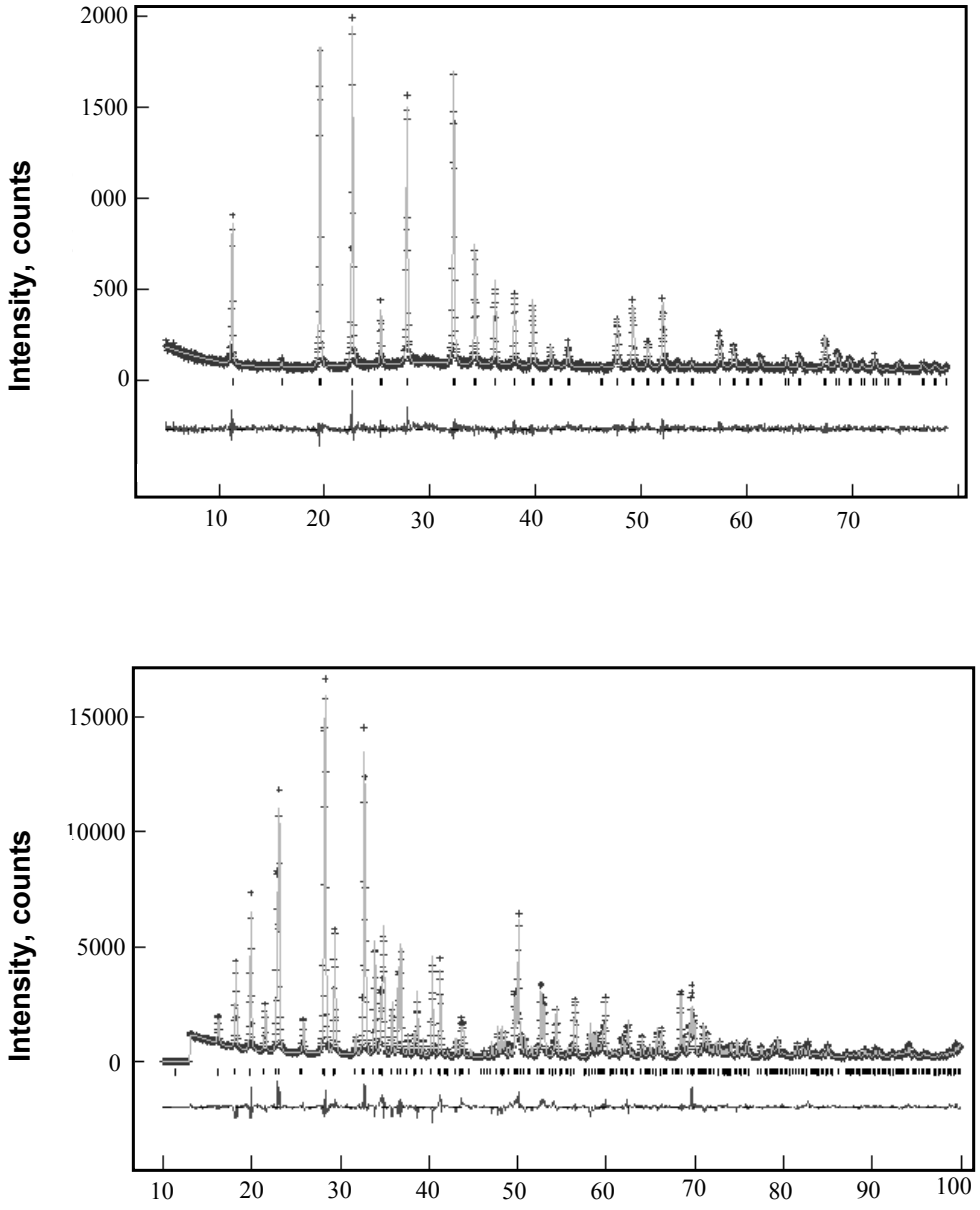

Figure 5.3. Observed (+) and calculated (—) X-ray powder diffraction profiles of KCs-NbSP (top) and KCs-GeGeP (bottom). The top data set was collected on Bruker-D8 diffractometer, whereas the bottom data set is from Rigaku RU-200 diffractometer

were set equal to the ratio determined from the electron microprobe analysis (EPMA) and their sum was constrained to a value equal to 1. The positions of Cs^+ and K^+ ions and water molecules in each of the structures were obtained from difference Fourier maps, followed by Rietveld refinement of the full patterns. The atomic positions of the framework atoms were refined with soft constraints consisting of bond distances, Ti/Nb/Ge-O = 2.00(2) Å for $Ti^{IV}/Nb^{V}/Ge^{IV}$ octahedra, Si-O = 1.63(2) Å for Si tetrahedra and Ge-O = 1.75(2) for Ge tetrahedra. Non-bonded distances of 2.66(2) Å and 2.85(2) Å were used to constrain O-O atoms in the silicate and germanate tetrahedra, respectively. No bond distance constraints were applied for the refinement of alkali metal cations and water oxygen positions.

During the final cycle of refinement the occupancies of K^+, Cs^+ and water molecules were fixed close to the values calculated on the basis of EPMA and TGA. The refinement results showed that the cations and the lattice water molecules in these phases exhibited relatively larger thermal parameters, possibly due to disorder or partial occupancy. Observed and calculated X-ray powder diffraction profiles for selected phases are shown in Figure 5.3. Results of X-ray powder data collection and Rietveld refinement are shown in Tables 5.5-5.6. Refined fractional atomic coordinates and occupancy factors of nonframework atoms for the Ti/Si/Ge phases are shown in Table 5.7. Table 5.8 summarizes selected interatomic distances for the Ti/Si/Ge. The results for the Nb-substituted and Nb-free phases synthesized in K-form are presented in similar order: refined fractional atomic coordinates and occupancy factors of nonframework atoms are shown in the Table 5.9, selected interatomic distances are shown in the Table 5.10 including the data for KCs-GeGe-P phase. Refined fractional atomic coordinates and occupancy factors of atoms for KCs-GeGe-P phase are shown separately in Table 5.11 due to the change in the symmetry.

Table 5.5. XRD Powder Data Collection and Rietveld Refinement Results for Ti/Ge/Si Pharmacosiderite Phases

`	TSiGeP-24	TSiGeP-49	TSiGeP-74	TGeP-100
Symmetry/ SG	Cubic/$P\bar{4}3m$	Cubic/$P\bar{4}3m$	Cubic/$P\bar{4}3m$	Cubic/$P\bar{4}3m$
Cell constant (Å)	a = 7.8577(2)	a = 7.9000(2)	a = 7.9306(2)	a = 7.9769(4)
Volume (Å^3)	485.17(3)	493.05(2)	498.80(4)	507.57(2)
Z	1	1	1	1
R_P	0.0791	0.0768	0.0720	0.0848
χ^2	1.885	1.403	1.601	2.019
R_F	0.0904	0.1076	0.0780	0.0918
R_{WP}	0.1019	0.100	0.0867	0.1107
Sample	H-TSiGeP-24	H-TSiGeP-49	H-TSiGeP-74	H-TGeP-100
Symmetry/ SG	Cubic/$P\bar{4}3m$	Cubic/$P\bar{4}3m$	Cubic/$P\bar{4}3m$	Cubic/$P\bar{4}3m$
Cell constant (Å)	a = 7.8773(2)	a = 7.9275(2)	a = 7.9757(2)	a = 8.0237(2)
Volume (Å^3)	488.80(4)	498.21(3)	507.34(2)	516.57(6)
Z	1	1	1	1
R_P	0.0937	0.1028	0.0966	0.1013
χ^2	1.685	2.574	1.847	1.989
R_F	0.1052	0.1127	0.1082	0.1071
R_{WP}	0.1184	0.1293	0.1293	0.1341

Table 5.6. XRD Powder Data Collection and Rietveld Refinement Results for Ti/Si, Ti/Nb/Si, All Ge Pharmacosiderite Phases

Phase	K-TS-P	K-NbTS-P	K-GeGe-P*
Symmetry/ SG	Cubic/$P\bar{4}3m$	Cubic/$P\bar{4}3m$	Cubic/*I23*
Cell constant (Å)	7.7647(5)	7.7937(2)	15.418(8)
Volume (Å^3)	468.14(5)	473.40(4)	3665.1
Z	1	1	8
R_P	0.0907	0.0948	R = 0.090
χ^2	6.389	4.684	
R_F	0.1304	0.1403	
R_{WP}	0.1180	0.1216	
Phase	KCs-TS-P	KCs-NbTS-P	KCs-GeGe-P
Symmetry/ SG	Cubic/$P\bar{4}3m$	Cubic/$P\bar{4}3m$	Tetragonal/$P\bar{4}b2$
Cell constant (Å)	7.8416(3)	7.8622(12)	a = 10.9311(1); c = 7.7993(1)
Volume (Å^3)	482.20(2)	486.0(3)	931.94(5)
Z	1	1	2
R_P	0.0999	0.0897	0.0792
χ^2	3.14	1.896	2.356
R_F	0.1125	0.0648	0.1107
R_{WP}	0.1300	0.1092	0.1029

* Crystallographic data reported by Bialek and Gramlich [67]

Table 5.7 Refined Fractional Atomic Coordinates and Occupancies for Non Framework Atoms for Cs/Ti/Ge/Si Pharmacosiderite Phases

Atoms/Site	Phase	TSiGeP-24	TSiGeP-49	TSiGeP-74	TGeP-100	H-TSiGeP-24	H-TSiGeP-49	H-TSiGeP-74	H-TGeP-100
Cs1/ 6(g)	x = y	0.5	0.5	0.5	0.5	0.5	0.5	0.5	0.5
	z	0.0644(4)	0.0625(4)	0.0559(4)	0.0586(5)	0.0440(20)	0.0518(16)	0.0504(15)	0.0555(15)
	Occupancy	0.5	0.5	0.5	0.5	0.06	0.064	0.07	0.058
Ow1/4(e)	x = y= $\bar{z}$	0.3424(12)	0.3366(12)	0.3228(11)	0.3321(14)	0.3119(8)	0.3104(9)	0.3076(9)	0.3037(10)
Ow2/ 1(b)	x = y = z	0.5	0.5	0.5	0.5	0.5	0.5	0.5	0.5
	Occupancy		0.5	1.0	0.5	0.56	0.6168	0.52	0.5
Ow3*/ 6(g)	x = y	n/a	n/a	n/a	n/a	0.5	0.5	0.5	0.5
	z	n/a	n/a	n/a	n/a	0.0440(20)	0.0518(16)	0.0504(15)	0.0555(15)
	Occupancy	n/a	n/a	n/a	n/a	0.44	0.436	0.43	0.44

*Disordered with Cs1

Table 5.8 Selected Interatomic Distances (Å) and Angles (degrees) in Cs/Ti/Ge/Si Pharmacosiderite Phases

Phase	Cs-TS-P*	TSiGeP-24	TSiGeP-49	TSiGeP-74	TGeP-100	H-TSiGeP-24	H-TSiGeP-49	H-TSiGeP-74	H-TGeP-100
Cs1-O1x4	3.143(3)	3.124(5)	3.141(5)	3.163(5)	3.165(6)	3.193(6)	3.195(7)	3.196(6)	3.238(7)
Cs1-O1x4	3.408(2)	3.426(4)	3.440(4)	3.430(4)	3.457(4)	3.392(8)	3.434(7)	3.438(6)	3.502(7)
Average	3.125	3.275	3.290	3.296	3.311	3.292	3.314	3.317	3.37
Cs1-Ow1x2	2.820(2)	2.799(3)	2.831(3)	2.903(3)	2.889(3)	2.974(11)	2.953(9)	2.987(9)	2.988(9)
Cs1-Ow1x2	3.624(3)	3.644(3)	3.643(3)	3.601(3)	3.647(3)	3.500(12)	3.573(10)	3.586(9)	3.642(9)
Average	3.222	3.221	3.237	3.252	3.268	3.237	3.263	3.286	3.315
Cs1-Ow2		3.422(3)	3.455(3)	3.522(3)	3.521(4)	3.592(16)	3.553(12)	3.586(12)	3.567(12)

*Cs-TS-P = $HCs_3Ti_4O_4(SiO_4)_3.4H_2O$; reported by Behrens et al[66]

Table 5.9. Refined Fractional Atomic Coordinates for Ti/Si and Ti/Nb/Si Pharmacosiderite Phases

Atoms/Site	Phase	K-TS-P	K-NbTS-P	KCs-TS-P	KCs-NbTS-P
K1* / 6(g)	x = y	0.5	0.5	0.5	0.5
	z	0	0	0	0
	Occupancy	1	0.73	0.07	0.03
	U_{ISO} (Å^2)$^{\#}$	0.130(4)		0.0332(9)	0.054(9)
Cs1/ 6(g)	x = y			0.5	0.5
	z			0.0571(3)	0.078(20)
	Occupancy			0.465	0.24
Ow1/ 4(e)	x = y	0.3232(12)	0.3158(7)	0.3297(9)	0.310(7)
	z	0.6768(12)	0.6842(7)	0.6703(9)	0.690(7)
Ow2/ 4(e)	x = y = z			0.5	0.5

*Disordered with Cs2 in KCs-NbTS-P

Table 5.10. Selected Interatomic Distances (Å) in Ti/Si and Ti/Nb/Si Pharmacosiderite Phases

Atoms	K-TS-P	K-NbTS-P	KCs-TS-P	KCs-NbTS-P	Atoms	KCs-GeGe-P
Cs1-O1x4			3.136(4)	3.130(18)	Cs1-O1x2	3.277(9)
Cs1-O1x4			3.401(3)	3.49(7)	Cs1-O2x2	3.183(8)
Cs1-Ow1x2			3.573(2)	3.71(13)	Cs1-O4x2	3.302(11)
Cs1-Ow1x2			2.852(2)	2.79(10)	Cs1-O4x2	3.236(10)
Cs1-Ow2			3.473(2)	3.32(16)	Cs1-Ow1x2	3.194(9)
Cs2-O1x8				3.2574(13)	Cs1-Ow1x2	3.400(10)
Cs2-Ow1x4				3.225(9)	K1-O1x4	3.378(10)
K1- O1x8	3.219(9)	3.241(3)	3.240(3)		K1-O2x4	2.924(10)
K1-Ow1x4	3.172(7)	3.190(7)	3.201(2)		K1- Ow1x4	3.036(11)

Table 5.11. Refined Fractional Atomic Coordinates for KCs-GeGe-P

Atom	Site	*x*	*y*	*z*
Ge1	*8i*	0.1379(2)	-0.0063(2)	0.1399(3)
Ge2	*4g*	0.2670(1)	0.2329(1)	0
Ge3	*2c*	0	0	0.5
O1	*8i*	0.1431(6)	0.2458(8)	-0.1428(10)
O2	*8i*	0.2671(9)	0.0990(5)	0.1218(10)
O3	*8i*	0.1054(8)	-0.0204(12)	-0.1055(11)
O4	*8i*	-0.1264(3)	0.0194(11)	0.3676(5)
Cs1	*4h*	0.2955(1)	0.2045(1)	0.5
K1	*2b*	0.5	0	0
Ow1	*8i*	0.3376(10)	-0.0501(8)	0.6921(13)

5.3. Results

5.3.1. Ion exchange studies

Complications in the remediation of nuclear waste accumulated at the DOE sites results from high alkalinity (up to 1-3 M NaOH) and high ionic strength of the solutions (up to 5-6 M Na^+). The ion-exchange process for the target ion M^+ in the H-form of TS-P can be described by reactions (5.2a) and (5.2b):

$$M^+ + \overline{HZ} \leftrightarrows \overline{MZ} + H^+ \qquad (5.2a)$$

$$H^+ + OH^- \leftrightarrows H_2O\,. \qquad (5.2b)$$

Reaction (5.2a) is followed by the formation of water: protons, liberated from the ion-exchanger, $\overline{HZ}$, combine with hydroxide ions present in the solution shifting the equilibrium to the products side. Thus, the samples were pretreated with acid and used in H-form for ion exchange experiments.

The Ti/Nb/Ge/Si phases were tested in a number of simulants with various compositions. Satisfactory performance was not observed in any of the phases for solutions consisting of 0.015 M KNO_3, 0.00014 M CsCl, and up to 5.6 M Na^+. This solution closely matches the composition of a tank waste at the Savannah River site. No appreciable difference in Cs^+ concentration was observed after 100 mL of such a solution was treated with 40 mg of ion-exchanger for 72 hours. For a comparative ion-exchange study solutions with lower ionic strength were prepared. In Figure 5.4 cesium distribution coefficients for the Ti/Nb/Ge/Si phases are plotted against the time of agitation for a solution consisting of 0.05 M NaOH and 0.05 M $NaNO_3$. The plot indicates a better performance by K-NbTS-P compared to K-TS-P as the cesium K_d values obtained after 24 hours for K-NbTS-P are almost three times higher than K-TS-P. Although higher capacity is observed for K-NbTS-P, the kinetics of the removal is slower than that in K-TS-P. There is almost no increase in the K_d values for the non-niobium phase (K-TS-P) after 3 hours of agitation whereas in K-NbTS-P it increases by at least 50%. The inferior kinetics of the Nb-substituted phase can be explained by

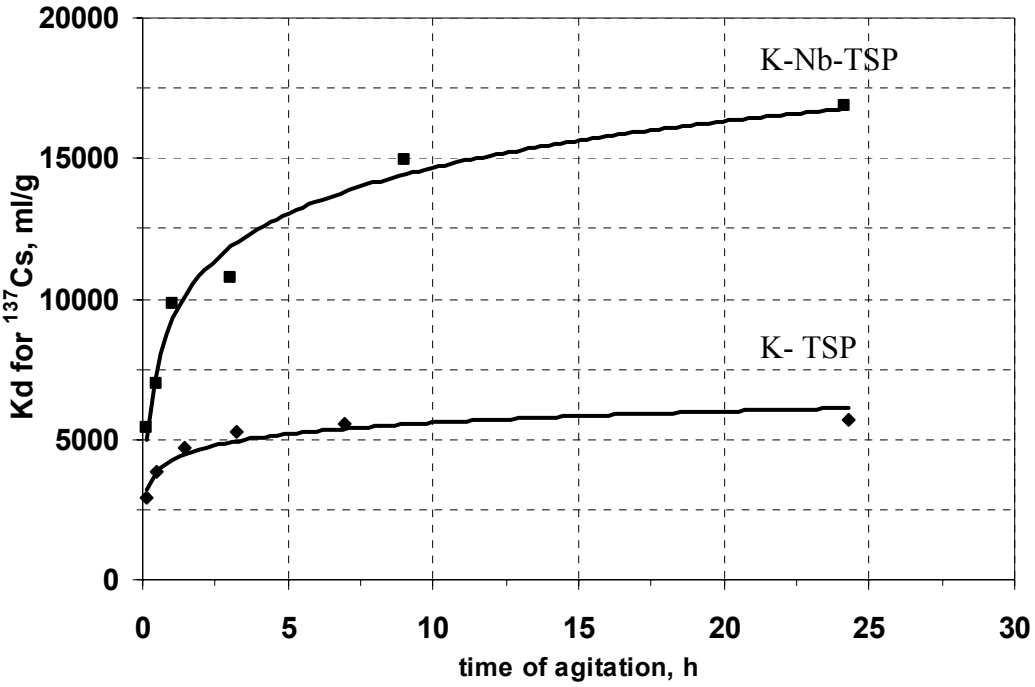

Figure 5.4. K_d values for Cs^+ uptake by K-TS-P and K-NbTS-P as a function of time. Negligible K_d values were observed for K-GeGe-P. Simulant composition: 0.05M NaOH, 0.05M $NaNO_3$, ^{137}Cs-trace

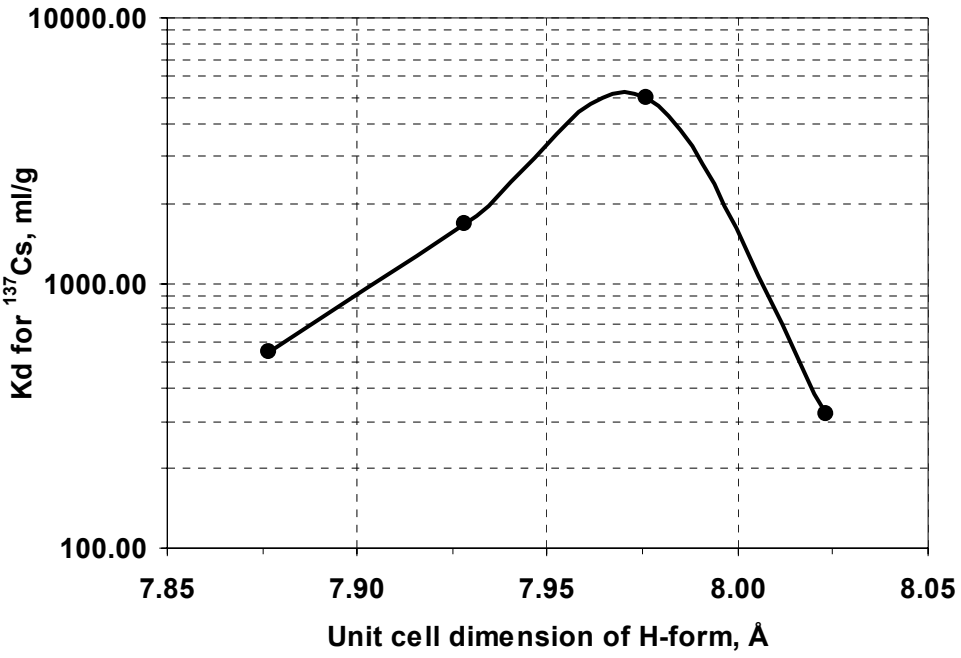

Figure 5.5. K_d values for H-TGeSiP-24, H-TGeSiP-49, H-TGeSiP-74, H-TGeP-100 as a function of unit cell dimensions. The unit cell dimension increase from sample 24 to 100. Simulant composition is the same as in Figure 5.4

slower diffusion of Cs to (½, ½, ½) sites (see discussion section). No appreciable amount of cesium was removed by the K-GeGe-P sample.

The K_d values for Cs were also measured from the solution consisting of 0.05 M NaOH and 0.05 M $NaNO_3$ for Ti/Ge/Si phases. The best K_d values were observed for the H-TSiGeP-74 sample as shown in Figure 5.5. The K_d values for samples TSiGeP-24 and H-TGeP-100 are below 1000 mL/g compared to 1100 mL/g for TSiGeP-49.

5.3.2. Structure of various substituted forms: reasons for improved selectivity

The structure of TSP with composition $HM_3Ti_4O_4(SiO_4)_3 \cdot 4H_2O$ (M = Cs, K etc) and mineral sitinakite topology was described previously.[66,68] The structure is similar to the titanium silicate sitinakite, except the Ti_4O_4 clusters are connected through silica tetrahedra in all three crystallographic dimensions. Such connectivity results in a cubic unit cell with channels, forming a 3-dimensional network. Each face of a cube is formed by an 8-membered ring (8MR) opening with alternating silicon tetrahedra and titanium octahedra (Figure 5.6). Each cavity is filled by charge neutralizing extra framework cations that occupy sites in the center of the cube faces (symmetry $\bar{4}2m$), such as K^+ (½, ½, 0) or slightly displaced from the center (symmetry 2.*mm*), such as Cs^+ (½, ½, z) or close to the wall of the spherical cavities (symmetry *m*) such as Sr^{2+} (x, x, z) and water molecules. The K cation with a smaller ionic radius than Cs^+ usually occupies sites in the face centers with eight binding sites from silicate oxygen (O1) at about 3.234Å and four binding sites from the water oxygen at about 3.169Å. The Cs cations are disordered in the displaced sites on either side of the ideal face center positions and also have eight binding sites from silicate oxygen but there are two sets of bond lengths; one being shorter than 3.143 Å and other being longer than about 3.408 Å. Only two water molecules are bonded to Cs.

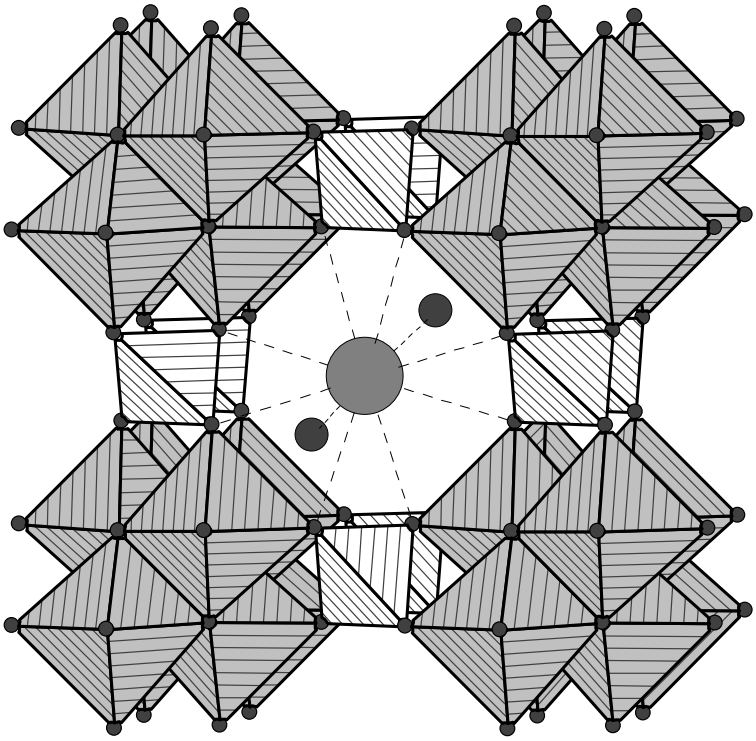

Figure 5.6. A polyhedral representation of the crystal structure of Cs-form of pharmacosiderite. Dark and light gray spheres in the eight ring channel represent water molecules and Cs^{+} cations respectively

Ti/Si/Ge phases. The idea has been posited that a more thermodynamically stable structure would form if Cs ions fit exactly in the middle of a face at (½, ½, 0), where it could ideally form eight equal bonds (3.5 Å) with framework oxygens.[58] One of the ways to achieve this is to increase the size of the cavity. By variation of gel compositions we have increased the unit cell dimensions of Cs forms by ≈ 0.12 Å and the diameter of the spherical 8MR opening by 0.048 Å from TSiGeP-24 to TSiGeP-100 (Table 5.7). The swelling of the channel is caused by germanium substituting for silicon in the tetrahedral sites. Though the Ge substitution of Ti in the octahedral site reduces the lattice parameter, it is offset by an overall increase in the lattice parameter due to a greater Ge substitution in the tetrahedral Si site. The increase of the pore size results in dislocation of the Cs cation towards the ideal site at the face center (Table 5.7). However, in the phase with full germanium substitution in tetrahedral sites, the cesium ion shifts back towards the center of the unit cell. Such a behavior can be correlated with possible interaction with water molecules.

Water contents in all the samples were derived from TGA studies in conjunction with refined occupancy obtained via the Rietveld refinement. The water molecule (Ow1) was observed in all four phases at the 4e site with 100% occupancy. In TSiGeP-49 through TSiGeP-100 phases, an additional water molecule (Ow2) with variable occupancy was observed at the center of the unit cell. Therefore, the cesium cations in all 4 phases had different coordination with water molecules. In TSiGeP-24, Cs1 has eight binding sites with framework oxygen (O1) and two with water molecules (Ow1) resulting in the usual ten coordinate complex. In the other phases, it has eight binding sites with framework oxygen (O1), two with water molecules (Ow1) and one with a half (TSiGeP-49 and TSiGeP-100) or fully (TSiGeP-74) occupied site (Ow2), which results in an eleven coordinate complex for TSiGeP-74 (see Figure 5.7) and a variable coordination between ten and eleven for TSiGeP-49 and TSiGeP-100. The average Cs-O1 bond lengths are 3.275, 3.290, 3.296, 3.311Å and average Cs-Ow1 bond lengths are 3.221, 3.237, 3.252 and 3.268 Å in TSiGeP-24 to 100, respectively (Table 5.8).

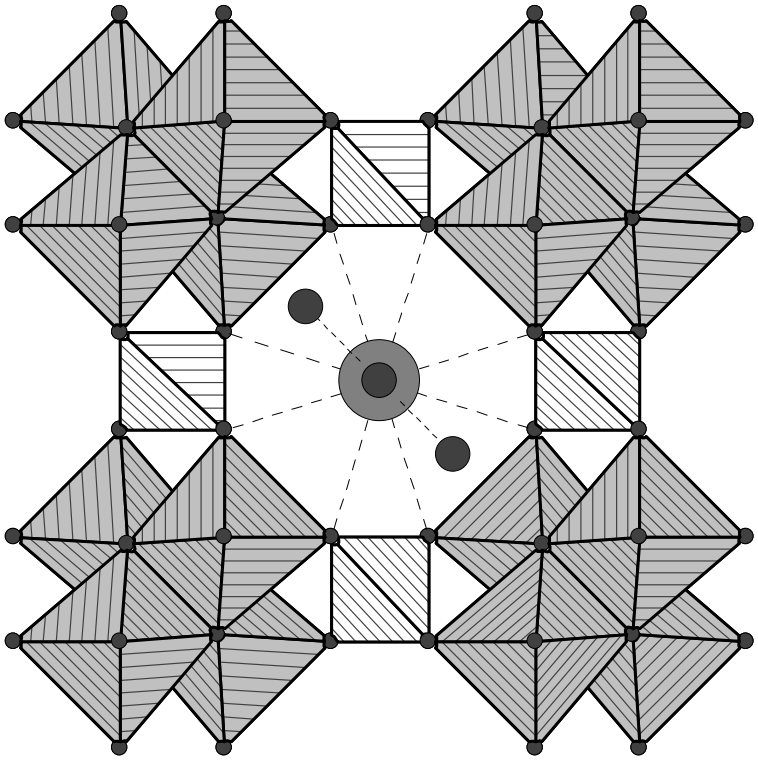

Figure 5.7. A polyhedral representation of the crystal structure of substituted pharmacosiderite along {001}. Dark and light gray spheres in the eight ring channel represent water molecules and Cs^+ cations respectively. Water molecule located above Cs^+ cation at (½, ½, ½) was observed.

The "as synthesized" Cs-forms were converted to H-forms by treatment with acid, as described in the experimental section. However, all Cs could not be exchanged for protons without destroying the structure in these compounds. The H-exchanged samples also indicated an increase of 0.146 Å in the unit cell dimensions from H-TSiGeP-24 to H-TSiGeP-100 while retaining the cubic symmetry and the space group, $P\bar{4}3m$ (Table 5.5). Each of the unit cell dimensions in the H-form samples is larger than the corresponding Cs-form due to an increase in hydration level. The Cs cations are disordered with water molecules, Ow3, at (1/2, 1/2, z). Water molecules (Ow2) with variable occupancy were also located at the center of the unit cell (½, ½, ½) besides the usual site for water (Ow1) at 3*m* (x, x, $\bar{z}$). Unlike. the case of TSiGeP-24, a water molecule was observed at (½, ½, ½) in H-TSiGeP-24.

K-forms of pharmacosiderite phases. In the second comparative study a 20% niobium substituted titanosilicate pharmacosiderite (K-NbTS) phase was prepared in K-form and its Cs^+ affinity was compared with titanosilicate (K-TS) and germanium germanate (K-GeGe-P). The K-GeGe-P crystallizes in the body-centered cubic supercell, defined in *I*23 (*a* = ~ 15.42 Å). The crystal structure of this all germanium form has been reported.[67] In K-TS-P and K-NbTS-P, a twelve coordinate K was observed with eight equal binding sites from framework oxygens (O1) and four equal binding sites from water molecules (Ow1) (Table 5.10). There are two different disordered sites for K in K-GeGe-P that have twelve and ten coordination with framework oxygen atoms and water molecules.[67]

The K-forms were converted directly to partially exchanged Cs forms via ion exchange. The exchanged KCs-GeGe-P resulted in a unit cell with tetragonal symmetry. Both the K and Cs cations form twelve coordinate complexes that include six bonds with framework oxygen and six bonds with water oxygen atoms in the Cs complex and eight bonds with framework oxygen and four bonds with water oxygen in the K complex. Potassium ions also form a twelve coordinate complex in KCs-NbTS-P and KCs-TS-P, however, they are disordered with Cs cations in KCs-NbTS-P13.

There is only one independent water position in KCs-GeGe-P while two water positions are observed in KCs-TS-P and KCs-NbTS-P. One of them is located at the center of the unit cell, (½, ½, ½), and the other site is close to the wall of the spherical cavities (x, x, z) (see Table 5.8).

4.4. Discussion

In Chapter VI we correlated an improved selectivity for cesium in Nb-substituted titanosilicate sitinakite with increased coordination of cesium ion within the tunnel. We pursued two approaches to modify pharmacosiderite. In the first approach, the size of the spherical 8MR was increased in a systematic way by modifying the gel composition so that the substitution of Ge for Si in the tetrahedral site is maximized and its substitution for Ti in the octahedral site is kept to a minimum. It was observed that as the unit cell increases Cs cations moves towards the ideal sites at the face center. However, in the phase with the largest unit cell, it is not in this desired position. On the contrary, it moves back closer to the center of the unit cell. The K_d values for ^{137}Cs from the partially H-exchanged samples indicated an increasing trend with the unit cell dimensions up to the third sample (H-TSiGeP-72) with unit cell dimension 7.9306(2) Å (Figure 5.5). The crystal structure of TSiGeP-72 revealed that Cs approaches closest to the ideal position (½, ½, 0.0559(4)) as shown in Figure 5.8. This position is more symmetrical compared to the other three samples in terms of Cs-O1 bonding distances. The two sets of four Cs-O1 bonds and two sets of two Cs-Ow1 are closest to each other (Table 5.9). It should be remembered that in the ideal site for Cs, the eight bonds to framework oxygen atoms and the four bonds to water oxygen are equal. However, we believe that it is the difference in the coordination environment around Cs that results in the different ion exchange behavior of these materials. In TSiGeP-24, there are four water molecules per formula unit resulting in a ten coordinate Cs complex with eight bonds to framework oxygen (O1) and two bonds to Ow1 for each of the split positions of Cs1.

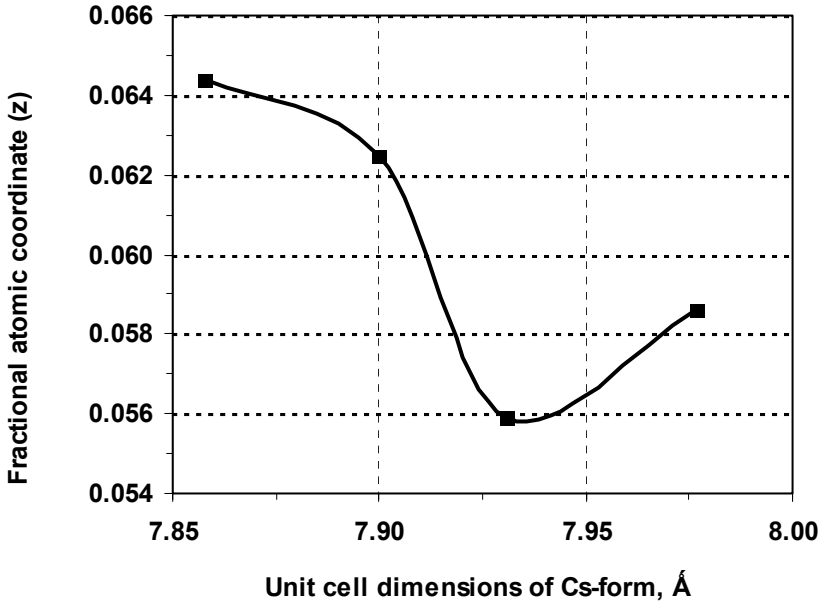

Figure 5.8. Fractional atomic coordinate (z) of Cs cation for Cs-forms of Ti/Si/Ge phases plotted against the unit cell dimensions of the phases

While in H-TSiGeP-72, there is an additional fully occupied water at (½, ½, ½) resulting in an eleven coordinate Cs complex. In H-TSiGeP-49 and H-TSiGeP-100, this $\bar{4}3m$ site is only half occupied thus a coordination number between ten and eleven can be assumed for the Cs cation in these two phases. The observed K_d values are consistent with different Cs coordination numbers.

In the second approach, a 20% Nb substituted titanosilicate pharmacosiderite sample was prepared and its K_d values were compared with pure germanium and titanosilicate phases. Our previous studies on the closely related structure of the 25% Nb substituted titanosilicate with sitinakite topology showed that the population of water vs. Na^+ in the channel adjusts to charge-balance the $Nb^{5+} \leftrightarrow Ti^{4+}$ substitution. This in turn modifies the coordination environment of Cs and hence its uptake by the exchanger. Higher K_d values for Cs were indeed observed for K-NbTS-P compared to K-TS-P while K-GeGe-P showed negligible K_d values. No change in Cs coordination number was observed for KCs-NbTS-P. Since K cations occupy the ideal site (½, ½, 0) in the center of spherical 8MR in K-TS-P, it could not be completely exchanged for Cs cations unlike the loosely fitting Na ions in the case of sitinakite which occupy sites close to the walls of the 8MR. The Nb substitution, therefore only results in a decrease in K occupancy at (½, ½, 0) and a stable model was obtained with disordered Cs/K cations at this site. Thus some Cs cations can be accommodated in the K sites due to a decrease in K cations in K-NbTS-P. The slow kinetics observed in K-NbTS-P can be correlated to slow migration of some Cs cations to this site. In KCs-TS-P a stable refinement could not be obtained with a disordered Cs/K model whereas negligible K_d values obtained in KCs-GeGe-P can be correlated to the ideally placed K1 cations that tightly fit in the 4*h* sites in the smallest 8MRs. In fact the negligible K_d values observed for this phase makes it an excellent candidate for K removal from tank waste simulants in the H-form. Among all the "as synthesized" K forms shortest K-O distances of 2.924 Å were observed in KCs-GeGe-P. Cs cations can only partially occupy sites with symmetry 2*b* to compensate for charge balance.

In general, we observed that in the case of the K-form of pharmacosiderite, it is difficult to remove all K from the ideal site (½, ½, 0) and the best K_d values are shown by Nb substituted samples which require less K due to overall charge balance in the compound.

5.5. Conclusions

We synthesized a range of compositions of materials with pharmacosiderite topology and studied their ion exchange properties. The origin of selectivity for Cs^+ cations in these phases has been correlated with the atomic structure. In the first set of mixed Ti/Ge/Si phases, the size of the 8-membered ring was systematically increased in order to shift the Cs cation as close as possible to the ideal site (½, ½, 0) that is usually occupied by the smaller K cations. This Cs movement in turn shifts the position of water molecules (Ow1) allowing enough space in the center of the channel (½, ½, ½) for another half (in TSiGe-49 and 100) or fully (in TSiGe-74) occupied water molecule (Ow2) to move in. The highest K_d values were observed in the phase that has Cs ions closest to the ideal site which results in the highest coordination number due to this additional water molecule at (½, ½, ½). In the phase that has Cs ion farthest from the ideal site, no additional water molecules were observed at (½, ½, ½). This site is too close to the fully occupied site with Ow1 molecules. In the case of Nb-substituted phases, better K_d values can be correlated with the decrease in charge balance requirement in the channels resulting from the substitution of Nb^{v} for Ti^{iv}. Upon Cs-exchange a disorder of Cs/K cations was observed in the Nb substituted sample in contrast to the non-Nb sample. It is difficult to remove K cations from the K-form of pharmacosiderites as they fit well in the ideal site with eight equal bonds with framework oxygen and four equal bonds with water molecules compared to the Na cations in the titanosilicate sitinakite.

CHAPTER VI
OPTIMIZING MONOSODIUM TITANATE AND SODIUM NONATITANATE FOR STRONTIUM REMOVAL

6.1. Introduction

In this Chapter, the ion-exchange properties of amorphous materials in particular monosodium titanate (MST) and sodium nonatitanate (SNT) and possible routes for optimization of their strontium removal capabilities will be discussed. Furthermore, decontamination properties of these materials will be compared with tunnel type titanosilicate, discussed in previous chapters.

The main limitation of current strontium and actinides separation stage of reprocessing technology at Savannah River Site is the insufficient ion-exchange capacity of the sorbents. Limited information is available on the mechanism of ion-exchange in amorphous materials. Taking into account the hypothesis that the nuclides are being sorbed on the surface we tried to improve the capacity by modification of the surface area. Modification of pore size and/or pore size distribution may increase the overall strontium and actinide capacity of the materials.

Mesoporous titania has received extensive attention because of its possible application in catalysis, separations, and applications in nanotechnology.[69-71] A great variety of methods for synthesizing of mesoporous titania was developed.[72,73] Sol-gel procedures carried out with the assistance of surface active substances (surfactants) as well as methods of direct precipitation from solution have received considerable attention since they resulted in mesoporous powders with high surface area.[74,75] Surfactants such as amines and polyethylene oxides with different molecular weights have been used to synthesize mesoporous titania with nanosized anatase walls[76] (amines) or hollow microspheres of mesoporous titania.[77]

Monosodium titanate is synthesized by slow hydrolysis of titanium isopropoxide in isopropanol media.[6,78] The baseline synthetic procedure received from Savannah

River Company was modified using template assisted precipitation. The effects of the template amount and synthetic variations on surface area, morphology and ion-exchange properties are discussed.

Another approach was chosen for sodium nonatitanate modification. Similarly to titanosilicate sitinakite (see Chapter III) the effect of crystallinity on ion-exchange properties was studied.

6.2. Experimental methods

6.2.1. Synthesis of monosodium titanate

General procedure. The synthesis procedure for monosodium titanate was received from Savannah River Company.[78] The stoichiometry for a baseline procedure can be described by the following reaction carried out in isopropanol:

$$2Ti(OC_3H_7)_4 + NaOCH_3 + 5H_2O = NaTi_2O_5H + CH_3OH + 8C_3H_7OH$$

Based on the above equation for 10g of solid the following amounts of chemicals were used:

30 mL of Titanium isopropoxide (TIP)

154.3 mL of Isopropanol (IP)

11.6 mL of 25% (4.4 M) of sodium methoxide (SM)

4.05 mL of deionized H_2O

The synthetic procedure was started with preparation of 120 mL of solution (Solution 1) having 65.3% (78 mL) of IP, 9.7% (11.6 mL) of SM solution and 25% (30 mL) of TIP in a plastic bottle. In a separate bottle, a total of 32.5 mL of solution 2 (87.5 % of IP, 12.5% H_2O by volume) was prepared by mixing 28.43 mL of IPA with 4.06 mL of ddi H_2O. The synthesis was carried out in a two neck 250 mL round bottom flask with a setup for reflux. A 0.5 mL of solution 2 was mixed with 47.5 mL of IP in round bottom

flask followed by 2.0 mL of solution 1. The solutions were charged below liquid level. The mixture was agitated for about 10 minutes to initiate the precipitation. Furthermore, the remaining 118 mL of solution 1 was charged at a rate of 4.0 mL/min and 32 mL of solution 2 was charged at a flow rate of 1.0 mL/min. Solutions were charged through polyethylene tubing using a peristaltic pump. The flow rate was set prior to the experiment by adjusting the speed of the pump with water.

After addition of both solutions the reaction was heated on an oil bath to 82^{o}C, refluxed for 1 hour, and cooled down. Excess alcohol was removed by successive decantation and addition of water. The slurry was transferred to a polyethylene bottle; ddi water was added to adjust the solid concentration to 10-20%, sealed and kept for further experiments.

Modified preparations. The monosodium titanate synthesis procedure was modified using the template approach. Two types of templates, hexylamine ($C_6H_5NH_2$) and tetraethylene glycol (TEG) were used.

Synthesis of MST-amine (DM4-46-1). The baseline procedure was modified in a following way:

1. A total of 26.5 mL (0.2 mol) of hexylamine (Aldrich) was added to solution 1

2. The cooled slurry received additional washing with 200 mL of IP, ddi water, 3 times with 200 mL of ethanol and 2 times with water.

Synthesis of MST-TEG-2 (Ti:TEG=1:2, DM4-48-2).

Modifications:

1. A total of 38.9 g of TEG was added to 47.5 mL of IP was placed into the round bottom flask prior to the addition of solution 1 and 2 to the round bottom flask.
2. The final slurry was washed twice with isopropanol, and once with ddi water.

In further synthesis the amount of reagents was decreased by half compared to the baseline procedure

Synthesis of MST-TEG-1 (Ti:TEG=1:1, DM5-261-1)

Modifications:

1. A total of 9.09 g of TEG was mixed with 23.7 mL of IP in a round bottom flask prior to addition of solutions 1 and 2
2. The final slurry was shaken with ddi H_2O for 2 days, and the pH of final slurry was adjusted using 10 M NaOH.

Synthesis of MST-TEG-0.3 (Ti:TEG=1:0.3, DM5-271-1)

Modifications:

1. In this preparation the composition of solution 2 was modified in the following way: 3.1 g of TEG was added to solution 2 to replace water, 2.2 mL of water was added to the reaction mixture later to trigger precipitation, after half of the solutions 1 and 2 were charged into the round bottom flask.
2. Final slurry was washed with isopropanol and water.

Synthesis of MST-TEG-0.29 (Ti:TEG=1:0.29, DM5-28-1)

Preparation:

The amount of chemicals was close to the one in the MST-TEG-0.3 preparation.

1. A total of 2.9 g of TEG was added to solution 2
2. The slurry was washed with isopropanol and ddi water

Synthesis of MST-TEG-0.58 (Ti:TEG=1:0.58, DM5-281-1)

The preparation was similar to MST-TEG-0.29, but more TEG was added:

1. 5.84 g of TEG was added to solution 2
2. Final mixture was washed with isopropanol, ddi water, pH was adjusted to 10 using 10 M NaOH.

6.2.2. Synthesis of sodium nonatitanates and mixtures of sodium titanate-titanosilicate

The SNT samples were synthesized by a hydrothermal technique from the gel with composition of 1.0 TiO_2 : 4.63 Na_2O : 120.0 H_2O at temperatures 165 – 180^oC. Time of hydrothermal treatment varied from 21 hours to 3 days.

In a typical procedure a source of titanium, usually TIP, was added to ddi H_2O under vigorous stirring. To this mixture, sodium hydroxide was added as a 50% solution

in water followed by addition of 30% H_2O_2 to transfer titanium into a soluble form. The resultant mixture was treated hydrothermally, or by reflux.

In a typical SNT-TS synthesis the gel with composition of $1.0TiO_2$:$1.98SiO_2$:$6.77Na_2O$:$218H_2O$ was prepared by mixing of 3.5 mL of titanium isopropoxide in 20mL of ddi H_2O, 8.5 mL of 10 M NaOH with 27 mL of 0.86 M silica solution in 2.6 M NaOH. The resulting mixture was treated hydrothermally at 200^oC for 10 hours. After heating, the final products in all reactions were treated in the following fashion: pressure vessels/reaction flasks were cooled down, the solid was separated by filtration, washed with ddi water converted to H-form by treatment with acidic solutions, with the exception of Na-SNT, which was washed only with ddi H_2O once. The preparations, sample names and other parameters are summarized in Table 6.1.

6.2.3. Characterizations

Surface area measurements. The surface areas of the MST and selected SNT phases were determined by adsorption of nitrogen. Sorption-desorption isotherms were obtained with a Quantachrome Autosorb-6 automated N_2 gas adsorption unit. Prior to the surface area measurements the slurry was filtered off, washed with ddi H_2O and alcohol, dried at 55 ^oC in air. Furthermore, the dried solids (0.2-0.6 g) were preheated at a 120 ^oC and then outgassed at 100 ^oC on the Quantachrome degasser at the pressure of 2×10^{-3} Torr. The isotherms were collected at 77 K and analyzed by the BET method. The micropore volume was determined by the DeBoer t-plot method, and the micropore distribution was calculated by the MP method.

Table 6.1. Summary of Synthetic Conditions of SNT Phases and Their Identifications

Prep ID	Phase ID	Temperature, ^{o}C	Time, h	Remarks
DM4-43-1	c-SNT	175	72	*c* stands for crystalline
DM4-45-1	c-SNT-w	175	72	w stands for washing
DM4-45-2	SNT-amine	175	72	Ti:amine=1:2
JD1-01-1A	Na-SNT	175	21	pH=12
JD1-01-1B	H-SNT	From Na-SNT	n/a	pH=6
DM5-44-2	SNT-IP	80, reflux	32	24 h reflux in IP, 8 h in NaOH
DM5-441-1	SNT-water	80, reflux	19	19 h reflux in NaOH solution
DM5-50-2	SNT-TS	200	10	Hydrothermal reaction

Table 6.2. Summary of MST Samples Synthesized for Strontium Removal

Prep. ID	Phase ID	Template	Slurrry pH	BET SA, m^2/g	Microporous SA, m^2/g	Sr Kd, mL/g
DM4-46-1	MST-amine	hexylamine	9.226	232	204.2	917000 at 23.2 h
DM5-261-1	MST-TEG-1.0	TEG	9.532	288	143	301000 at 24 h
DM5-27-1	MST	No template	9.26	458	178	336000 at 24 h
DM5-271-1	MST-TEG-0.3	TEG	10.085	219	97	308000 at 21.5h
DM5-28-1	MST-TEG-0.29	TEG	9.924	292	163	294000 at 24 h
DM5-281-1	MST-TEG-0.58	TEG	11.596	16	0	332000 at 21.5 h
00-QAB-417	Comm. MST*	as received	11.87	141	0	259598 at 22 h

* - Baseline MST

Scanning Electron Microscopy. The dried samples for SEM acquisition were coated with palladium-platinum alloy. The photographs were acquired using Leo VP1530 FE SEM scanning electron microscope.

Ion-exchange studies. Ion-exchange studies were carried out by a technique and under conditions described in Chapter III.

6.3. Results and Discussion

6.3.1. Monosodium titanate

MST samples, their identifications, and summary of surface area measurements are shown in Table 6.2. SEM images and corresponding nitrogen adsorption isotherms are shown in Figure 6.1. Kinetics of strontium removal from highly alkaline simulant is shown in Figure 6.2.

It should be noted that the N_2 isotherms of MST samples are not uniform. The amine templated sample had a high surface area with most of the pores in the micropore (under 20Å) range. It also had the highest strontium uptake (Figure 6.3). The isotherm (Figure 6.2, top) is a Type I indicative of a microporous material.[49] The increase in volume at the high pressure end of the isotherm indicates the filling of large pores with N_2. The SEM photograph shows that particle size is small with relatively large pores formed by particle aggregates. Sample MST-TEG-1.0 has similar isotherm but the upward bend at ~0.4 P/P_0 indicates a broad distribution of mesopores (20-500Å). In fact, roughly half the large surface area is present as larger pores or as external surface.

The sample with no template had the highest surface area and an isotherm (Figure 6.1) that illustrates the presence mainly of mesopores. This fact is in agreement with the bulk of the pores, 61%, being larger than micropores. The particles aggregate into spherical agglomerates that are larger than those of the other samples.

MST-amine

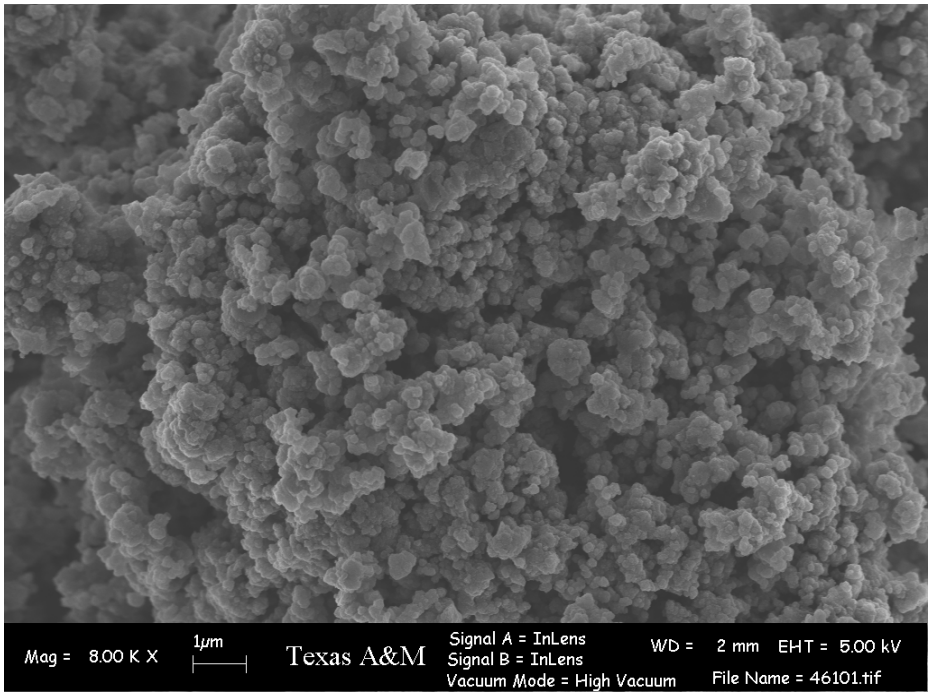

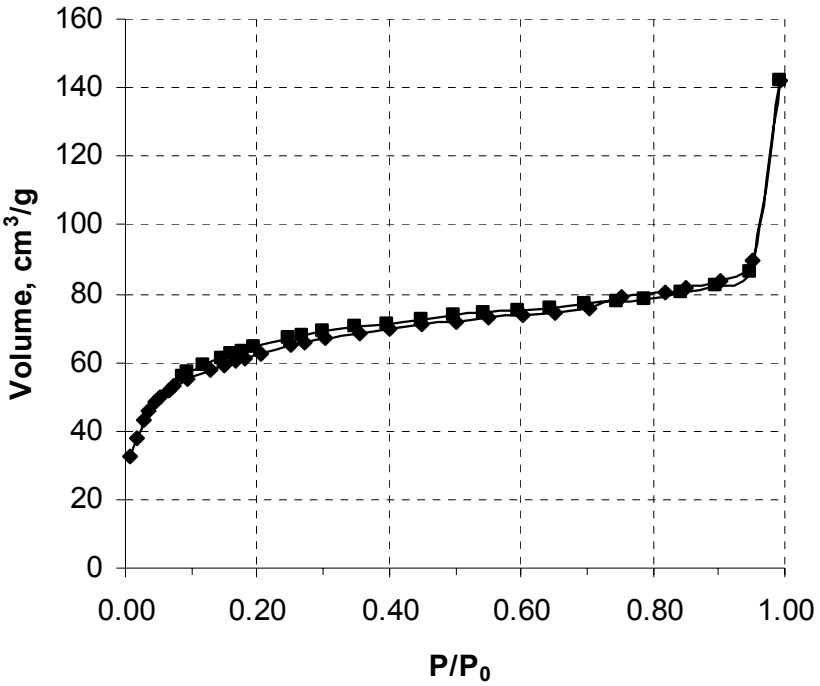

Figure 6.1. SEM images (top) and nitrogen adsorption isotherms (bottom) of MST samples. See Table 5.2 for surface area data and experimental section for synthetic procedures

MST-TEG-1

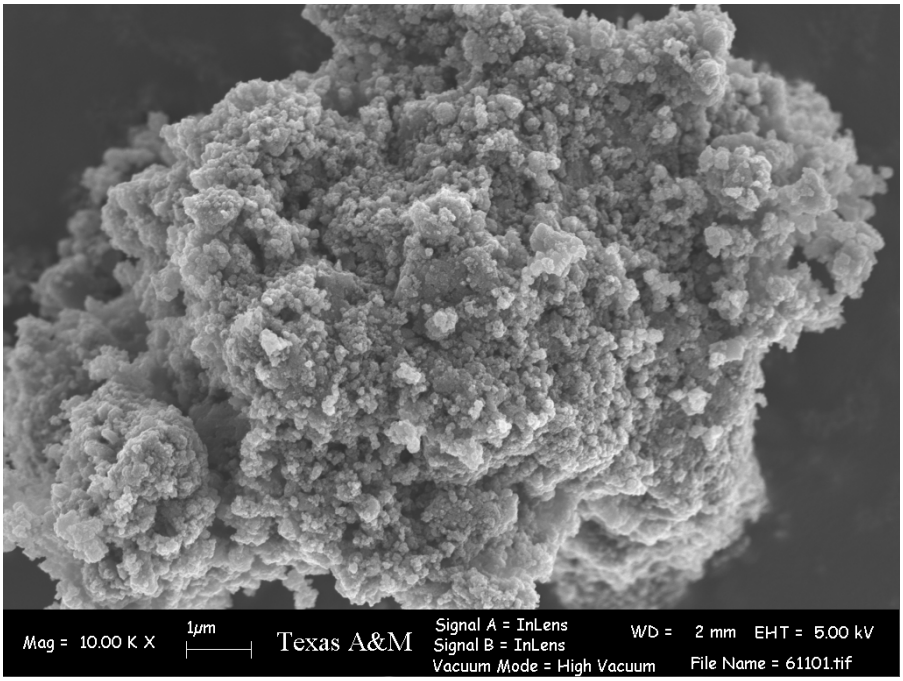

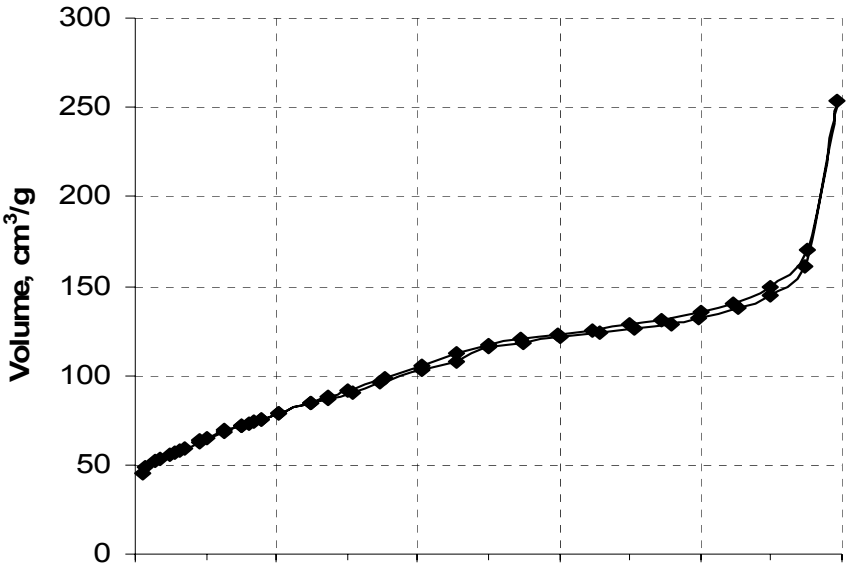

Figure 6.1. (Continued)

MST (no template)

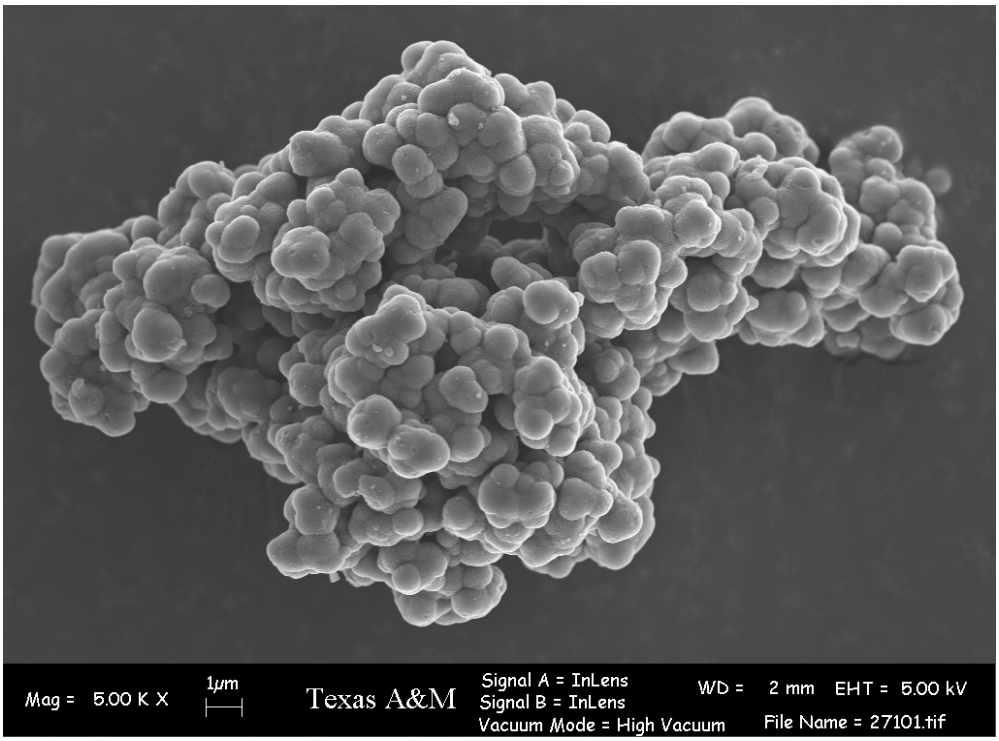

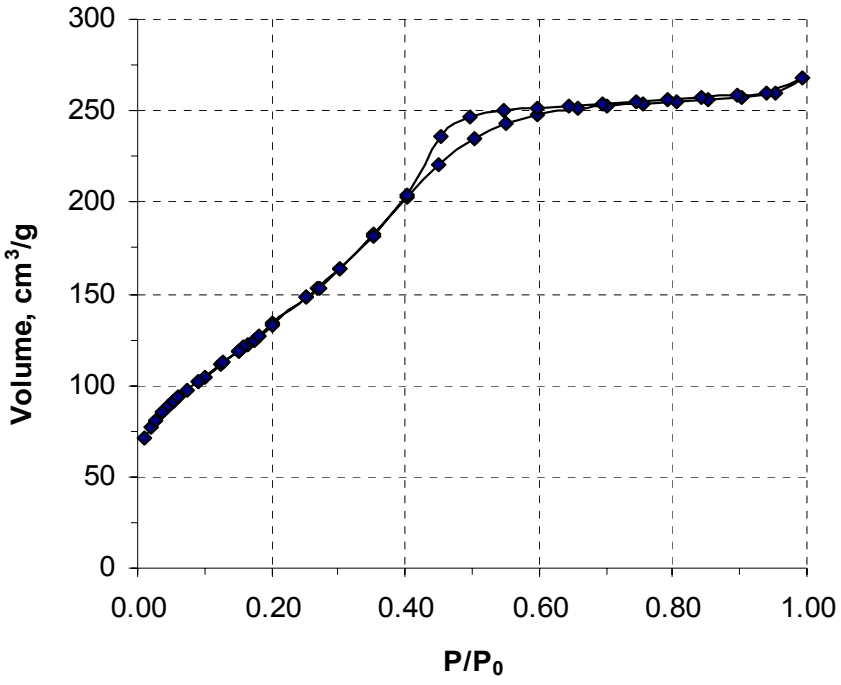

Figure 6.1. (Continued)

MST-TEG-0.3

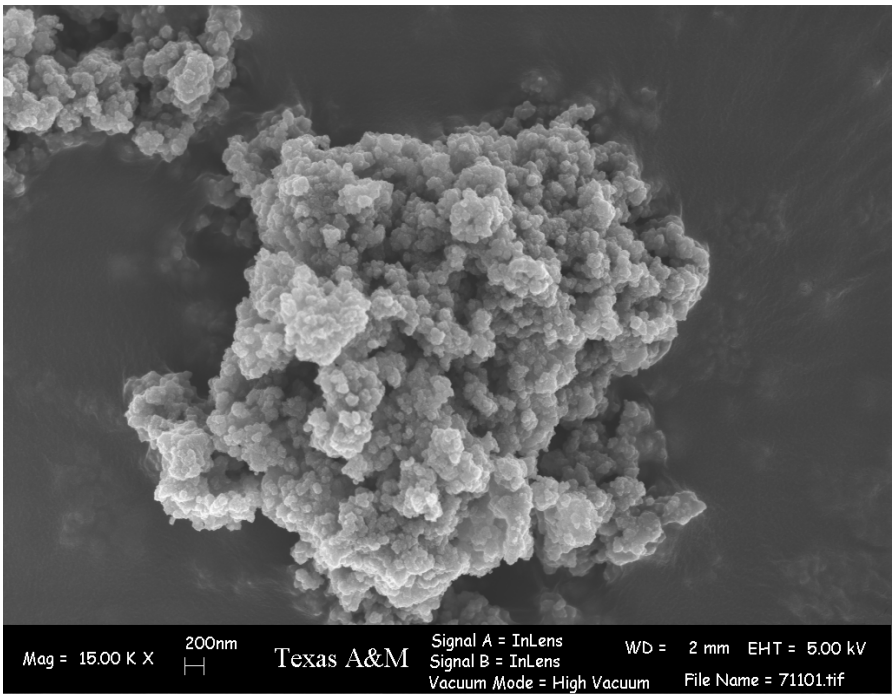

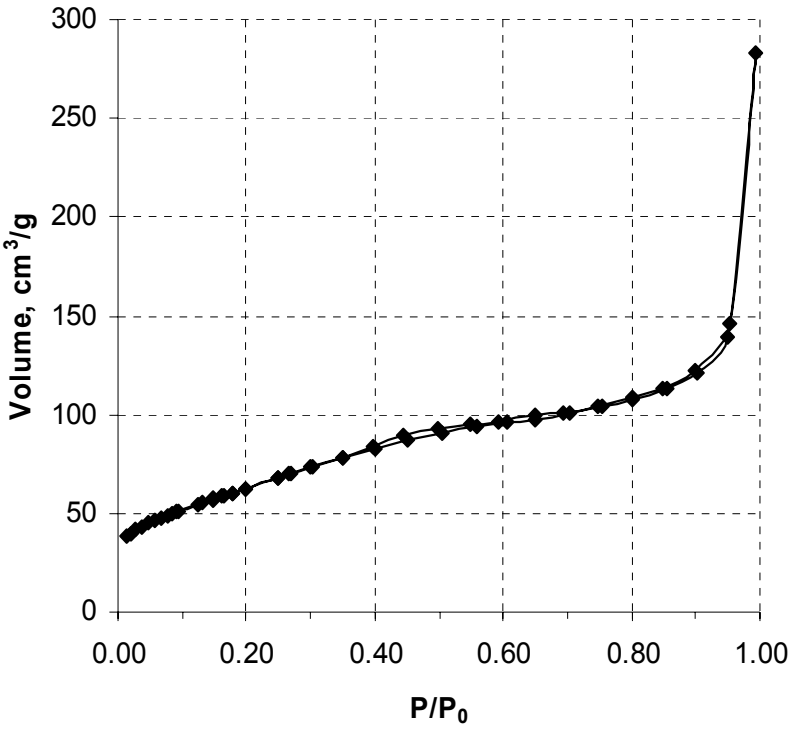

Figure 6.1. (Continued)

MST-TEG-0.29

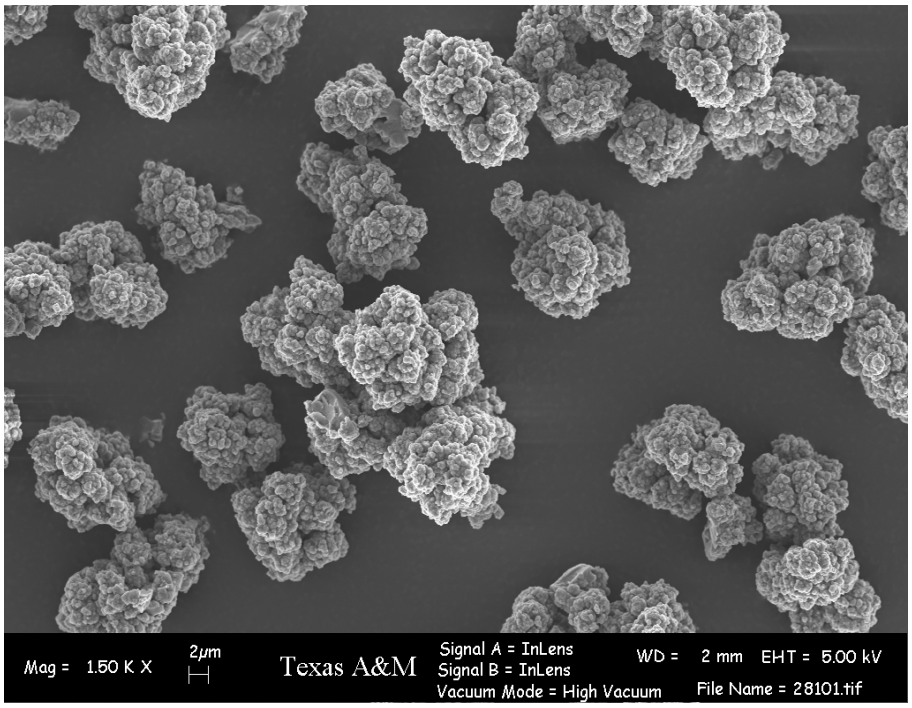

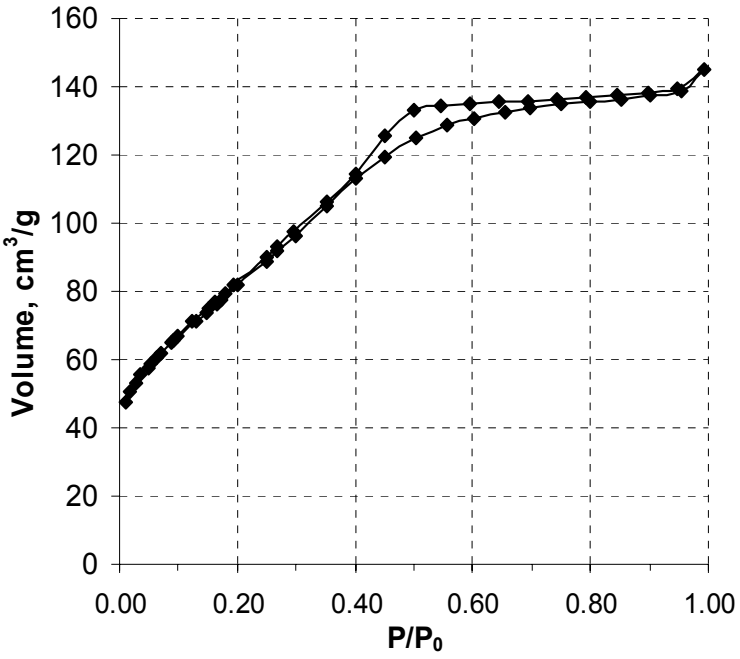

Figure 6.1. (Continued)

MST-TEG-0.58

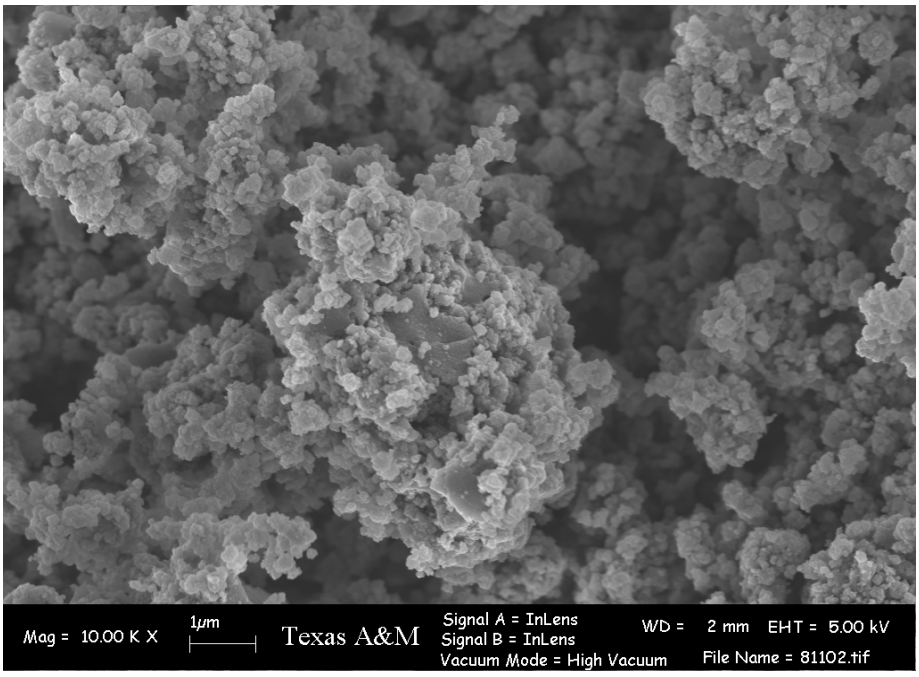

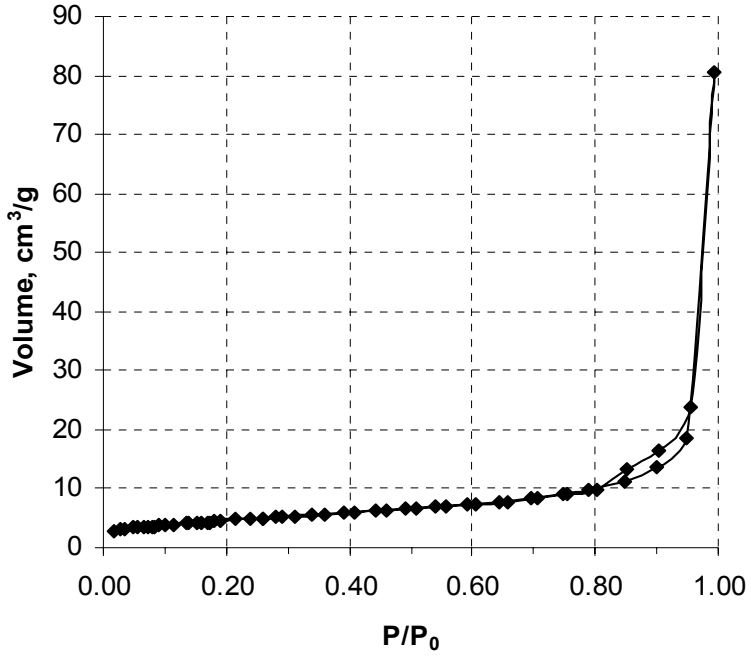

Figure 6.1. (Continued)

Commercial MST

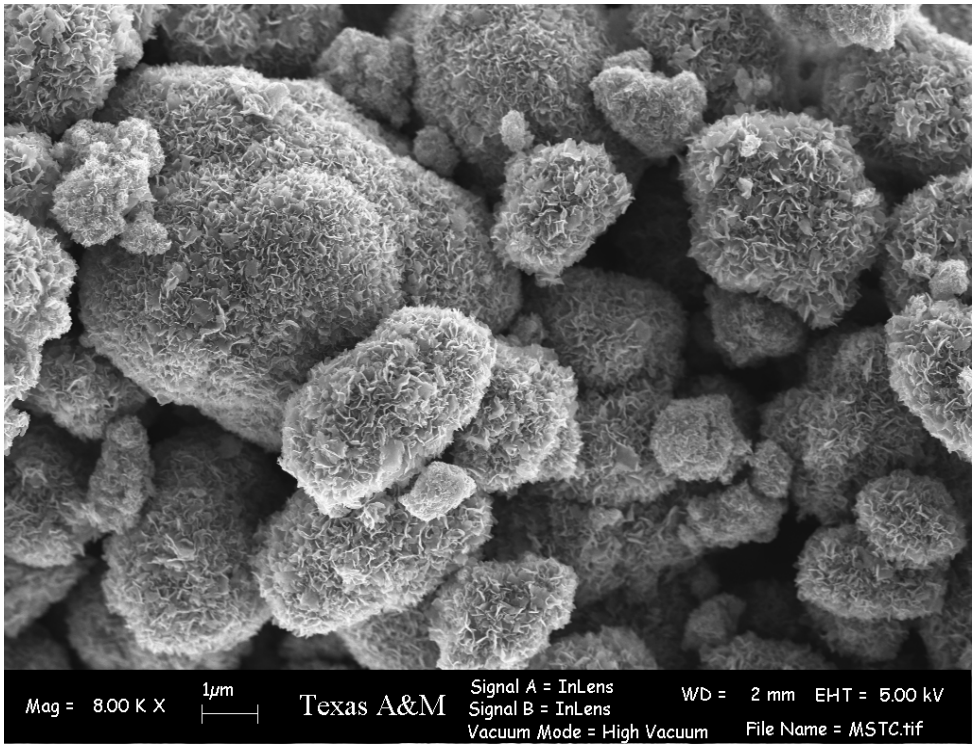

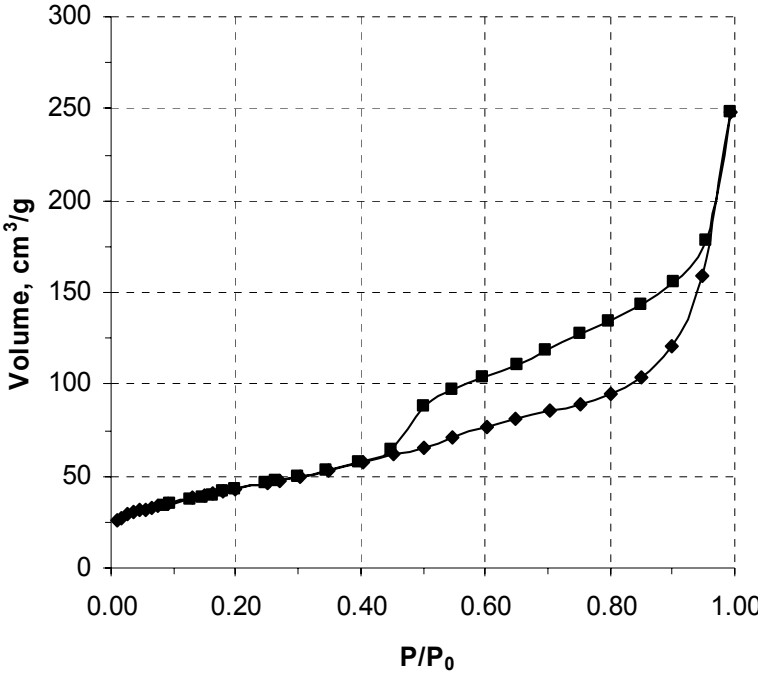

Figure 6.1. (Continued)

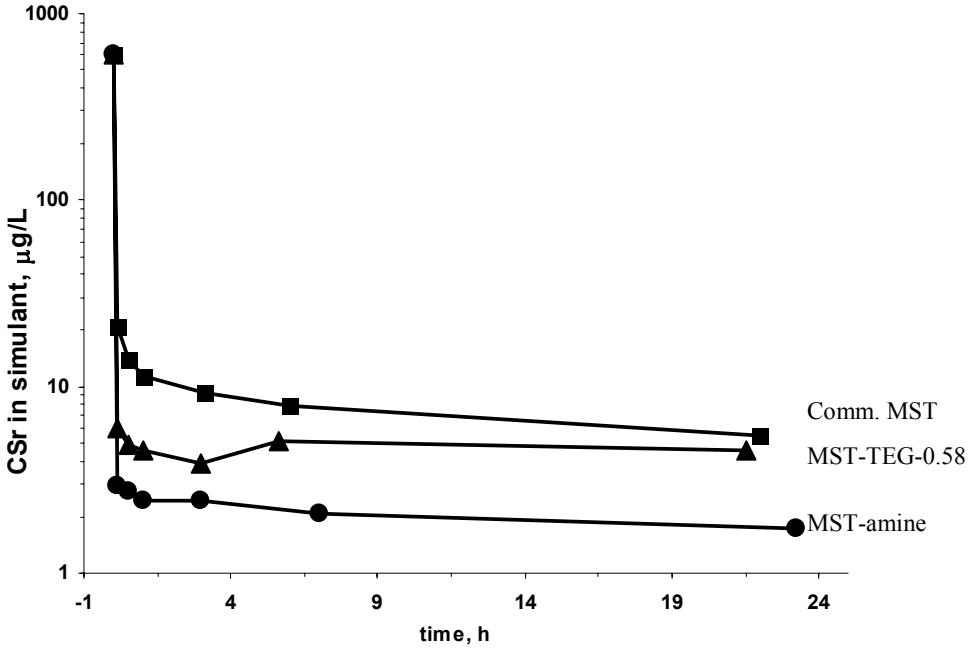

Figure 6.2. Strontium removal from highly alkaline simulant. The curves for the other MST samples from Table 6.2 fell into the region between MST-amine and commercial MST plots and are omitted for clarity. K_d values for all the samples are shown in Table 6.2

For the remaining samples we see that the TEG-0.3 sample isotherm is similar to that of TEG-1, MST-TEG-0.29 isotherm is similar to that of the template free samples and the isotherm for TEG-0.58 is the external surface isotherm.

In the remaining TEG samples, the TEG was added to solution 2. The surface area data showed that the final product is sensitive to the amount of TEG added. At a ratio of 0.58, no pores developed and as the amount of TEG is lowered, the surface area increases.

The commercially prepared MST phase has the surface area lower than any of the modified samples except the TEG-0.58 and the lowest K_d (Table 6.2). The isotherm is a composite of a type II and a type III isotherm with a broad distribution of mesopores and large interparticle voids.

Comparison of the Sr^{2+} uptake in the SR type simulant indicated that the best result was obtained by the amine treated sample. These results indicate that there is no correlation between surface area and ion-exchange capacity in amorphous titanates.

6.3.2. Sodium nonatitanate

An important distinction between SNT samples is their crystallinity, the less crystalline the sample, the better the uptake. Figure 6.3 shows the X-ray powder patterns of three poorly crystalline samples and one sample, SNT-TS, as a mixture of SNT and TS (the sharp peak).

Crystalline products were obtained after 3 days of hydrothermal treatment (Table 6.1). Heating under reflux resulted in less crystalline phases. Hydrothermal treatment of the SNT gel for 21 hours yielded a poorly crystalline phase as well.

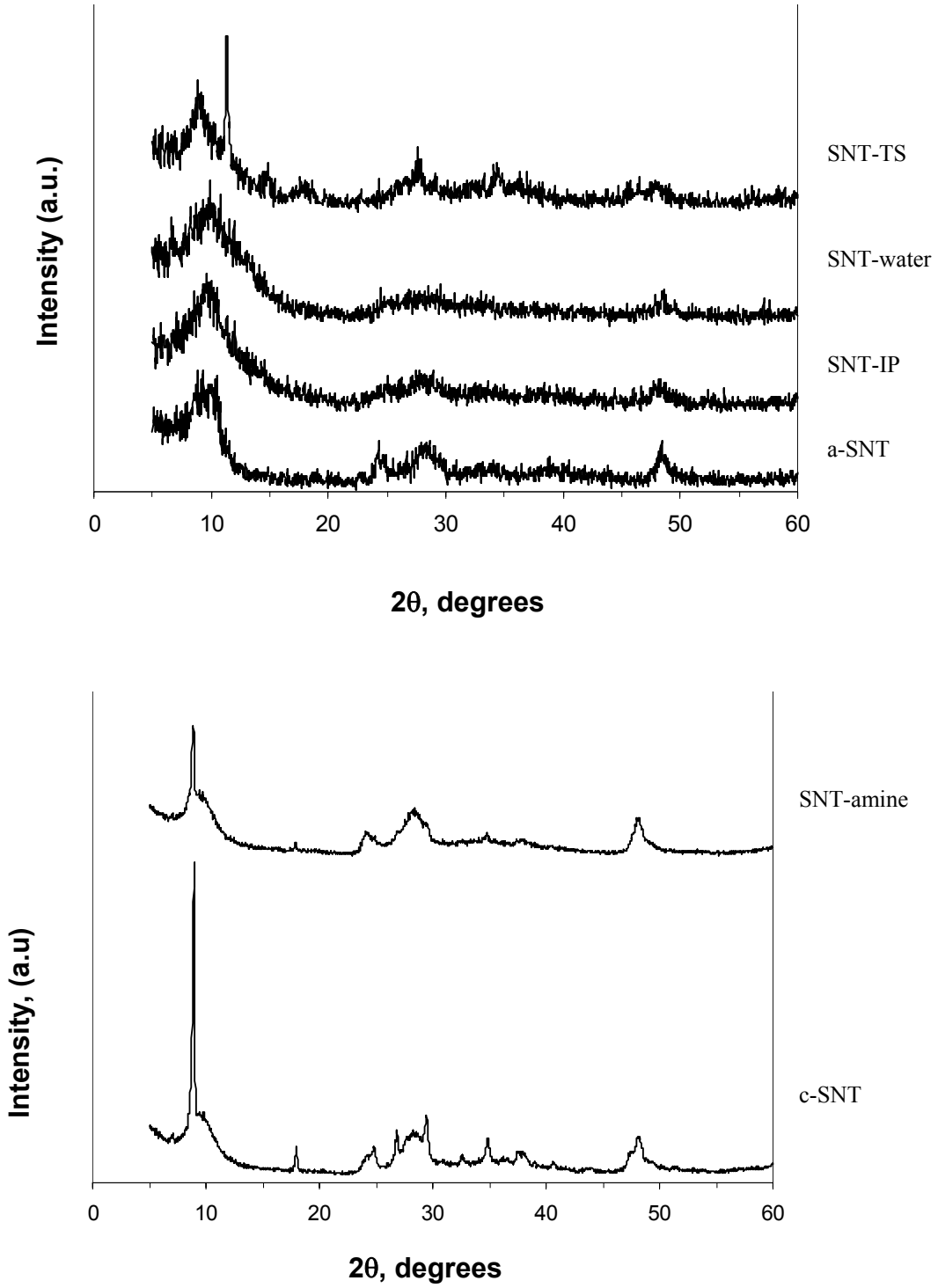

Figure 6.3. X-ray powder patterns of amorphous SNT and SNT-TS phases (top) and crystalline SNT phases (bottom)

The SEM micrographs of two of the samples (Figure 6.4 (top)) indicate that the particles are flat rectangular shaped about ½ micron in width and several microns long. They are very thin in thickness which is common for layered materials. The amine treated sample appears to have a slightly different morphology. Preliminary studies showed that 24 hours K_d values (Table 6.3) for crystalline phases were inferior to those for the commercially manufactured MST phase. Further studies were focused on poorly crystalline phases.

Table 6.3. K_d Values for Monosodium Titanate and Sodium Nonatitanate Phases*

Sample	phase	Comment	Kd, mL/g, after 1 hour, waste simulant
DM4-43-1	SnT_w	h/t, washed	3159.88
DM4-45-1	SnT	h/t	878.11
DM4-45-2	SnT_amine	h/t, with hexylamine	8183.46
00-QAB-417	MST	commercial	22009.45

*simulant used: 1.33M NaOH; 4.27M $NaNO_3$, 88mg/L Sr-cold

Performance of the SNT samples is shown in Figure 6.4 (bottom). The H-SNT phase showed the best removal of strontium, in terms of ion-exchange capacity. This phase was prepared from the sodium form of SNT by washing with hydrochloric acid. The protons replaced sodium ions in $Na_4Ti_9O_{20}•xH_2O$. Microprobe analyses of the H-SNT phase revealed the following composition: $Na_2H_2Ti_9O_{20}$, anal: Na-5.53%, Ti – 50.97 wt.%. calc:Na-5.76%, Ti – 53.93 wt.%. As can be seen from the results, only two out of four sodium atoms were replaced by the protons. The sodium form of the same sample behaved better then commercial MST but was not as effective as the H-form.

Two other samples were also converted in H-form and behaved slightly better than the commercially prepared MST. Their X-ray patterns are shown in Figure 6.3.

a)

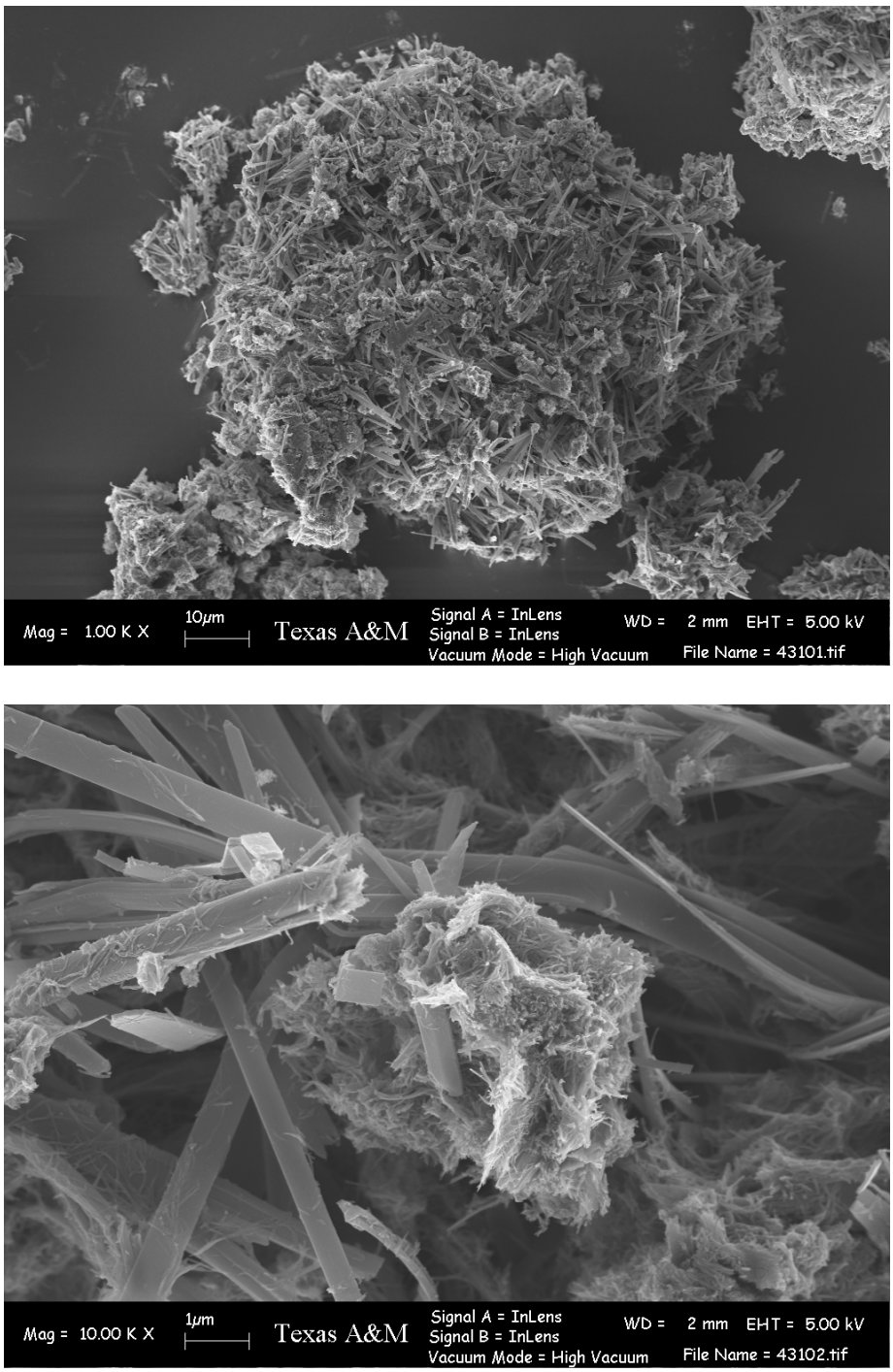

Figure 6.4. SEM images of SNT-w phase (a) and SNT-amine phase (b) with low (top) and high (bottom) resolutions.

b)

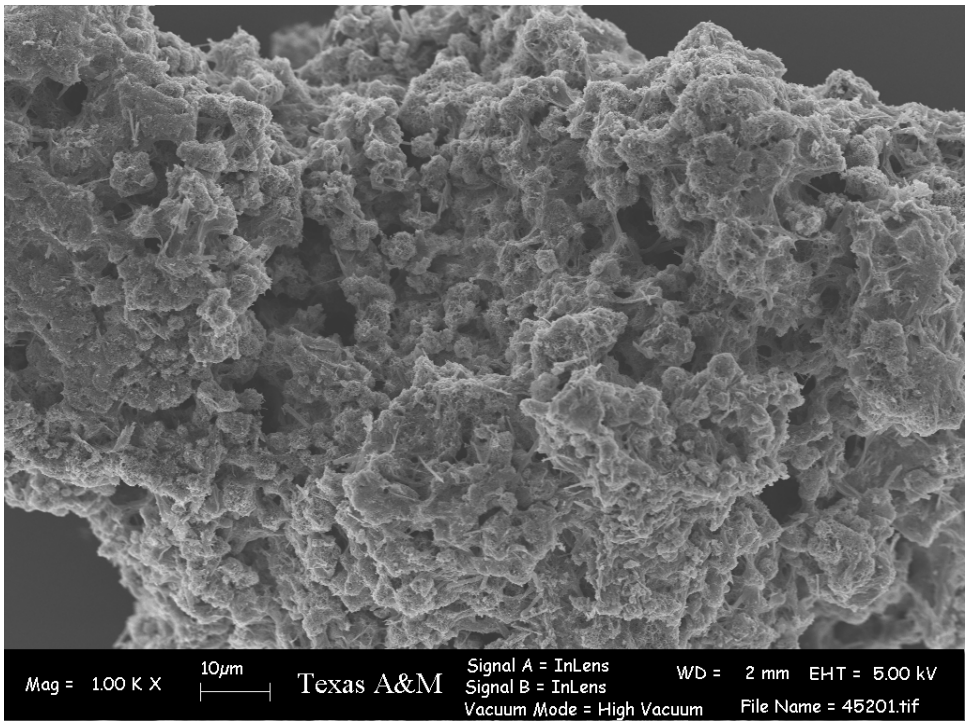

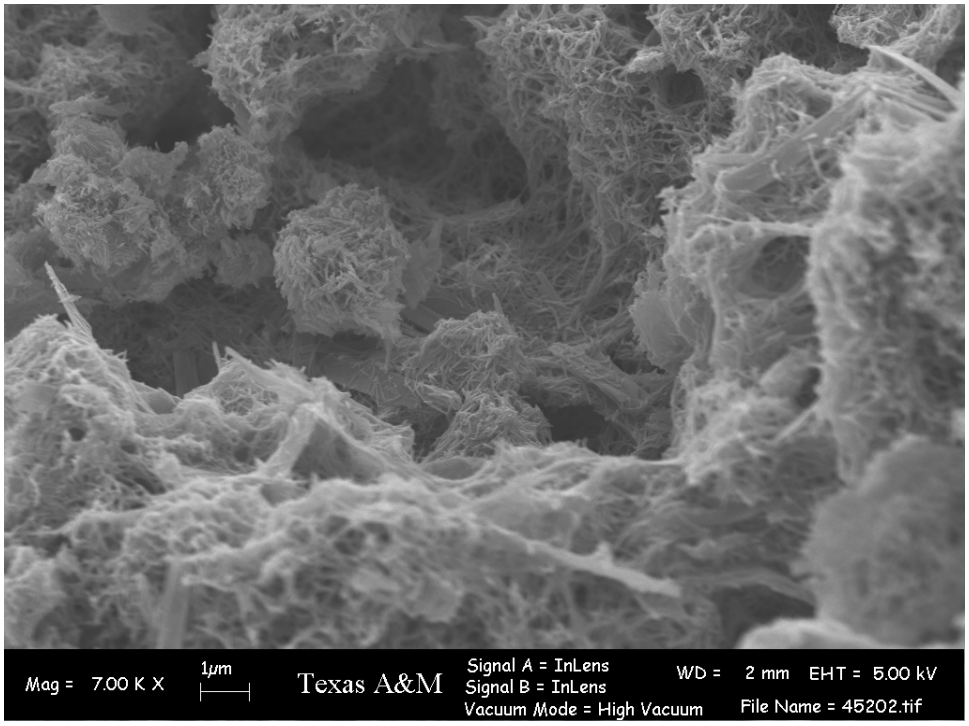

Figure 6.4. (Continued)

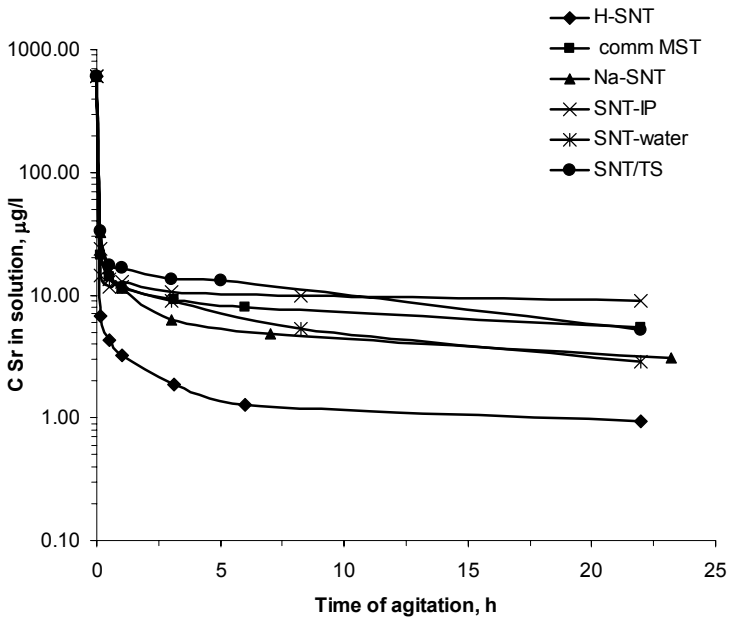

Figure 6.5. Comparative strontium removal with sodium nonatitanate phases (see Table 6.1).

It is noteworthy, that the SNT-TS mixture, synthesized from one precursor removed as much strontium as the commercial MST.

The enhanced strontium removal of the H-form of the material can be explained from the perspective of Le Chatelier principle. Suppose an H-form of the ion-exchanged material is introduced to highly alkaline waste solutions. Then, the ion-exchange process for the target ion M^+ in the H-form can be described by reactions (6.1a) and (6.1b):

$$M^+ + \overline{HZ} \leftrightarrows \overline{MZ} + H^+ \qquad (6.1a)$$

$$H^+ + OH \leftrightarrows H_2O \qquad (6.1b)$$

Reaction (6.1a) is followed by formation of water: protons, liberated from the ion-exchanger, $\overline{HZ}$, combine with hydroxide ion present in the solution shifting the

equilibrium to the products side. Therefore, more ions can be exchanged in the ion-exchanger.

The idea of utilizing of H-form of ion-exchanger for treatment of highly alkaline nuclear waste was applied to pharmacosiderite (TSP) phases. To improve the behavior of TSP sample the "as synthesized form" of K-NbTS-P (see Chapter V) was treated with a mixture of 0.2 M tetraphenyl borate, 1.0 M NaCl and 0.01 M EDTA followed by exhaustive washing with acetone, and 2 M HNO_3 for 2 hours to obtain the H-form. The obtained solid was washed with ddi H_2O, dried in the oven at 55^oC. The H-form was divided into three parts, one part of this phase was further exchanged with 50 mL of 0.1M $NaNO_3$-NaOH solution to obtain sodium form (Na-NbTS-P), and another was exchanged with 50 mL of 0.1M of KOH-KNO_3 to obtain the potassium form of the phase (K1-NbTS-P). The remaining sample was used for ion-exchange experiments without further treatment (H-NbTS-P). The results of this study are shown in Figure 6.5 (top). Similarly to SNT case the H-form exhibits the best performance, compared to potassium and sodium forms. The reason also can be correlated with the equilibrium shift due to protons combining with hydroxyl ions present on the simulant.

Figure 6.6 (bottom) represents a comparative ion-exchange behavior of a number of phases; two MST samples, two SNT samples and a niobium substituted pharmacosiderite. The best strontium sorbent is a proton form of SNT (H-SNT), followed by the MST-amine phase. The Nb substituted pharmacosiderite removed the least amount of strontium.

6.4. Conclusions

In this chapter we discussed the optimization and ion-exchange studies of the amorphous sorbents suitable for alkaline high level waste treatment. Monosodium titanate (MST) was synthesized by template-assisted precipitation in isopropanol using either hexylamine or tetraethylene glycol as surfactants.

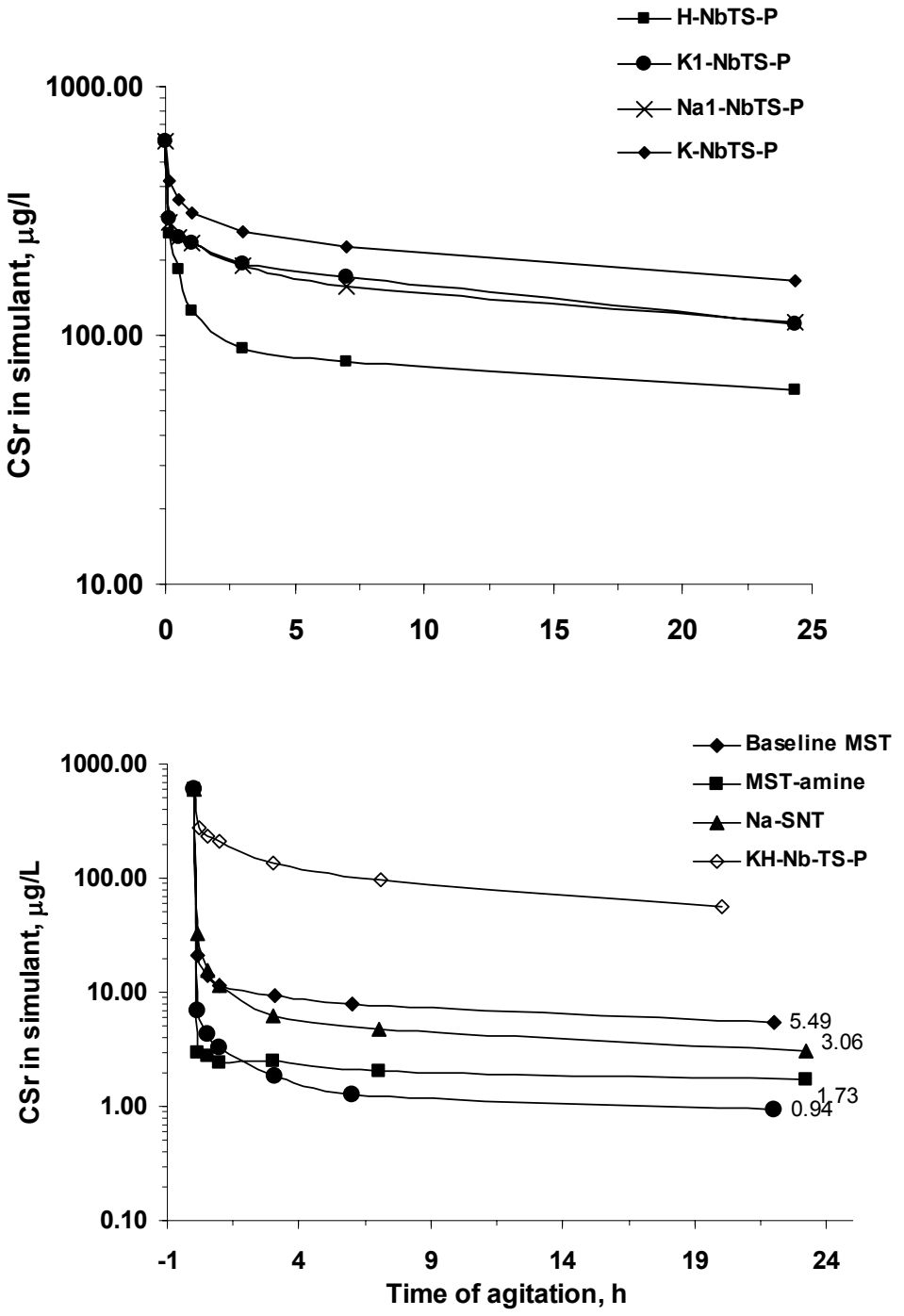

Figure 6.6. Comparative Sr removal by amorphous and tunnel type phases (top) and by HK-forms of Nb-substituted pharmacosiderite phases (bottom).

As a result, a number of samples with surface areas ranging from 16 to 400 m^2/g and broad range of pore size distributions were prepared. Ion-exchange properties of the templated samples were studied.

It was found, that there is no correlation between the surface area and strontium ion-exchange capacity in MST samples, which indicates that surface area is most likely not a key parameter in the mechanism of adsorption. Further studies are needed to rule out this statement. The MST sample prepared by the hexylamine assisted precipitation procedure exhibited the best ion-exchange capacity.

Several sodium nonatitanate (SNT) samples with different degrees of crystallinity was prepared by hydrothermal and reflux techniques. All phases demonstrated excellent ion-exchange behavior, comparable with the commercially available MST phase. The increase in ion-exchange capacity was noted for the H-form of the SNT material, compared to "as synthesized" sodium form, which can be related to equilibrium shift due to water formation as a result of the reaction. A similar trend was observed for pharmacosiderite phases. It should be noted, that a mixture of SNT/TS phases removed as much strontium as the baseline MST sample, which opens the possibility for utilization of this sample for combined cesium and strontium removal.

CHAPTER VII
SUMMARY AND SUGGESTIONS FOR FUTURE WORK

This dissertation is a part of on-going research project on the ion-exchange selectivity in inorganic ion-exchangers. The main purpose of this study is to find a way to improve currently available sorbents and synthesize new materials with predictable properties. This can be accomplished in part through understanding of the reasons of ion-exchange selectivity. Furthermore, the materials with enhanced properties can be utilized in several areas ranging from radioactive waste segregation to separation of nuclides for medical purposes.

Two groups of materials were considered in this work. The first group was titanium based zeotype materials whose framework consists of alternating clusters of TO_6 ($T=Ti^{4+}$, Nb^{5+}, Ge^{4+}) octahedra and Ge/Si tetrahedra. The negative charge of the framework is compensated by the cations, which fill the tunnels. In titanosilicate sitinakite (TS, ideal formula $Na_2Ti_2O_3SiO_4 \bullet 2H_2O$) the clusters share corners in one crystallographic dimension forming one-dimensional channels, whereas in the pharmacosiderite ($HM_3Ti_4O_4(SiO_4)_3 \bullet 4H_2O$, $M=Cs^+$, Na^+, K^+) structure the clusters are connected by silicon tetrahedra forming a three-dimensional network of channels.

Two strategies were used to improve the ion-exchange properties of the sitinakite. In the first approach the synthetic procedure was modified resulting in a less crystalline phase. The poorly crystalline phase exhibited higher strontium decontamination factors both in groundwater and radioactive waste simulants. The total ion-exchange capacity of the poorly crystalline phase was found to be 115% of that of the highly crystalline phase. The enhanced strontium removal capabilities of the less crystalline phase were correlated with differences in morphology and surface area between the two phases. The crystalline phase was mainly microporous with a surface area of 90 m^2/g, whereas the amorphous phase was macroporous with surface area of 200 m^2/g (see Chapter III for details).

A second approach to the TS optimization was a heteroatom framework substitution of Nb^{v} for Ti^{vi}. The sodium in the TS occupies two positions: one in the framework cavities and the other one inside the tunnel, where it is disordered with water molecules. A substitution of Nb for 25% of Ti resulted in a decrease of the negative framework charge, which in turn leads to Na depopulation of the tunnel. Cesium is too large to fit in the framework sites so it occupies the position in the center of the tunnel forming 8 bonds with framework oxygens. Due to sodium depopulation of the tunnel additional water molecules could enter the tunnel resulting in a higher cesium coordination number (12: 8 framework + 4 water bonds) in Nb-substituted material, compared to the Nb-free exchanger. For strontium, the situation is the opposite, as strontium is located near the walls and not in the center of the tunnel. Ion-exchange studies showed higher distribution constants for Cs in Nb-TS, compared to pure TS (see Chapter IV for details).

Similar conclusions were drawn from the studies on pharmacosiderite material, which crystallizes in a cubic unit cell. Several phases with increasing degree of germanium substitution in tetrahedral sites were hydrothermally prepared in cesium form. Unlike the Nb^{+5}, germanium, being +4 charged does not alter the framework charge. However, having ionic radius smaller than Ti^{4+} (r = 0.605Å) and larger then Si^{4+} (r = 0.26 Å), Ge^{4+} (r = 0.40 Å) can be used to decrease the unit cell size when occupying octahedral (titanium) sites and increase the unit cell when substituting for silicon occupying tetrahedral sites. It was found, that the cesium ion migrates toward the face center of the cube as the unit cell dimensions increase. However, the displacement was not the biggest in the phase with the largest volume. Although the tunnel site is the largest, cesium moves to the center of the unit cell possibly due to the interaction with water molecules. Similar to the titanium silicate case, we observed the best K_d values for the sample having the highest cesium coordination number. In the 20% Nb-substituted pharmacosiderite phase some cesium was observed in the face center due to possibly depopulation of the potassium sites (see Chapter V for details). The Nb-substituted phase demonstrated higher affinity to cesium compared to the titanium silicate phase.

The second group of materials in a focus was amorphous sodium titanates. Monosodium titanate was synthesized by a template-assisted technique, resulting in a number of samples with surface areas ranging from 20 to 400 m^2/g. The best strontium removal was demonstrated by the amine treated phase. Our preliminary results showed that surface area is not an essential factor in determining ion-exchange capacity in this type of materials. Ion-exchange properties of sodium nonatitanate phases of different crystallinities in radioactive waste simulant were examined as well. The correlation between crystallinity and strontium removal was observed. The best sample was synthesized hydrothermally and was poorly crystalline. It should be noted that the proton form of this material demonstrated an enhanced strontium capacity compared to the as synthesized sodium form (see Chapter VI for details).

Last but not the least; we discovered the route of crystallization of the titanium silicate sitinakite using in-situ X-ray diffraction technique. It was found that the process is very sensitive to the alkalinity of the starting gels and starts with formation of the sodium nonatitanate phase which is an excellent strontium sorbent. The idea was posited that sodium nonatitanate can be utilized in the ion-exchange mode in combination with titanium silicate for combined cesium and strontium removal[2]. By adjusting the synthetic condition the SNT-TS mixture was synthesized from one precursor and tested for strontium removal. It turned out that the SNT-TS phase removed as much strontium as the baseline monosodium titanate. Significant cost cutting can result from utilization of a single step in-tank process as opposed to a two-step process adopted currently.

Future work can be outlined in light of the results presented in this dissertation. The cesium removal of the TS-SNT mixture can be improved by substituting up to 25% of Nb in the TS part. Successful optimization of the synthesis of SNT-Nb-TS can be done utilizing a combination of in-situ and ex-situ methods.

The process of SNT-TS transformation, described in Chapter II can be further studied using the pair-density factor (PDF) method. The PDF describes the distribution of the separation between two atoms in the system. This method is applicable to crystalline powders and polycrystalline solids without texture. Since the SNT is a

semicrystalline material the idea of its structure can be obtained using the PDF technique.

Further optimization of sitinakite is possible through Nb-substiution in poorly crystalline samples converted to the hydrogen form. Finally, the structures of Sr-loaded pharmacosiderite phase studies by combination of single crystal and powder methods are underway as single crystal of germanium germanate was obtained towards the end of this work by modification of the technique described in Chapter V.

REFERENCES

(1) GAO: Fierce challenges still lie ahead for DOE, *Nuclear News* **2003**; *46*, 52.

(2) Alternatives for High-Level Waste Salt Processing at the Savannah River Site, National Research Council, Washington, DC, 2000.

(3) Anthony, R. G.; Dosch, R. G.; Gu, D.; Philip, C. V. *Ind. Eng. Chem. Res.* **1994**, *11*, 2702.

(4) Hritzko, B. J.; Walker, D. D.; Wang, N. H. L. *AIChE J.* **2000**, *46*, 552.

(5) Walker, J. F., Jr.; Taylor, P. A. *Book of Abstracts,* 214th ACS National Meeting, Las Vegas, NV, 1997, NUCL-097.

(6) Dosch, R. G. *Conversion of Radioactive Materials from Liquid to Solid Form*, German patent, DE2554891, 1976.

(7) Hobbs, D. T.; Walker, D. D. Plutonium and uranium adsorption on monosodium titanate, Westinghouse Savannah River Co.,Aiken, SC, 1992.

(8) Hobbs, D. T.; Fleischman, S. D. Fissile [material] solubility and monosodium titanate loading tests, Westinghouse Savannah River Co., Aiken, SC, 1993.

(9) Chandler, G. T.; Hobbs, D. T. Monosodium titanate particle characterization, Westinghouse Savannah River Co., Aiken, SC, 1993.

(10) Dosch, R. G.; Brown, N. E.; Stephens, H. P.; Anthony, R. G. *Technology and Programs for Radioactive Waste Management and Environmental Restoration* Sandia National Laboratories, Albuquerque, NM, *Vol. 2*, 1751, 1993.

(11) Sokolova, E. V.; Rastsvetaeva, R. K.; Andrianov, V. I.; Egorov-Tismenko, Y. K.; Men'shikov, Y. P. *Dokl. Akad. Nauk SSSR* **1989**, *307*, 114.

(12) Menshikov, Y. P.; Sokolova, E. V.; Yegorov-Tismenko, Y. K.; Khomjakov, A. P.; Polezhaeva, L. I. *Zap. Vses. Mineral. O-va.* **1992**, *121*, 94.

(13) Poojary, D. M.; Cahill, R. A.; Clearfield, A. *Chem. Mater.* **1994**, *6*, 2364.

(14) Lehto, J.; Clearfield, A. *J. Radioanal. Nucl. Chem.* **1987**, *118*, 1.

(15) Dadachov, M. S.; Hunter, B. A.; Bartlett, J. R. *Book of Abstracts,* ACS National Meeting, Orlando, FL, 1996, INOR-390.

(16) DeFilippi, I.; Yates, S.; Sedath, R.; Straszewski, M.; Andren, M.; Gaita, R. *Separation Science and Technology* **1997**, *32*, 93.

(17) Chapman, D. M.; Roe, A. L. *Zeolites* **1990**, *10*, 730.

(18) Behrens, E. A.; Clearfield, A. *Microporous Materials* **1997**, *11*, 65.

(19) Mooler, W. J.; Koenigsberger, J. *Z. Anorg. Allgem. Chem.* **1918**, *104*, 1.

(20) Cundy, C. S.; Cox, P. A. *Chem. Rev.* **2003**, *103*, 663.

(21) Davis, M.; Lobo, R. *Chem. Mater.* **1992**, *4*, 756.

(22) Nagy, J. B.; Bodart, P.; Hannus, I.; Kiricsi, I. *Synthesys, characterization and use of zeolitic microporous materials*; DecaGen Ltd: Szeged, Hungary, 1998.

(23) Rocha, J.; Anderson, M. W. *Eur. J. Inorg. Chem.* **2000**, 801.

(24) McCabe, D. J. *Book of Abstracts,* 214th ACS National Meeting, Las Vegas, NV, 1997, NUCL-100.

(25) Miller, J. E.; Trudell, D. E.; Krumhansl, J. L.; Anthony, R. G.; Philip, C. V.; Huckman, M.; Latheef, I. *Book of Abstracts,* 214th ACS National Meeting, Las Vegas, NV, 1997, I&EC-097

(26) Miller, J. E.; Brown, N. E.; Krumhansl, J. L.; Trudell, D. E.; Anthony, R. G.; Philip, C. V. *Proceedings of the ACS Symp. Science Techn. Disposal Rad. Tank Wastes,* Las Vegas, Nev., 1998, 269

(27) Luca, V.; Hanna, J. V.; Smith, M. E.; James, M.; Mitchell, D. R. G.; Bartlett, J. R. *Microporous and Mesoporous Materials* **2002**, *55*, 1.

(28) Norby, P. *J. Amer. Chem. Soc.* **1997**, *119*, 5215.

(29) Parise, J. B.; Cahill, C. L.; Lee, Y. *Canadian Mineralogist* **2000**, *38*, 777.

(30) Hammersley, A. P.; Svensson, S. O.; Thompson, A. *Nucl. Instr. Meth.* **1994**, *A346*, 312.

(31) Hammersley, A. P.; Svensson, S. O.; Hanfland, M.; Finch, A. N.; Hausermann, D. *High Pressure Research* **1996**, *14*, 235.

(32) Bowden, M., ConvX program, 1998, http://ccp14.minerals.csiro.au/ccp/web-mirrors/convx/

(33) EVA: data evaluation and plotting software, 4.0.0.2 ed. Bruker AXS: Karlsruhe, Germany, 1998.

(34) Shirley R. The CRYSFIRE System for Automatic Powder Indexing: User's Manual, The Lattice Press, 41 Guildford Park Avenue, Guildford, Surrey GU2 7NL, England, 2000

(35) Cheary, R. W. & Coelho, A. A.. Programs XFIT, deposited in CCP14 Powder Diffraction Library, Engineering and Physical Sciences Research Council, Daresbury Laboratory, Warrington, England, 1996, http://www.ccp14.ac.uk/tutorial/xfit-95/xfit.htm

(36) Toby, B. H. *J. Appl. Crystallogr.* **2001**, *34*, 210.

(37) Nikitin, A. V.; Ilyukhin, V. V.; Litvin, B. N.; Mel'nikov, O. K.; Belov, N. V. *Dokl. Akad. Nauk SSSR* **1964**, *6*, 1355.

(38) Men'shikov, Y. P.; Pakhomovskii, Y. A.; Goiko, E. A.; Bussen, I. V.; Mer'kov, A. N. *Zap. Vses. Mineral. O-va.* **1975**, *3*, 314.

(39) Nyman, H.; O'Keeffe, M. *Acta Crystallogr., Sect. A: Found. Crystallogr.* **1978**, 905.

(40) Clearfield, A.; Lehto, J. *J. Solid State Chem.* **1988**, *73*, 98.

(41) Nyman, M.; Tripathi, A.; Parise, J. B.; Maxwell, R. S.; Harrison, W. T. A.; Nenoff, T. M. *J. Am. Chem. Soc.* **2001**, *123*, 1529.

(42) Gould, R. O.; Lowe, B. M.; MacGilp, N. A. *Chem. Commun.* **1974**, 720.

(43) Stallings, W. E.; Lamb, H. H. *Langmiur* **2003**, *19*, 2989.

(44) Clearfield, A.; Stynes, J. A. *J. Inorg. Nucl. Chem.* **1964**, *26*, 117.

(45) Clearfield, A.; Smith, G. D. *J. Inorg. Nucl. Chem.* **1968**, *30*, 327.

(46) Clearfield, A.; Oskarsson, A. *Ion Exchange and Membranes* **1974**, *4*, 205.

(47) Poojary, D. M.; Bortun, A. I.; Bortun, L. N.; Clearfield, A. *Inorg. Chem.* **1996**, *35*, 6131.

(48) Bortun, A. I.; Bortun, L. N.; Clearfield, A. *Solvent Extraction and Ion Exchange* **1996**, *14*, 341.

(49) Sing, K. S. W.; Everett, D. H.; Haul, R. A. W.; Moscou, L.; Pierotti, R. A.; Rouquerol, J.; Siemieniewska, T. *Pure Appl. Chem.* **1985**, *57*, 603.

(50) Barton, T. J.; Bull, L. M.; Klemperer, W. G.; Loy, D. A.; McEnaney, B.; Misono, M.; Monson, P. A.; Pez, G.; Scherer, G. W.; Vartuli, J. C.; Yaghi, O. M. *Chem. Mater.* **1999**, *11*, 2633.

(51) Tripathi, A.; Medvedev, D.; Clearfield, A. *J. Solid State Chem.* **2004**, submitted.

(52) Flanigen, E. M.; Grose, R. W. *Advances in Chemistry Series* **1971**, *101*, 76.

(53) Ben Taarit, Y. *NATO ASI Ser., Ser. C* **1992**, *352*, 291.

(54) Vaughan, D. E. W.; Strohmaier, K. G.; Pickering, I. J.; George, G. N. *Solid State Ionics* **1992**, *53-56*, 1282.

(55) Joshi, P. N.; Joseph, E. M.; Shiralkar, V. P. *J. Chem. Soc., Faraday Trans.* **1994**, *90*, 387.

(56) Hunsicker, R. A.; Klier, K.; Gaffney, T. S.; Kirner, J. G. *Chem. Mater.* **2002**, *14*, 4807.

(57) Rocha, J.; Brandao, P.; Lin, Z.; Esculcas, A. P.; Ferreira, A.; Anderson, M. W. *J. Phys. Chem.* **1996**, *100*, 14978.

(58) Behrens, E. A.; Poojary, D. M.; Clearfield, A. *Chem. Mater.* **1998**, *10*, 959.

(59) Poojary, D. M.; Clearfield, A. *Inorg. Chem.* **1994**, *33*, 3685.

(60) Anthony, R. G.; Dosch, R. G.; Philip, C. V.; Sandia Corporation, Albuquerque, NM 2000.

(61) Eisenman, G. *Biophys. J.* **1962**, 259.

(62) Cotton, F. A.; Wilkinson, G. *Advanced Inorganic Chemistry*; fourth ed.; John Wiley & Sons: New York 1980.

(63) Shannon, R. D.; Prewitt, C. T. *Acta Crystallogr., Sect. B: Struct. Sci.* **1969**, *25*, 925.

(64) Roberts, M. A.; Fitch, A. N. *Z. Kristallogr.* **1996**, *211*, 378.

(65) Nenoff, T. M.; Harrison, W. T. A.; Stucky, G. D. *Chem. Mater.* **1994**, *6*, 525.

(66) Behrens, E. A.; Poojary, D. M.; Clearfield, A. *Chem. Mater.* **1996**, *8*, 1236.

(67) Bialek, R.; Gramlich, V. *Z. Kristallogr.* **1992**, *198*, 67.

(68) Harrison, W. G., T; Stucky, G. *Zeolites* **1995**, *15*, 408.

(69) Bach, U.; Lupo, D.; Comte, P.; Moser, J. E.; Weissortel, F.; Salbeck, J.; Spreitzer, H.; Gratzel, M. *Nature (London)* **1998**, *395*, 583.

(70) Athanassov, Y.; Rotzinger, F. P.; Pechy, P.; Graetzel, M. *J. Phys. Chem. B* **1997**, *101*, 2558.

(71) Hutter, R.; Mallat, T.; Baiker, A. *J. Chem. Soc., Chem. Commun.* **1995**, 2487.

(72) Antonelli, D. M.; Ying, J. Y. *Angew. Chem., Int. Ed. Engl.* **1995**, *34*, 2014.

(73) Antonelli, D. M. *Microporous and Mesoporous Materials* **1999**, *30*, 315.

(74) Dutoit, D. C. M.; Schneider, M.; Baiker, A. *J. Catal.* **1995**, *153*, 165.

(75) Takahashi, R.; Takenaka, S.; Sato, S.; Sodesawa, T.; Ogura, K.; Nakanishi, K. *J. Chem. Soc., Faraday Trans.* **1998**, *94*, 3161.

(76) Cassiers, K.; Linssen, T.; Meynen, V.; Van Der Voort, P.; Cool, P.; Vansant, E. F. *Chem. Commun.* **2003**, 1178.

(77) Ren, T.-Z.; Yuan, Z.-Y.; Su, B.-L. *Chem. Phys. Lett.* **2003**, *374*, 170.

(78) Hobbs, D. T., MST synthesis.

VITA

Dmitry Gennadievich Medvedev

Department of Nuclear Engineering
Texas A&M University,
College Station, TX, 77840-3133
E-mail: medvmitr@cedar.tamu.edu

EDUCATION

Ph.D./Nuclear Engineering/Health Physics
Texas A&M University, College Station, TX, 2004
Diploma of Chemical Engineer
D. I. Mendeleyev University of Chemical Technology of Russia, Moscow, Russia, 1999

PROFESSIONAL EXPERIENCE

May 2000-August 2004
Texas A&M University, College Station, TX, graduate research assistant
Sequestering of radioactive waste utilizing ion-exchange process. Synthesized ion-exchangers for radionuclides removal. Studied reasons for selectivity

June 1999-December 1999
Mayak Product Association, Central Facility Laboratory, Ozersk, Russia, research engineer
Optimized U, Np, and Pu separation in a large scale solvent extraction process.

February 1998-February 1999
D.I. Mendeleev University of Chemical Technology of Russia, Moscow, Russia, graduate research assistant
Solidification of radioactive waste in SYNROCK matrix. Synthesized and characterized zirconolite and perovskite ceramic.

HONORS AND AWARDS

State scholarship (1993-1999)
Ministry of Atomic Energy of Russia (MINATOM) scholarship (Spring 1995-Spring 1999)
Mayor of Moscow scholarship (Spring 1996)
Best Presentation Award in the Fuel Cycle Technical Session at 2003 American Nuclear Society Student Conference, University of California, Berkeley, April 2-5, 2003
Travel award of Environmental Sciences Division of the American Nuclear Society